OXYGEN GRADIENTS AND EXTRACELULLAR MATRIX INTERACTIONS SYNERGISTIC EFFECT ON SARCOMA CELL MIGRATION

by
Daniel M. Lewis

A dissertation submitted to The Johns Hopkins University in conformity with the requirements for the degree of Doctor of Philosophy

Baltimore, Maryland
March 2018

Abstract

Soft tissue sarcomas are a heterogeneous group of malignant cancers derived from transformed cells of mesenchymal origin. Approximately 13,000 new cases per year are diagnosed in the US alone, with 25–50% of patients developing recurrent and metastatic disease. Current clinical data suggest that undifferentiated pleomorphic sarcoma (UPS) is one of the most aggressive sarcoma subtypes, which frequently results in lethal pulmonary metastases that are insensitive to radio/chemotherapy. It has recently become apparent that sarcoma progression and metastasis are regulated by microenvironmental cues such as extracellular matrix (ECM) remodeling, cell-to-cell/matrix interactions, signaling factors, and spatial gradients. Current hydrogel platforms to study the tumor microenvironment do not fully capture complexity of the tumor microenvironment. Addressing the need for hydrogel platforms that more closely mimic the tumor microenvironment, we developed a new class of hydrogels to study oxygen gradients, collagen architecture, as well as stress relaxation as how it effects sarcoma cell migration.

First we utilized a novel gelatin based hydrogel to create a fast forming hypoxic gradient to explore the effect of varying oxygen tensions on sarcoma cell migration. To accurately model the effect of the O_2 gradient, we examined individual sarcoma cells embedded in the O_2-controllable hydrogel. We observed that hypoxic gradients guide sarcoma cell motility and matrix remodeling through hypoxia inducible factor one alpha (HIF–1α) activation. We further found that in the three-dimensional hypoxic gradient, individual cells migrate quicker, across longer distances, and in the direction of increasing O_2 tension. Treatment with minoxidil, an inhibitor of hypoxia-induced

sarcoma metastasis, abrogated cell migration and matrix remodeling in the hypoxic gradient. To determine the impact of collagen fiber density and hypoxic gradient on sarcoma cell migration, we then generated hypoxic collagen gels. Sarcoma cells encapsulated in high fiber density hypoxic gels migrated faster and degraded the matrix more rapidly compared to the low fiber density hypoxic constructs. Finally, we explored the effect of stress relaxation in the hypoxic collagen platform. From this study we can conclude that a quicker stress relaxation in hypoxic gradients lead to an increase in cell migration due to an increase procollagen-lysine,2-oxoglutarate 5-dioxygenase 2 (PLOD2) expression. We determined the quicker stress relaxation increases PLOD2 via transforming growth factor beta (TGF-β). Indeed, *In*-vivo we found an increase in tumor growth in the quicker stress relaxation hydrogels as well as an increase in collagen secretion and PLDO2 expression. Analyzing data from the cancer genome atlas (TCGA), we found a significant decrease in patient survival with an increase in PLOD2. Finally, when sarcoma from primary patient tissue was encapsulated in the system the cells demonstrated the same predicted phenotype as the mouse sarcoma line.

Thesis Advisor:

Prof. Sharon Gerecht, Ph.D.

Thesis Committee:

Prof. Zhiyong Xia, Ph.D.

Prof. Denis Wirtz, Ph.D

Prof. Hai-Quan Mao, Ph.D.

Prof. Tzipora Sarah Karn Eisinger, Ph.D. (University of Pennsylvania)

Prof. Konstantinos Konstantopoulos, Ph.D. (internal alternate)

Prof. Peter Searson (external alternate)

Acknowledgments

First and foremost, I would like to express my sincerest gratitude to my advisor and mentor, Dr. Sharon Gerecht. Over my years at Johns Hopkins, she has been there to foster my research career. Dr. Gerecht took me as a freshman and not only allowed me to stay for my master's but encouraged me to stay for my Ph.D. She has had the utmost belief in me through the highs and lows or research. I was truly lucky to have been mentored by Dr. Gerecht.

I would like to thank Dr. Dennis Wirtz, Dr. Tzipora Sarah Karn Eisinger, and Dr. Zhiyong Xia, to serve my graduate review board member to evaluate my research progress during the last three years, and Dr. Searson, Dr. Kostas Konstantopoulos, and Dr. Hai-Quan Mao for taking the time from their busy schedule to serve as members of my thesis committee.

I have been so fortunate to have so many wonderful lab members with whom I have built friendships throughout the past many years. Dr. Guoming Sun, Dr. Abigail Cuddy, Dr. Donny Hanjaya-Putra, Dr. Sravanti Kusuma, Dr. Maureen Wanjare, Dr. Kyungmin Park, Dr. Xin Yi Chan, Dr. Ying Wang, Dr. Sebastian F. Barretto, Dr. Quinton Smith, Dr. Yu-I Shen, Dr. Hawley Pruitt, Dr. Zhao Wei, Michael Blatchley, Greco Song, Matt Davenport, Kim Ellis, Ana Maria Carmo, Jacqueline Trivero, Joon Eoh, Franklyn Hall, Eugenia Volkova, Kristen Nicholes, Bria Macklin, John Jamieson, Justin Lowenthal, Morgan Elliot and many undergraduates in the lab. I would like to give a special thanks to Dr. Laura Dickinson and Dr. Hasan Erbil Abaci who took the time to train and mentor me as an undergraduate and really help me find what type of research I was passionate in.

I want to give gratitude to Yu Xu, Vitor Tang, Nupur Jain, and Mark Ciccaglione who helped facilitate the progress of my work through by taking time out of their school schedule to perform research.

I would also like to thank all the ChemBE and INBT staff who have been there helping me with a variety of administration classes, from registering for classes to dealing with purchasing.

Lastly, I would like to thank my family and friends. After being at Hopkins for the last 8 years they have been there to support me and my goals. My friends were an amazing support system at Hopkins and were with me in the library at 2 o'clock in the morning and celebrating when it was all done on a Friday night. My family was there to listen support my wishes and let me follow my heart to do the things I truly enjoy.

Table of Contents

List of Figures & Tables

List of Supplemental Figures & Tables

1 Introduction

1.1 *Physiochemical Properties of the Tumor Microenvironment*

In developing new cancer therapeutics there has been a great motivation to develop *in-vitro* platforms to better screen novel treatments. The NIH has estimated that in the year of 2016, 1.68 million people will be diagnosed with cancer with 595,690 people estimated to die of cancer[1]. The average cost of a new therapy is around $2.6 billion[2]. One of major factors of these costs in the cost of research and development, and the extensive amount of animal testing necessary to comply with FDA guidelines. In addition to the costs, these therapies also have a high failure rate due to current *in*-vitro and even *in*-vivo models that are unable to predict efficacy and effects of therapies in humans. Currently there is a 12% success rates for a drug to complete all stages of clinical trials, with most drugs failing in phase 2 clinical trials at a rate of 67%[3]. As such, there is a need to better understand the mechanism of action of potential target of therapeutics and to better predict treatment outcomes of such potential therapeutics. Toward this, a better understanding of the cancer microenvironment needs to be established, to enable the development of research tools that more accurately portray the patho-physiological aspects of the tumor and its surroundings. Moreover, such research and development tools could potentially be used for diagnostic applications. The average cost of a cancer therapy is $8,500 per patient per month with global spending on cancer therapy estimated

at $91 billion dollars[4]. In addition, many patients have to go through multiple rounds of treatment without in order to have their cancer eradicated. Thus, the technologies developed to better mimic the tumor microenvironment (TME) to study and screen potential therapeutics, can be adapted for diagnostic and preventive applications.

The tumor microenvironment is a intricate and dynamic milieu containing supporting cells, blood vessels and extracellular matrix (ECM) proteins. In addition, there is a complex combination of chemical, mechanical and physical cues that regulate cancer progression such as stiffness of the ECM, pressure of the growing tumor mass, secreted and sequestrated cytokines/growth factors, oxygen, pH, and glucose concentration. All of these cues contribute to the decision of cancer cells to grow or migrate. These environmental cues are typically present in a three-dimensional environment. This system is drastically different than conventional two-dimensional culture regimes used to study mechanisms that regulate cancer growth. These *in vitro* two-dimensional culture regimes have minimal physiological relevance, as they do not accurately portray the complexity of the tumor environment. As a result, current studies using two-dimensional culture regimes have shown limited translational impact as well as a low screening ability for successful therapies.

One approach could be to develop biomaterials and hydrogel technologies that mimic the cancer microenvironment in the three-dimension. Hydrogels are cross-linked polymeric networks that are extensively swollen with water[5]. These polymer networks can be made up of a wide variety of materials such as natural, synthetic, or a natural/synthetic hybrid[6]. Hydrogel properties such as stiffness, cell adhesion domains, and degradation sites can be modified to tune a hydrogel to suite any cell type[7]. Such

platforms can be applied to study mechanisms underlying cancer development, growth and metastasis, as well as to screen cancer therapeutics. Towards the design of these novel hydrogel materials, a better understanding of the tumor microenvironment must be established.

The native tumor microenvironment is composed of a complex structure of ECM proteins with varying chemical and mechanical gradients that lead to the migration and proliferation of cancer cells. The extracellular environment has many cues that lead to cancer cell migration. In the following sections we focus on key aspects in the tumor microenvironment that regulate cancer cell fates, including the ECM composition, matrix remolding, oxygen, pH, cytokines, and stiffness.

1.1.1 **Extraceullular Matrix**

The ECM is the acellular component of a tissue made of a meshwork of highly cross-linked proteins[8]. The ECM is made up of a wide variety of proteins, such as fibronectins, collagens, laminins, glycoproteins, etc.)[8]. Collagen is the most abundant protein in the ECM, which constitutes up to 30% of the total proteins in the body and 90% of the ECM[9, 10]_. Collagen is a substantial structural feature of the ECM that regulate tensile strength and cell adhesion[11]. Collagen molecules are made up of three alpha helical structures that together form a fibril structure. These fibers form larger supramolecular structures that create the backbone of collagen bundles[10]. These fibrous bundles are modified through the hydroxylation of proline and lysine resides, allowing for the strengthening and crosslinking of collagen fibers[12]. Another major ECM component is fibronectin. Fibronectin is made from a dimer that is joined by c-terminal disulfide bonds. These bonds can bind to other fibronectin dimers, to collagen, and to cell

integrin receptors[13]. Laminin is another crucial ECM protein. This molecule is crucial for cell attachment to the matrix[14]. Laminin has been shown to increase migration in breast carcinomas[15, 16]. All of these proteins in conjunction create a fibrillar network. This fibrillar network morphology can be imaged using second harmonic generation (SHG) microscopy [17]. SHG microscopy is a process where two photons are up-converted to half of the wavelength of the excitation laser. These lasers when funneled through polarized optics allow for a detailed structure of collagen to be produced. [18].

Within the ECM there are cancer-associated fibroblasts (CAFs), which have been shown to modify the ECM, leading to fibrillar ECM[19]. Specifically, CAFs have been shown to contribute to the synthesis of type I, type III, and type IV collagen, fibronectin and laminin[20-22]. It has been shown that increased number of fibroblasts leads to an increase in type I collagen deposition. These fibroblasts lead to an higher deposition of ECM as well as remodeling of the matrix. All of these factors lead to a higher chance of tumorgenesis.[23].

1.1.2 **Matrix Remodeling**

CAF's as well as cancer cells secrete a wide variety of proteases and ECM modifiers. Two of the most studied enzymes are matrix metalloproteinase (MMP) and thrombospondin motifs (ADAMTS), which specialize in degrading the ECM[23]. There are about 23 members in the MMP family[24]. MMPs target a large range of extracellular proteins, including MMP-1 that targets collagen, MMP-2 that targets gelatin (denatured collagen), and MMP-7 that targets fibronectin[25, 26]. These MMP's have two classifications: soluble (secreted)-type and membrane-anchored MMPs[27, 28]. Soluble MMPs are secreted from the cell and are made up of proMMPs[29]. In the pro-domain of

the soluble MMP's resides a cysteine residue which ligates catalytic zinc[29]. This cysteine-zinc interaction is disrupted in a two-step reaction. The reaction starts by cleaving the pro-peptide region to remove the n-terminal polypeptide. The second step occurs through an auto-proteolytic reaction, which generates an active enzyme[30]. Membrane-type (MT)-MMP are anchored to the membrane and are activated by pro-protein convertases[28]. ADAMTS share a similar structure to MMPs in which they both have pro-domains that needs to be activated, degrading the surrounding matrix. The difference between MMPs and ADMATS is that instead of a cytosine rich domain, ADMATS have a thrombospondin domain[31].

Besides matrix degradation, cancer cells modify the ECM to facilitate migration. Because of the prevalence of interstitial collagen in the tumor microenvironment, it is subject to a large number of posttranslational modifications[32]. Collagen crosslinking is primarily mediated by lysyl oxidase (LOX) and LOX-like enzymes. The LOX crosslinking has been shown to increase cancer cell migration as well as increase ECM stiffness[33, 34]. Baker et al, have shown that this increase in stiffness due to LOX crosslinking lead to an increased in colorectal cancer migration[35]. In breast cancer, it has been shown that LOX crosslinking induces β1 integrin clustering, PI3K signaling and focal adhesions[36]. Another key collagen modifier is pro-collagen-lysine, 2-oxoglutarate 5-dioxygenase (PLOD2), which initiates lysine hydroxylation of collagen[37-39]. These crosslinks are crucial in the formation of mature collagen fibers, are regulated by hypoxia, and lead to an increase in tumorgensis[40, 41].

.

1.1.3 O_2 and pH

Oxygen and pH are two important cues that regulate normal cell growth. These factors have lead to changes cancer cell growth to migration[42, 43]. The relative distance to a blood vessel determines oxygen tension and pH in the tumor microenvironment. Datta et al show when the tumor vasculature is re-established due to anti-vascular endothelial growth factor (VEGF) therapy they can observe the change in the oxygen and pH gradients around the tumor[44]. This therapy and similar therapies have been shown to effect tumor vascular, which will be discussed later in the review. However, as the distance from the blood vessel to the tumor increases, there is a decrease in oxygen concentration to levels bellow 2% oxygen, known as hypoxia[45]. Oxygen concentration is mediated by the distance that a tumor mass is away from a blood vessel. When a tumor is approximately ~200 μm away from a blood vessel which leads to hypoxia and server hypoxia [46]. Hypoxia has been shown to lead to increase in angiogenesis[47], metastatic potential[48, 49], DNA replication[49, 50], and reduced protein synthesis[51]. The oxygen sensing mechanism has been identified to be linked to transcription factor termed hypoxia inducible factor (HIF). HIF are made up of an α and β subunit[52]. HIF1 is accumulated at 1% oxygen[53] and rapidly degraded at 21%. There are three types of HIFs; HIF1, HIF2, and HIF3. The main difference between these factors is that HIF1α is constantly expressed ubiquitously in most tissues, while HIF2α and HIF 3α are found in a subset of tissues[54-56]. Hypoxia in general leads to up regulation of a variety of factors (**Figure 1-1**), from pro-angiogenic to ECM modifiers for example collagen remodeling genes such as PLOD2 and LOX to angiogenic and intravasation factors such as VEGF[57]. Hypoxia has also had a negative effect clinically,

cells exposed to hypoxia are usually far away from blood vessels, and therefore less exposed to drugs, as well as lower proliferation rates and less sensitivity to radiotherapy and p53-mediated apoptosis[58]. Recently our lab has developed a platform to better screen potential cancer therapeutics in a hypoxic cancer tumor microenvironment[59].

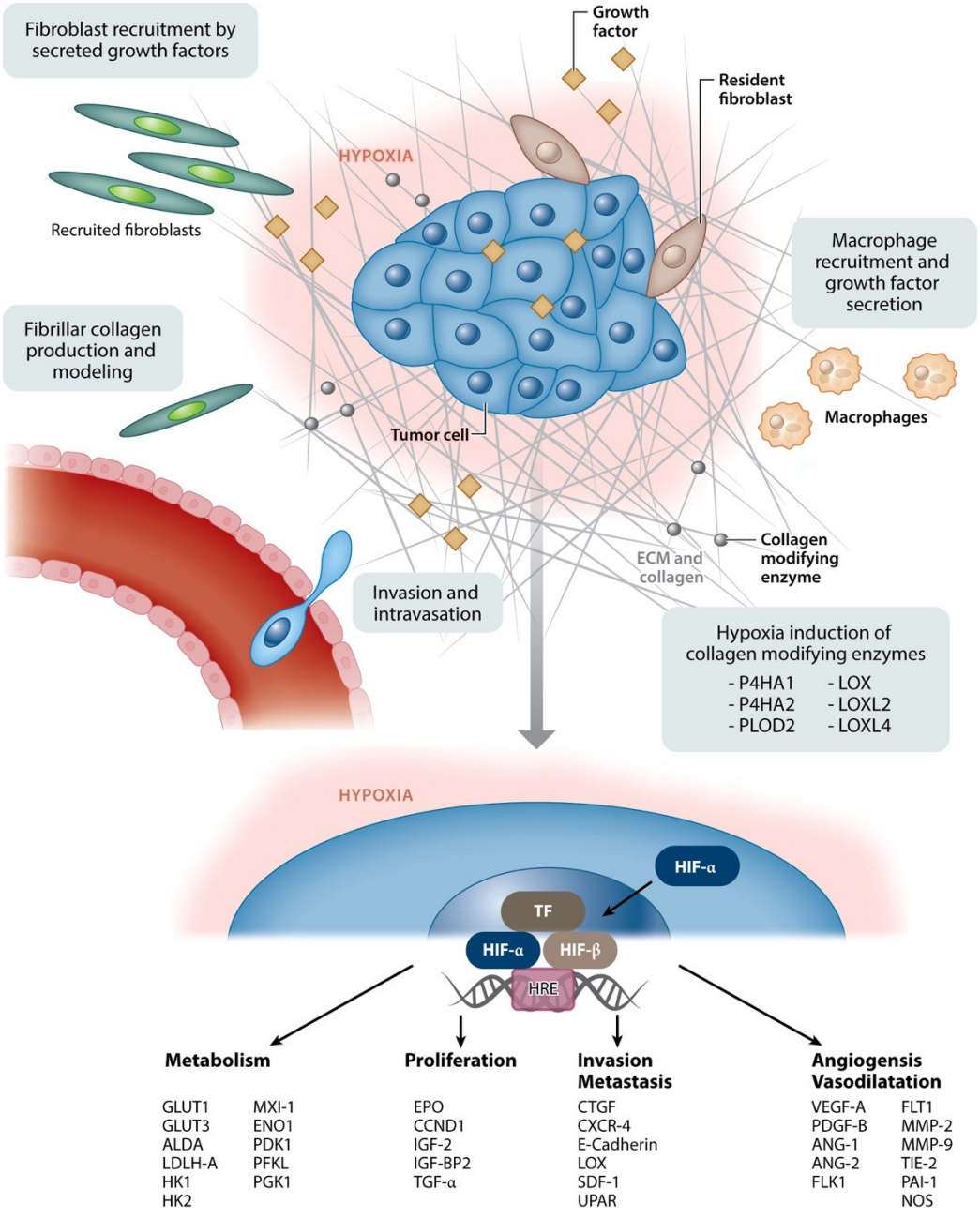

Figure 1-1: Cancerous pathways affected by accumulation of hypoxia-inducible factor.

Modified from Reference 46. Abbreviations: ALDA, aldolase A; ANG-1, angiopoietin 1; ANG-2, angiopoietin 2; BMDSC, bone marrow derived stem cell; CCND1, cyclin D1; CTGF, connective tissue growth factor; CXCR4, C-X-C chemokine receptor type 4; ECM, extracellular matrix; ENO1, enolase 1; EPO, erythropoietin; FLK-1, VEGF receptor 2; FLT-1, VEGF receptor 1; GLUT, glucose transporter; HIF, hypoxia-inducible factor; HK, hexokinase; IGF-2, insulin growth factor-2; IGF-BP2, IGF-factor-binding protein 2; LDH-A, lactate dehydrogenase A; LOX, lysyl oxidase; miRNA, micro-RNA; LOXL, lysyl oxidase homolog 1; MMP, matrix metalloproteinase; MXI-1, max interactor 1; P4HA, Prolyl 4-hydroxylase subunit alpha-1; PAI-1, plasminogen activator inhibitor-1; PDGF-B, platelet-derived growth factor-B; PDK1, pyruvate dehydrogenase kinase 1; PFKL, phosphofructokinase L; PGK1, phosphoglycerate kinase 1; PLOD, procollagen-lysine 2-oxoglutarate 5-dioxygenase; SDF-1, stromal-derived factor 1; TF, transcription factors; TGF-a, transforming growth factor-a; TIE-2, angiopoietin receptor 2; UPAR, urokinase plasminogen activator receptor; VEGF, vascular endothelial growth factor

In addition to an up regulation of many cytokines, hypoxia also affects the metabolism of the cell. The normal metabolism and generation of adenosine triphosphate (ATP) is highly sensitive to oxygen concentration. It has been shown that hypoxia causes a substantial decrease in ATP production[60]. Normally, cancer cells have to change their metabolism to rapidly produce ATP[61]. Under hypoxia, cancer cells switch from their normal oxidative phosphorylation to glycolysis. In order to maintain the high levels of ATP, these cells drastically increase their glucose uptake to maintain the ATP level. By using glycolysis, cancer cells can very quickly generate ATP even faster then conventional oxidative phosphorylation. However, due to this type of metabolism, the pH in extracellular environment drops from a physiological pH of 7.2 to an acidic microenvironment to a pH between 5.6-6.8[46].

1.1.4 **Stiffness**

Stiffness of the ECM is a crucial characteristic of the tumor microenvironment, with the majority of the ECM made out of collagen 1. As detailed above, the density of ECM in the tumor microenvironment increases as a result of new ECM secretion and up-

regulation of crosslinkers by the CAFs and cancer cells. In fact, an increase in collagen crosslinkers such as LOX and PLOD2 have been shown to lead to facilitate tumor progression[62]. Because of this increase in LOX secretion cancer cells have responded by clustering non-receptor tyrosine kinases, specifically focal adhesion kinase (FAK). Paszek et al have shown that 3D matrices with a Young's modulus of 400 Pa to have a significant increase in the size of colonies compared to colonies cultured in 3D matrices with a Young's modulus of 160-170 Pa[33]. They linked this increase in size to clustering of α5β1-integrin, which caused stimulation of FAK phosphorylation, RhoA activity and cytoskeletal contractility.

In addition to stiffness, another factor of the tumor microenvironment that plays a roll the pore size of the surrounding matrix. Patheck et all have shown how ECM matrix stiffness and confinement play a role in cancer cell migration, demonstrating that cells in stiffer and narrower channels migrating faster[63]. Haeger et al explored this concept of confinement and cell-cell junctions in collagen gels[64]. They concluded that depending on the type and density of the ECM the mode of migration changes, with cells in denser matrixes have a "follow the leader" type migration, while in less porous matrixes, single cell migration was observed. The ECM stiffness has also been shown to increase the differentiation of epithelial cancer cells to a more mesenchymal phenotype. Wei et al recently published that nuclear translocation of TWIST1, leads to an increase in mesenchymal transition via this mechano-transduction pathway[65].

1.1.5 **Stress Relaxation**

In addition to ECM stiffness, another mechanical property of the ECM that is recently being explored is stress relaxation. Stress relaxation is the decrease in stress under a

constant strain. When the stress relaxation modulus decreases that is similar as having a lower resistance to deformation over time. Recently, it has been shown that different organs have different stress relaxation times[66]. Different stress relaxation times were also reported in different tumor types[67]. Previous work has examined the effect of stress relaxation on cell behavior[68-71]. Stress relaxation has been shown to affect including cell motility[72], mesenchymal stem cell differentiation [66], and the cell's ECM sensing capability [73].

1.2 *Polymeric Hydrogels as Engineering Three-Dimensional Microenvironments*

Polymeric Polymeric hydrogels, which are composed of a three-dimensional (3D) hydrophilic network, have been recognized as a promising material for regenerative medicine and pharmacological applications due to their multi-tunable properties and structural similarity to the native extracellular matrices (ECMs).[74-79] Their physico-chemical and biological properties, such as mechanical strength, degradation behavior, nutrient transport, and spatiotemporal topography, can be regulated by the types of polymers and their compositions, crosslinking density, and tailoring with various bioactive molecules (*i.e* cell adhesion ligands, proteolytic degradation sites, etc). In addition, these matrices are utilized as artificial cellular microenvironments for recapitulating ECMs in soft tissues due to their high swelling properties and mechanical resemblance. In particular, *in situ* crosslinkable hydrogels, which show phase transition from solution to gel through various crosslinking chemistries, have attracted substantial attention as engineered cellular microenvironments and drug delivery carriers owing to easy encapsulation of therapeutic agents during hydrogel formation under mild condition

as well as minimally invasive properties.[80-82] With advances in materials engineering, various *in situ* forming hydrogels and crosslinking strategies have been developed to create engineered microenvironments for supporting cell growth and directing their fate (**Figure 1-2**).[83] In this section, we discuss various types of polymeric hydrogels and their crosslinking chemistries to create 3D hydrogel matrices for a broad range of biomedical applications.

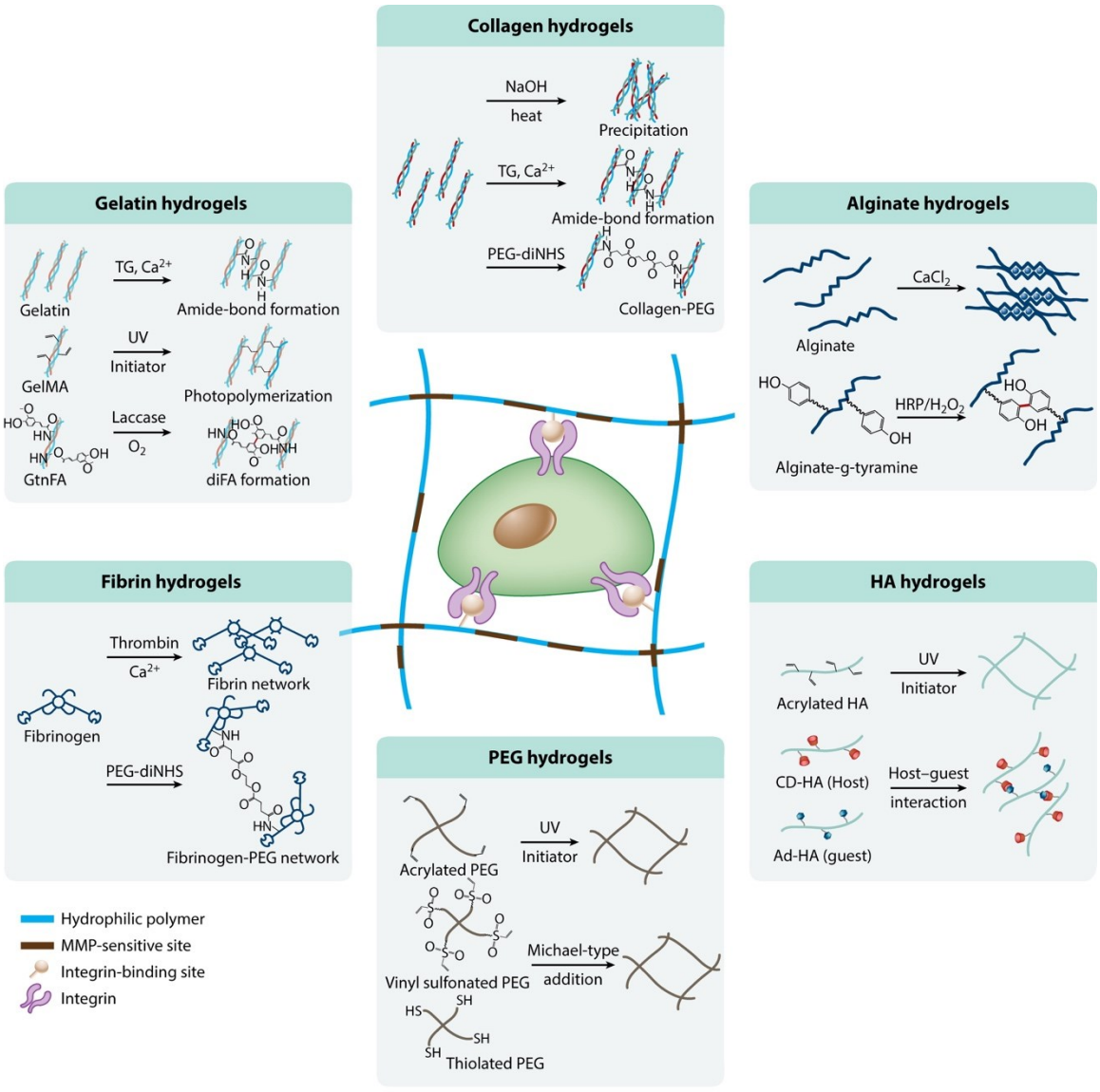

Figure 1-2: In situ cross-linakble hydrogels as an artificial cellular microenvironment.
Cross-linking strategies are detailed for each hydrogel system. Abbreviations: CD-HA, β-cyclodextrin-modified hyaluronic acid; FA, ferulic acid; GelMA, methacrylated gelatin; GtnFA, gelatin grafted with ferulic acid; HA, hyaluronic acid; MMP, matrix metalloproteinase; PEG, poly(ethylene glycol); PEG-diNHS, poly(ethylene glycol) conjugated to di(succinic acid *N*-hydroxysuccinimide ester); TG.

1.2.1 **Natural Hydrogel Materials**

Collagen type I is a well-known ECM protein that provides structural frame to support cell growth and adhesion through cell-to-cell and cell-to-matrix interaction since it has various binding sites that interact to cell-surface receptors and to other ECM components (*e.g.*, fibronectin).[84, 85] It also includes proteolytic degradable sites for ECM remodeling within cellular microenvironments, which is a critical parameter for regulating cell behaviors in the microenvironments.[84] Generally, collagen hydrogels are prepared *via* physical crosslinking by pH and temperature-sensitivity, which can 3D fibrillar matrices recapitulating the ECMs *in vivo*. Increasing pH and temperature of acidic collagen precursor solution induces fibrilar hydrogel matrices.[86] Based on their unique properties, collagen has been widely used as scaffolds for tissue engineering and regenerative medicine as well as other biomedical applications. However, the critical disadvantages of collagen are the weak mechanical properties and batch-to-batch variation. To improve these limitations, many chemical crosslinking methods have been developed, including chemical glycation[87] and enzyme-mediated crosslinking reaction[88] to give more stable and stiff collagen hydrogels through chemical crosslinking. For example, David and colleagues developed a method to fabricate chemically crosslinked collagen hydrogels using transglutaminase that catalyze the amide crosslinking from the specific functional groups (*e.g.*, γ-carboxamide and primary amine in collagen chains).[88] Using this approach, they fabricated more stable collagen hydrogels compared to physically crosslinked collagen hydrogels. Baoxing and colleagues utilized a different crosslinking condition using genipin that an excellent natural cross-linker for proteins (*e.g.*, collagen and gelatin) with low cytotoxicity.[89]

The mechanical properties can be controlled by varying genipin concentrations, showing from 2 to 50 kPa of compressive strength. However, this system has a disadvantage such as slow chemical reaction (over 24 h to fully cross-link the networks). More recently, Hyunjoon and his colleagues developed a novel strategy to create more stable and multi-tunable collagen hydrogels using poly(ethylene glycol) conjugated with di-(succinic acid *N*-hydroxysuccinimidly ester) (PEG-diNHS) that induce interconnection between collagen fibers through crosslinking of primary amines in polymer backbones.[90] Using the engineered collagen hydrogels, they investigated the effect of matric stiffness on the behaviors of cancer spheroids of hepatocarcinoma cells (HCCs). While many approaches have been developed to enhance the stability of collagen matrices, advanced engineering technologies are still required to improve cyto-compatibility and multi-tunable properties.

Fibrin has been widely used in a wide range of biomedical applications due to their biocompatibility and biodegradability as well as easy to fabrication.[91] Fibrin hydrogels were fabricated by the crosslinking of fibrinogens through thrombin-mediated ionic interactions.[92, 93] In this reaction, thrombin cleaves the *N*-terminal end of fibrinogen that can induce polymerization of fibrin into fibrous hydrogel matrices.[92, 93] These fibrin matrices also possesses various cellular responsible domains, including integrin, heparin, and fibronectin binding sites that are critical in regulating cellular activities in wound healing and tissue regeneration.[94] Based on their unique properties, fibrin gels have been widely utilized as either therapeutic implants or vehicles for regenerative medicine and drug delivery carriers as well as clinical treatments. Compared to collagen hydrogel, fibrin gels showed relatively higher and broader range of matrix mechanical properties (approximately 1 to 30 kPa) by varying fibrinogen and thrombin

concentrations. However, the fibrin gels have a problem with fast degradation of hydrogel matrices through tissue factors and other enzymes secreted by the cells, which is difficult to fully support cell growth and activities. Therefore, many studies have been reported to improve matrix stability of fibrin gels, allowing long-term cell culture to fully understand of the effect of 3D matrices on cellular activities. The representative strategy is to incorporate functionalized PEG as a crosslinker, defined as PEGylations. Francesca *et al.* utilized PEG-fibrin hydrogels to provide artificial tumor microenvironments for cancer researches.[95] They prepared PEGylated fibrin hydrogels by simple mixing of fibrinogen and functionalized PEG that can induce crosslinking between the polymer backbones through chemical reactions. Using the stable matrices, they investigated the effect of 3D microenvironments on the cancer cell growth (*e.g.*, lung adenocarcinoma cell lines, A549 and H1299) for day 18, resulting the 3D matrices showed similar tumor growth compared to *in vivo* models.

1.2.2 **Synthetic Hydrogel Matrices**

Synthetic polymers have several advantages compared to natural polymers, such as more controllable physicochemical properties. Among these, Poly(ethylene glycol) (PEG) is well known as the representative biomaterial for medical uses. PEG is a bio-inert and hydrophilic polymer, thus used as surface grafting materials to create anti-fouling surfaces of biomaterials and as coating materials to enhance lubricity of medical catheters. In addition, PEG hydrogels are commercially used as clinical tissue sealants. Furthermore, a PEG has been utilized as hydrogel matrices for tissue regeneration and drug delivery systems due to its biocompatibility and multi-tunable properties. However, PEG should be decorated with bioactive molecules (*e.g.*, cell adhesion sites and MMP-

sensitive moieties) to support cell growth within 3D microenvironments. The most common strategy is to fabricate PEG hydrogels through photo-polymerization of diacrylated-PEG (PEGDA) chains.[96] During hydrogel formation, the bioactive molecules can be incorporated within the matrices. Anseth and her colleagues utilized the photo-curable PEG hydrogels as a template to study the effect of mechanical memory on stem cell fate, demonstrating stem cells have mechanical memory that stores information from past phsico-chemical conditions and regulates their fate.[97] There are many other approaches to create PEG hydrogels, including Michael-type additionreaction, thiol-ene reaction, and enzyme-mediated crosslinking reactions. Lutolf *et al*. developed a PEG hydrogels incorporating cysteine coligopeptides *via* Michael-type additions.[98] The conjugative reaction occurs under mild conditions, which is critical for *in vitro* and *in vivo* applications. Segura and her colleagues developed the similar PEG hydrogels through thiol-maleimide Michael-type addition using zinc (Zn), demonstrating multi-tunable properties of the hydrogel matrices, such as kinetics of hydrogel formation and matrix stiffness.[99] Using the matrix, they investigated the impact of matric stiffness on cellular activities of human dermal fibroblasts (HDFs).

1.2.3 **Semi-Synthetic Hydrogels**

While the natural and synthetic hydrogels have been widely used as 3D matrices in tissue engineering and regenerative medicine, there are some limitations to be improved, such as matrix stability; batch-to-batch variation; accurately mimicking native extracellular matrices. To overcome these limitations, chemically modified natural hydrogels (defined as semi-synthetic hydrogels) have been developed. There are various

approaches to create the engineered polymeric hydrogels for tissue engineering and regenerative medicine.

Alginate is a naturally derived anionic polymer, which is composed of the repeating units of (1-4)-linked *β-D*-mannurinate (M units) and α-*L*-gluronate (G units).[100] Alginate hydrogels forms in the presence of divalent cations (*e.g.*, Ca++ and Mg++) through ionic interaction between the G units in the polymer backbones. Due to its biocompatibility and easy fabrication process, alginate hydrogels have been used in various clinical applications, including wound dressing, drug delivery, and tissue regeneration as well as treatments of myocardial infraction.[101, 102] While it is useful in various biomedical applications, it remains a challenge to improve its mechanical properties and bioactivity. To improve these limitations, many research have been endeavored to introduce chemical modifications of alginate chains. Dhoot *et al.* have conjugated cell adhesive sites (Arg-Gly-Asp, RGD) into alginate chains to enhance cellular activities.[103] Zhu and colleagues have developed an enzymatically crosslinked alginate hydrogels, which is composed of tyramine-conjugated alginate that can form chemically cross-linked hydrogels through horseradish peroxidase (HRP)-mediated oxidative reaction.[104] More recently, Mooney and his colleagues developed a novel strategy to create highly stretchable and tough alginate hydrogels through the formation of interpenetrating networks (IPNs).[105] To improve mechanical stiffness and hydrogel stability, they fabricated the hydrogels by hybridization of ionically crosslinked alginate networks using Ca++ and photocrosslinkable polyacrylamide gels, resulting in highly elastomeric alginate hydrogels. With advanced in engineering approaches, alginate

hydrogels with biological activities are promising materials to provide 3D matrices in tissue regeneration and other clinical applications.

Gelatin, denatured collagen type I, has been widely used in tissue engineering and regenerative medicine due to its desirable features, including biocompatibility, biodegradability, cost effect, and easy to fabrication (reviewed by Barbara *et al.*[106]). In addition, it has a cellular responsive sites, such as integrin biding sites and proteolytically degradable domains that plays a critical roles in regulating cellular activities within 3D microenvironments.[107] To utilize gelatin as a biomaterial, it is required to introduce chemical crosslinking of polymer backbone to create stable gelatin matrices at body temperature. There are various ways to form a covalently crosslinked gelatin networks, including enzyme-mediated crosslinking and photo-crosslinking reactions. Using transglutaminase and formaldehyde, we can prepare gelatin hydrogels using unmodified gelatin. However, the process showed critical limitations for use in biomedical applications, such as slow phase transition and cytotoxicity. To improve these limitations, many approaches have been developed to create gelatin hydrogels using chemically modified gelatin. Khademhosseini and his colleagues developed methacrylated-gelatin (GelMA) that can form hydrogels through photo-polymerizations.[108] Using the bioactive hydrogels, they created various cell-laden matrices for regenerative medicine as well as engineered tissue models.[109-111] Recently, they also developed grapheme oxide (GO)-incorporated GelMA hydrogels to enhance mechanical properties through additional physical interaction between GO and polymer chains.[112] More recently, we also developed a novel gelatin hydrogel composed of gelatin-grafted with ferulic acid (GtnFA) that formed hydrogel matrices with oxygen consuming in the laccase-mediated

chemical crosslinking reaction.[81] In this reaction, lacase catalyzes the crosslinking of ferulic acid (FA) with oxygen consumption, resulting in 3D hydrogel networks through diFA formations. We demonstrated the oxygen-controllable hydrogels provided artificial hypoxic microenvironment to support enhanced vascular differentiation and tube formations of endothelial progenitor cells (EPCs). Using the advanced hydrogel matrices, we are trying to apply the engineered vasculatures to the treatment ischemic tissues and to utilize engineered tumor models to study cancer research.

Hyaluronic acid (HA), an anionic linear glycosaminoglycan consisting of *D*-glucuronic acid and *N*-acetyl-*D*-glucosamine, has been commonly used in clinical applications as soft tissue filler and Anti-adhesion adjuvants as well as various preclinical uses.[113, 114] While HA is very viscous solutions, it also needs chemical crosslinking to create stable HA matrices for *in vitro* and *in vivo* applications. HA hydrogels have been widely utilized as 3D cellular microenvironments to support vascular morphogenesis and cancer cell growth as it has several integrin biding sites (*e.g.*, CD44 and CD168) that play a critical role in regulating growth factor signaling.[115] However, there is no key cell adhesion site in the HA backbone, thus cell adhesion moiety should be incorporated to enhance cell binding affinity into the hydrogel matrices. In addition, HA does not have propetoytic degradable sites (*e.g.*, MMP-sensitive sites) that are pivotal in matrix remodeling within cellular microenvironments. Therefore, we should consider to incorporate both cell adhesion and MMP-sensitive sites when design 3D cellular microenvironments using HA hydrogels. There are a lot of approaches to create the engineered microenvironments using HA hydrogels. Burdick and his colleagues developed physically crosslinked HA hydrogels through host-guest interactions.[116]

They synthesized two kinds of precursor polymers, such as adamantine modified HA (guest macromer, Ad-HA) and β-cyclodextrin modified HA (host macromer, CD-HA). The HA hydrogels are rapidly formed by simple mixing of the solutions, resulting in physically crosslinked HA networks through guest-host bonds. They also developed a photo-curable HA hydrogels consisting of RGD-modified methacrylated HA (MeHA).[117] The functionalized HA hydrogels were formed by photo-polymerization and their mechanical properties and degradation behaviors could be controlled by varying relevant parameters (*e.g.*, crosslinking density, polymer concentrations, degree of substitution of methacrylate, MMP-sensitive sites). Using the multi-tunable HA hydrogel matrices, they investigated the effect of matrix stiffness and degradation on stem cell fate. In addition to stem cell microenvironments, we also utilized the MeHA hydrogels as 3D microenvironments to support vascular differentiation of human pluripotent stem cell (PSCs)-derived early vascular cells (EVCs) to create stable engineered vasculatures.[118] We encapsulated the EVCs within RGD-modified MeHA hydrogels, which can mature in to endothelial cells (ECs) and pericytes to create matured vasculatures within 3D matrices. We also demonstrated that the engineered vasculatures are connected to host vasculatures with blood perfusion.

With advanced in biomaterials engineering, various polymeric hydrogels have been used as 3D matrices for a wide range of medical applications. While these engineered matrices are promising materials, well-defined 3D cellular microenvironments are still required to accurately recapitulate the native cellular environments that present myriad physical, chemical and biological parameters as well as spatiotemporal complexity.

1.3 *Engineering the Tumor Microenvioerment*

The tumor microenvironments shows the complexity, diversity and dynamic nature, which play a critical role in cancer development and progression.[119, 120] Thus, many researches have endeavored to create artificial tumor microenvironment recapitulating the native tumors using various engineered biomaterials.[121] With advances in materials engineering, various polymeric hydrogels have been widely utilized as engineered 3D matrices to recapitulate the pathological tumor extracellular matrices to study basic cancer biology and to screen drug efficacy of anti-cancer agents for new aspects of cancer research.[122, 123] In this section, we discuss the most recent engineered tumor microenvironments for better understanding of cancer biology as well as emerging anticancer therapeutics. In particular, we are focusing on modeling the tumor extracellular matrices to study the tumor angiogenesis, invasion and metastasis occurring in the native tumor microenvironments as well as drug screening of anti-cancer agents.

1.3.1 **Tuning Biomaterials to the Tumor Microenviorment**

In all of the hydrogel platforms there is needed to tune the specific environment to the tumor type of interest or origin for that specific type of cancer. Each tumor model the ECM needs to be tuned for pore size, binding sight availability, stiffness, and degradability. Breast cancer is the most common and deadly tumor in women in the world.[124] Various polymeric hydrogels have been used to study the effect of myriad parameters in the primary tumors on breast cancer progression, including invasion and metastasis as well as tumor-associated angiogenesis.[125] In addition, the engineered platform provide a great chance to evaluate drug efficacy and to screen the newly

developed anti-cancer drugs for better understanding of breast cancer biology and better clinical outcomes in the cancer treatment.

Kristie *et al.* utilized a biomimetic 3D breast cancer models using collagen hydrogels encapsulating multicellular spheroids (MDA-MB-231) to evaluate the anti-cancer therapeutic effect of paclitaxel-loaded polymeric nanoparticles.[126] They fabricated the multicellular spheroids by culturing the cells on the top of aggarose hydrogels that is not available to attach the cells due to its bioinnert properties. The size of tumor spheroids was controlled by varying cell-seeding density, ranging from 100 to 400 um. The cancer spheroids were encapsulated within collagen hydrogels by simple mixing of cell suspension and polymer solutions. Using the tumor models, they investigated the therapeutic efficacy of nanoparticles encapsulating paclitaxel compared to delivering the drug without carriers. Toward this, they loaded the drugs to the pH-sensitive polymeric nanoparticles and treated to the tumor models. Interestingly, they found that the drug-combination with nanoparticles showed higher therapeutic effect compared to naked drug, suggesting that the engineered tumor models have a promising potential as a platform to evaluate drug candidates and delivery systems for a new cancer therapy development.

Shoichet and her colleagues utilized HA hydrogels as a platform for studying breast cancer cell invasion depending on matrix stiffness, MMP-sensitivity, and concentration of cell adhesion sites.[127] They fabricated HA hydrogels that varied crosslinking density (mechanical) and ligand (chemical) densities independently for studying the effects of each parameter on breast cancer invasion. They noticed that soft hydrogels tailored with MMP-sensitive moiety exhibited extensive cancer invasion

compared to stiff matrices without MMP-sensitive sites, demonstrating the importance of matrix stiffness and cell-mediated matrix degradation to breast cancer invasion. Interestingly, they also demonstrated that the cell-adhesive ligand density affected on cancer cell proliferation rather than migration.

Sarcomas are heterogeneous mesenchymal tumors diagnosed annually over 2,000 people in the world. [128] Anseth and her colleagues utilized PEG-based hydrogels for investigating the effect of biochemical and biophysical matrix properties on fibrosarcoma (HT1080) migration.[129] For the study, they prepared peptide functionalized PEG hydrogels through thiol-ene photopolymerization that can be spatially and temporally patterned using standard lithographic method. Using the technique, they fabricated the hydrogel matrices with mechanical gradients (60 Pa to 260 Pa) and examined the effect of matrix adhesion at different moduli on HT1080 migration, demonstrating that the HT1080 motility was determined by a complex trend in which positives and negative matrix effects on tumor cell migration. They noticed that HT1080 on soft matrices showed faster and longer migration distance compared to stiff ones. In addition, they found that the cells tended to migrate from stiff region to soft areas. The results suggest that the engineered tumor models provide innovative tools for investigating several unresolved questions in tumor developments, including the effect of tissue interfaces on tumor motility and invasion.

Glioblastoma multiforme (GBM) is the common and deadly form of brain tumor, which is aggressive and malignancy.[130] Various engineering approaches have been developed to recapitulate and model the GBM tumor microenvironments in vitro for better understanding of molecular and systems biology in GBM.[131] Wang *et al.*

developed bioengineered 3D brain tumor models to investigate the effects of matrix stiffness on GBM cell using PEG-based hydrogels.[132] The hydrogels were prepared through photo-polymerization, incorporating RGD and MMP-sensitive sites to support 3D cell growth and matrix remodeling. In addition, HA was incorporated to mimic the concentration in the brain extracellular matrix. To examine the effect of matric moduli on GBM cell fate in 3D, they encapsulated U87 cells as a model GBM cell line in soft (1 kPa) or stiff (26 kPa) hydrogels, mimicking the matrix stiffness of normal brain or GBM tissues. Interestingly, they noticed that increasing stiffness let to slower cell proliferation, but cells formed denser tumor spheroids as well as upregulation of matrix degradation factors (*e.g.*, HA synthease 1 and MMP-1), demonstrating the stiffness modulate the extracellular matrix decomposition and remodeling that plays a pivotal roles in tumor invasion and metastasis. This bioengineered 3D hydrogel platform may provide an innovative 3D brain tumor model for investigating the mechanisms underlying GBM progression as well as evaluating the efficacy of potential drug candidates for treatment of GBM.

Prostate cancer is one of the most common and diagnosed in men in the worldwide.[133] Many researchers have tried to elucidate molecular biology in the prostate cancer using advanced engineered platform.[134] Fong *et al.* utilized HA hydrogel-based 3D models using patient-derived prostate tumors for drug screening.[135] It is well known that the patient-derived xenograft (PDX) cells show poor cell viability in standard culture condition. To overcome this limitation, they encapsulated the PDX cells within 3D hydrogel matrices and evaluated the cell viability as well as drug efficacy. They observed that most cells were viable within the matrices for day 14. They also

investigated the drug sensitivity of the 3D tumor models with different patient origin to docetaxel. Interestingly, they found that the 3D PDX PCa cells showed a significant higher drug resistance to the drug as compared to the cell lines. This result suggests that the primary culture system have a great potential for directly culturing patient tumor tissues for rapid drug screening, and thus provide an innovative platform for personalized cancer therapeutics.

While prostate cancer is the most commonly diagnosed cancer in men (with 29% of all incident cases), ovarian cancer accounts only for 3% of all incident cancer cases in women per year.[136] It is challenging to model ovarian cancer that have genetically complexity, diverse pathology, and the unique mechanisms of metastasis. Thus, many studies have been reported to recreate the sophisticated ovarian cancer microenvironments for studying growing cancer spheroids and metastasis of ovarian cancer cells.[134, 137] Elke *et al.* developed 3D ovarian cancer models using gelMA hydrogels encapsulating the human epithelial ovarian cancer cell line (OV-MZ-6) derived from a patient.[138] They investigated the effect of matrix stiffness, matrix degradation, and incorporation of ECM components (laminin-411 and HA) on cancer spheroid formation. The matrix stiffness of hydrogels was modulated by varying the polymer concentrations (0.5 kPa-9.0 kPa). The medium stiffness (3.4 kPa) allowed tumor spheroid formation and high proliferation compared to other groups. In addition, they noticed that inhibition of proteolytic degradation of matrices reduced spheroids formation. They also found that incorporating laminin-411 and HA further facilitated spheroid growth within the gelatin-based hydrogels. These results demonstrate that the semi-synthetic gelatin

hydrogels may provide an alternative, bioengineered 3D ovarian cancer culture models *in vitro*.

Thesis Overview

In the field of cancer research there is a key gap in the use of novel biomaterials to control and mimic the tumor microenvironment. Combining improved biomaterials designs, with control over mass transfer in hydrogel system allows us to create novel approaches to study the tumor microenviorment (TME) and test possible new therapeutics. The overall hypothesis of this thesis is that the combinatory effect of oxygen and ECM on sarcoma cell migration leads to an increase in migration due to an increase in crosslinking. This thesis can be divided into three specific aims:

Specific Aim 1: Intratumoral Oxygen Gradients Lead to Sarcoma Cell Migration.

Toward *in vitro* modeling of biological events in sarcoma growth, we utilized 3D hydrogel scaffold that mimic the oxygen gradients commonly seen and study their effect on sarcoma cell migration. The study for this specific aim is presented in Chapter **Error! eference source not found.**.

Specific Aim 2: Collagen Fiber Architecture Regulates Hypoxic Sarcoma Cell Migration

In addition to oxygen gradients there is a growing need to determine the architecture of the tumor microenvironment, with specific focus on collagen fiber features. We examined the effect of collagen fiber density and architecture on sarcoma cell migration in oxygen gradients. The study for this specific aim is presented in Chapter 4.

Specific Aim 3: Quicker stress relaxation increases migration of sarcoma cells in hypoxic gradients

Mechanical properties in the tumor microenvironment have been correlated with tumor progression. We studied the effect of matrix stress relaxation on sarcoma cell migration, by developing a new hydrogel platform to explore stress relaxation in oxygen gradients. The study for this specific aim is presented in Chapter **Error! Reference ource not found.**.

2 *Overview of Experimental Methods*

2.1 *Gelatin-Hypoxic Hydrogels*

2.1.1 **Synthesis of Gelatin-Hypoxic Gels**

Gelatin (Gtn, type A from porcine skin, less than 300 bloom), laccase (lyophilized powder from mushroom, ≥4.0 units/mg), 3−methoxy−4−hydroxycinnamic acid (ferulic acid, FA), *N*−(3−dimethylaminopropyl)−*N′*−ethylcarbodiimide hydrochloride (EDC), *N*−hydroxysuccinimide (NHS), dimethyl sulfoxide (DMSO), and deuterium oxide (D_2O) were supplied from Sigma−Aldrich (Saint Louis, MO) and used as obtained without purification. Dialysis membrane (molecular cutoff = 3500 Da) was purchased from Spectrum Laboratories (Rancho Dominguez, CA) Gelatin−based hypoxia−inducible (Gtn−HI) hydrogels were synthesized by carbodiimide-mediated coupling reaction as we previously reported[139]. Prior to polymer synthesis, we prepared a solvent by mixing DMSO and distilled (DI) water with 1 to 1 volume ratio. We dissolved gelatin (1.0 g) in 50 ml of the solvent at 40 °C. FA (0.78 g, 4.0 mmol) was dissolved in 20 ml of the solvent and activated with EDC (0.92 g, 4.8 mmol, 1.2 eq. of carboxyl unit of FA) and NHS (0.64 g, 5.6 mmol, 1.4 eq. of carboxyl unit of FA) at room temperature for 15 minutes to give amine reactive FA molecules. The activated solution was then applied to the Gtn solution and the conjugative chemical reaction was conducted at 40 °C. After 24 hours, the reacted solution was dialyzed against DI water using a dialysis membrane

(molecular cutoff = 3500 Da) for five days. After dialysis, we obtained GtnFA polymers by freeze−drying and kept the product in a refrigerator (below 4 °C) before use. As previously [139], the chemical structure was confirmed using a ^{1}H NMR spectrometer (Bruker AMX−300 NMR spectrometer, Billerica, MA) and the degree of substitution of FA molecules was measured using an UV/Vis spectrometer (SpectraMax; Molecular Devices, Sunnyvale, CA).

Gelatin−based hypoxia−inducible (Gtn−HI) hydrogels were synthesized by carbodiimide-mediated coupling reaction as we previously reported[139]. Prior to polymer synthesis, we prepared a solvent by mixing DMSO and distilled (DI) water with 1 to 1 volume ratio. We dissolved gelatin (1.0 g) in 50 ml of the solvent at 40 °C. FA (0.78 g, 4.0 mmol) was dissolved in 20 ml of the solvent and activated with EDC (0.92 g, 4.8 mmol, 1.2 eq. of carboxyl unit of FA) and NHS (0.64 g, 5.6 mmol, 1.4 eq. of carboxyl unit of FA) at room temperature for 15 minutes to give amine reactive FA molecules. The activated solution was then applied to the Gtn solution and the conjugative chemical reaction was conducted at 40 °C. After 24 hours, the reacted solution was dialyzed against DI water using a dialysis membrane (molecular cutoff = 3500 Da) for five days. After dialysis, we obtained GtnFA polymers by freeze−drying and kept the product in a refrigerator (below 4 °C) before use. As previously [139], the chemical structure was confirmed using a ^{1}H NMR spectrometer (Bruker AMX−300 NMR spectrometer, Billerica, MA) and the degree of substitution of FA molecules was measured using an UV/Vis spectrometer (SpectraMax; Molecular Devices, Sunnyvale, CA).

2.1.2 **Cancer cell Encapsulation within Geltain-Hypoxic Inducible Hydrogels**

For cancer cell encapsulation, all solutions were prepared using Dulbecco's Phosphate−Buffered Saline (DPBS, Invitrogen) and filtered for sterilization using a syringe filter with a pore size of 0.2 μm. First, we prepared cell pellets of and KIA or KIA-GFP or KIA- HIF−1α - or KIA-Scr (1.0×10^6 cells; derived from a genetic murine model of sarcoma, *LSL-Kras$^{G12D/+}$; Ink4a/Arf$^{fl/fl}$* as established previously [140] in 1.5 ml eppendorf tubes. We then mixed the pellets with 375 μl of polymer stock solution (4% Gtn−FA solution) by gentle pipetting to give homogeneous cell suspensions and added 125 μl of laccase stock solution (100 U/ml). After mixing the enzyme, the solution was incubated at 37 °C for 2 minutes and then transferred to a 96−well plate (BD Bioscience). The cells were cultured within the hydrogel matrices under standard culture conditions (37 °C and 5% CO_2) in high−glucose DMEM with 10% fetal bovine serum (FBS), 1% Penicillin−Streptomycin (PS, Invitrogen) and 1% *L*−glutamine (Invitrogen). The final concentration of cells, polymers, and laccase were $1.0-2.0 \times 10^6$ cells/ml, 3%, and 25 U/ml, respectively. The cancer cell morphology was observed by light microscopy (in phase−contrast mode) and fluorescence microscopy (BX60, Olympus, Tokyo, Japan).

2.2 *Collagen Gels*

2.2.1 **Collagen Gel Formation**

The collagen gel synthesis protocol was adapted from previously established protocols [118, 141, 142]. In order to make 1 mL of 3 mg/mL collagen solution, we first mixed 35.96 µL of M199 10x media (Thermo Fisher Scientific) with 11.51 µL of 1M NaOH. This solution was mixed until it turned dark pink. Next we used acid soluble rat tail collagen I at 9.61 mg/mL (Corning #354249). A total of 312 µL of collagen was

added to the dark pink solution and mixed thoroughly. 640.35 mL of M199 1x media (Thermo Fisher Scientific) was then mixed with the solution to create our final collagen gel solution. The solution was then incubated for 30 minutes on ice to create a low fiber density solution and 2 hours on ice to create a high fiber density solution.

2.2.2 **Cacner Cell Encapsulation in Collagen Gels**

KIA was derived from a genetic murine model of sarcoma, LSL-KrasG12D/+; Ink4a/Arffl/fl as established previously [40], KIA-GFP was expanded under standard culture conditions (37°C and 5% CO_2) in high glucose DMEM with 10% FBS, 1% penicillin/streptomycin (PS; Invitrogen). For cancer cell encapsulation, we first prepared cell pellets of KIA and KIA-GFP cells (7.5 x 10^5 cells) in a 1.5 mL eppendorf tube. We then mixed the pellet with 0.5 mL of collagen solution by gentle pipetting to give a homogenous cell suspension. After mixing, the solution is pipetted into a 96 well plate (BD Bioscience) and incubated for 30 minutes at 37°C. The nonhypoxic gels were created with 50 μL of collagen while the hypoxic gels were made from 100 μL of collagen solution. The cells were then cultured within the hydrogel matrices under standard culture conditions in DMEM (Dow Corning) with 10% heat-inactivated fetal bovine serum (Gibco) and 1% penicillin streptomycin. 200 μL of media was used to culture the hypoxic gels and 100 μL was used to culture the nonhypoxic gels.

2.3 ***Rheology***

To analyze matrix stiffness, we performed rheological analysis of the hydrogels using a rheometric fluid spectrometer (RFS3, TA Instruments, New Castle, DE) as we previously reported[139]. In the rheological experiments, tumor constructs cultured within HI hydrogels were plated in the instrument. We performed dynamic time sweep on

the samples after day 3 in culture. We monitored the elastic modulus (*G'*) and viscous modulus (*G"*) at 1 percent of strain and a frequency of 10 Hz at 37 °C. A solvent trap wetted with deionized water was used to prevent sample evaporation.

Stress relaxation experiments were performed on RSAG2 dynamic mechanical analyzer from TA instruments. The initial elastic moduli and stress relaxation properties of collagen gels were measured from compression tests of the gel disks (6 mm in diameter, 2 mm thick, equilibrated in PBS for 24 h. The gel disks were compressed to 10% strain. Stress relaxation under shear mode was performed on an AR1500 EX rheometer from TA instruments. Collagen gel disks of 6 mm in size were used to perform the stress relaxation tests at 0.5% strain for 5 minutes. As previously performed[71], single element Maxwell model was used to fit the stress relaxation data in order to compare the time decay constants for different conditions Invasive and Non-Invasive Oxygen Measurements

The dissolved oxygen (DO) levels were monitored noninvasively and invasively as previously performed[59]. We used a commercially available sensor patch (PreSens) for the non-invasive measurements and a Needle-Type Housing Fiber-Optic Oxygen Microsensor (PreSens) for invasive measurements. Hydrogel cell constructs were created as stated above, and DO measurements were performed on day 3 of cell culture.

Tumors were generated as previously stated, and DO measurements were performed once tumors were visible. O_2 gradient measurements were performed using the needle sensor and a micromanipulator (PreSens). The tumor diameter was measured using a caliper and the needle was placed at the center of the tumor and moved outward

in 0.5 mm increments, recording a DO reading at each distance, until reaching the edge of the tumor. The volume of the tumor was calculated using the following equation:

$$V = \frac{1}{2} * L * W^2$$

where V is the volume of the tumor, L is the major axis, and W is the minor axis of the tumor [143]. The tumor O_2 measurements were averaged and the standard error mean was calculated for each distance from the center of the tumor.

This same technique was used to evaluate the O_2 gradient in the hydrogel at day 1,3,5 and 7 in the KIA encapsulated samples. It should be noted that *in vitro* invasive measurements might deviate a little from non-invasive measurements as the insertion of the needle can result in uncontrolled O_2 penetration into the hydrogel.

2.4 *Matrix Degradation and Migration Analysis*

To assess effect of O_2 levels on matrix degradation, we incorporated 10 μg/ml of DQ^{TM} gelatin or collagen (Invitrogen) into polymer solutions when preparing cell suspensions, and then mixed with the laccase solution as described above. After day 3, the hydrogels with DQ−gelatin or collagen was observed by the fluorescence microscopy (BX60, Olympus, Tokyo, Japan) and quantified by measuring the fluorescence intensity using a fluorescence spectrophotometer at wavelength of 495 nm excitation and 515 nm emission (Molecular Devices).

For the 3D cancer cell migration assay, we encapsulated KIA-GFP cells and tumor grafts in hydrogel to generate constructs with different O_2 levels as previously [139]. For non-gradient hydrogel controls, constructs were formed and incubated at 1% oxygen for 3 days and then tracked in that chamber at day 3. Cells were tracked at day 3 using live-cell three-dimensional confocal microscopy (LSM 780, Carl Zeiss,

Thornwood, NY, USA) equipped with a cell incubator (5% CO_2 and 37 °C). In order to properly optimize the experiment only cells that started in frame were included, with a shorter timeframe was used for the tumor encapsulated samples. The time-lapse and *z*−stack images (>200 μm thickness) were collected every 30 minutes up to 24 hours at five randomly selected positions. The images were analyzed using Imaris spot analysis (Imaris 8.1, Bitplane, South Windsor, CT, USA) software to track the time−dependent mobility. The 3D migration analysis was performed following the strategy developed by Wirtz and colleagues [144, 145]. A minimum of 100 individual cells at each point were tracked to generate x, y, and z coordinates at each time point. This data was then sorted to only include cells that were present at time zero. From this sorted data the time that the cells were in frame was calculated, and the most common time was used to pick cells for tracking analysis. This was done to maximize the sample size of cells that could be analyzed. Finally, velocity and speed profiles, mean squared displacements, and trajectory plots were calculated using code adapted from Wirtz et al [144, 145] for triplicate tracking trials (n=3) (Matlab, Mathworks Inc.). The statistical analysis was performed using MATLAB (Mathworks Inc.) to calculate the mean, standard deviation and standard error mean. A t-test was performed where appropriate to determine significance (GraphPad Prism 4.02). Graphed data is presented as average ±SD. Significance levels were set at: *P<0.05; ^P<0.01; #P<0.001[144, 145].

2.5 *Molecular Biology*

2.5.1 **Gene Expression**

To assess gene expression, we performed quantitative real time RT−PCR as described previously. Total RNA was extracted from cancer cells encapsulated in

hydrogels using TRIzol (Invitrogen), according to the manufacturer's instructions. In brief, we placed the hydrogel constructs into 500 μl of TRIzol and homogenized using a micro homogenizer. The suspension was centrifuged at 12,000 G for 15 minutes and the supernatant was separated. We then added 100 μl of chloroform to the solution and mixed manually for 20 seconds. The mixture was centrifuged at 12,000 G for 10 minutes and the supernatant was isolated. The solution was mixed with 250 μl isopropyl alcohol and kept at −4 °C for 1 hour. The precipitates were separated by centrifugation at 7,500 G for 5 minutes and then washed using 70% ethyl alcohol (EtOH). Total RNA was quantified using an ultraviolet (UV) spectrometer and validated by lack of DNA contamination. One microgram of RNA was transcribed using reverse transcriptase M−MLV and oligo(dT) primers (both from Promega, Madison, WI), according to the manufacturer's instructions. We used TaqMan Universal PCR MasterMix and Gene Expression Assay (Applied Biosystems, Foster City, CA), according to the manufacturer's instructions for *LOX, MMP2, MMP9, PLOD2, col1A, HPRT1,* and *β−actin*.

2.5.2 **Histology**

For histological analysis, hydrogel constructs or tumors were harvested and fixed using 3.7% paraformaldehyde and then dehydrated in graded EtOH (80−100%). We then embedded the samples in paraffin blocks and serially sectioned them using a microtome (5 μm). The slides were stained with either haematoxylin or eosin (H&E) or underwent immunohistochemistry for HIF−1α as previously described [140]. For quantification of HIF−1α positive cells in tumor sections, cells expressing nuclear HIF−1α were counted manually from 40x images (n=8). The total number of cells in the images were counted and percent positive cells were calculated. The standard deviation and t-test were

performed on the data to determine significance (GraphPad Prism 4.02). Graphed data is presented as average ±SD. Significance levels were set at: P<0.05; **P<0.01; ***P<0.001.

2.5.3 **Immunoflorescence Analysis**

Hydrogels were fixed using 3.7% paraformaldehyde and incubated at room temperature for 1 hour. For staining the cells were permabolized with 0.05% Triton-X for 30 minutes, washed with PBS and incubated with primary antibodies over night. The primary antibody used with collagen 1, HIF–1α (Novous Biologicals, Littleton, CO), YAP (Santa-Cruz), and Vinculin (Sigma-Aldrich) . Certain samples were rinsed with PBS and incubated with Alexa Fluor 546 (1:500; Invitrogen) for 1 hour, followed by incubation with Alexa Fluor 488 Phalloidin (1:40; Invitrogen) for 30 minutes and with 4-6-diamidino-2- phenylindole, DAPI, (1:1000; Roche Diagnostics) for 10 minutes. The labeled cells were examined using fluorescence microscopy (LSM 780, Carl Zeiss, Thornwood, NY, USA). Collagen fluorescence intensity was analyzed using ImageJ (ImageJ, National Institutes of Health, Bethesda, MD).

2.5.4 **Statistical Analysis**

All experiments were performed in triplicate for at least 3 biological replicates. We performed RT-PCR analysis in triplicate with duplicate readings. We performed statistical analysis using GraphPad Prism 4.02 (GraphPad Software Inc., La Jolla, CA). For all analyses other than the live migration (which its statistics is detailed above), the standard deviation and t-test were performed on the data to determine significance (GraphPad Prism 4.02). Graphed data is presented as average ±SD. Significance levels were set at: P<0.05; **P<0.01; ***P<0.001. All graphical data were reported.

3 *Intra-tumoral Oxygen Gradients Lead to Sarcoma Cell Migration*

3.1 *Introduction*

Soft tissue sarcomas are a heterogeneous group of malignant cancers derived from transformed cells of mesenchymal origin [146, 147]. Approximately 13,000 new cases per year are diagnosed in the US alone, with 25–50% of patients developing recurrent and metastatic disease [148-150]. Current clinical data suggest that undifferentiated pleomorphic sarcoma (UPS) is one of the most aggressive sarcoma subtypes, which frequently results in lethal pulmonary metastases that are insensitive to radio/chemotherapy. It has recently become apparent that sarcoma progression and metastasis are regulated by microenvironmental cues such as extracellular matrix (ECM) remodeling, stiffness modulation, cell-to-cell/matrix interactions, signaling factors, and spatial gradients [151-153]. Of all these factors, low intratumoral O_2 (hypoxia) is most dramatically associated with pulmonary metastasis, and poor clinical outcomes [154, 155].

Intratumoral hypoxia occurs when the partial pressure of O_2 falls below 5% and is a commonly observed feature of many sarcomas. Regional hypoxia develops as rapidly growing tumors outstrip their blood supply and as a consequence of aberrant tumor angiogenesis. As a result, O_2 gradients develop throughout the growing tumor. Tumor

hypoxia promotes chemo- and radiation resistance, primarily due to limited perfusion and reduced generation of reactive oxygen species (ROS), respectively[156]. Moreover, the stabilization and activation of Hypoxia Inducible Factor (HIF) transcriptional regulators promotes adaptation to hypoxic stress by modulating tumor cell metabolism, survival, angiogenesis, migration, invasion, and metastasis. Elevated HIF expression has been associated with poor prognosis in many cancers[157] and correlates with reduced survival for sarcoma patients. Recent transcriptome analyses have identified HIFs and HIF target genes as independent prognostic indicators[158] of clinical outcomes. Finally, high levels of intratumoral hypoxia and HIF1-α accumulation are among the most important predictors of metastatic potential in patients with sarcoma[159], although the underlying mechanisms for this correlation remain incompletely characterized. Importantly, while the effect of overall reduced O_2 on sarcoma cell responses has been studied; these cells are actually subjected to O_2 gradients. Currently, the impact of specific oxygen gradients on sarcoma cell migration is unclear.

In previous studies we found that deposition of immature collagen networks facilitated tumor cell metastasis to the lung in a HIF–1α dependent manner [140]. We also demonstrated that the HIF–1α regulated sarcoma metastasis through upregulation of procollagen–lysine, 2–oxoglutarate 5–dioxygenase (PLOD2) and the resulting increase in lysine hydroxylation of collagen molecules [140]. We have shown that PLOD2 expression promotes metastasis in a hypoxia- and □ HIF–1α □dependent manner in a genetic *in vivo* model of UPS [140]. However, we do not yet know how sarcoma cell migration/invasion is altered in the presence of the O_2 gradients that develop in tumors.

Using *in situ* O_2 measurements, we found that hypoxia gradients exist in small primary mouse sarcoma tumors while large primary mouse sarcoma tumors contain severe hypoxic cores (≤0.1% pO_2). To model intratumoral O_2-gradients we used novel O_2-controlling hydrogels that can serve as 3D hypoxic microenvironments [139]. In these hypoxia-inducible (HI) hydrogels, O_2 is consumed while polymerization occurs resulting in spatial O_2 gradients. Thus, with these hydrogels we can mimic physio-pathological O_2 gradients. By encapsulating small tumor grafts in the hydrogels, we found that hypoxic gradients promoted cell invasion with faster speeds and longer distance, compared to nonhypoxic gradients. We next demonstrate that the HI hydrogel culture system replicates HIF−1α-dependent collagen remodeling by sarcoma cells. Using this system, we then show that the hypoxic gradients guide the speed, distance, and direction of sarcoma cell motility compared with nonhypoxic hydrogels. Finally, we show that treatment of the encapsulated sarcoma cells with minoxidil abrogates cell migration and matrix remodeling in the O_2 gradient.

3.2 *Materials and Methods*

3.2.1 **Materials**

Gelatin (Gtn, type A from porcine skin, less than 300 bloom), laccase (lyophilized powder from mushroom, ≥4.0 units/mg), 3−methoxy−4−hydroxycinnamic acid (ferulic acid, FA), *N*−(3−dimethylaminopropyl)−*N′*−ethylcarbodiimide hydrochloride (EDC), *N*−hydroxysuccinimide (NHS), dimethyl sulfoxide (DMSO), and deuterium oxide (D_2O) were supplied from Sigma−Aldrich (Saint Louis, MO) and used as obtained without purification. Dialysis membrane (molecular cutoff = 3500 Da) was purchased from Spectrum Laboratories (Rancho Dominguez, CA).

3.2.2 **Synthesis of Gtn-HI hydrogels**

Gelatin based hypoxia−inducible (Gtn−HI) hydrogels were synthesized by carbodiimide-mediated coupling reaction as we previously reported[139]. Prior to polymer synthesis, we prepared a solvent by mixing DMSO and distilled (DI) water with 1 to 1 volume ratio. We dissolved gelatin (1.0 g) in 50 ml of the solvent at 40 °C. FA (0.78 g, 4.0 mmol) was dissolved in 20 ml of the solvent and activated with EDC (0.92 g, 4.8 mmol, 1.2 eq. of carboxyl unit of FA) and NHS (0.64 g, 5.6 mmol, 1.4 eq. of carboxyl unit of FA) at room temperature for 15 minutes to give amine reactive FA molecules. The activated solution was then applied to the Gtn solution and the conjugative chemical reaction was conducted at 40 °C. After 24 hours, the reacted solution was dialyzed against DI water using a dialysis membrane (molecular cutoff = 3500 Da) for five days. After dialysis, we obtained GtnFA polymers by freeze−drying and kept the product in a refrigerator (below 4 °C) before use. As previously [139], the chemical structure was confirmed using a ^{1}H NMR spectrometer (Bruker AMX−300 NMR spectrometer, Billerica, MA) and the degree of substitution of FA molecules was measured using an UV/Vis spectrometer (SpectraMax; Molecular Devices, Sunnyvale, CA).

3.2.3 **Cancer cell culture within Gtn-HI Hydrogels**

For cancer cell encapsulation, all solutions were prepared using Dulbecco's Phosphate−Buffered Saline (DPBS, Invitrogen) and filtered for sterilization using a syringe filter with a pore size of 0.2 μm. First, we prepared cell pellets of and KIA or KIA-GFP or KIA- HIF−1α - or KIA-Scr (1.0×10^6 cells; derived from a genetic murine model of sarcoma, *LSL-Kras$^{G12D/+}$; Ink4a/Arf$^{fl/fl}$* as established previously [140] in 1.5 ml eppendorf tubes. We then mixed the pellets with 375 μl of polymer stock solution (4%

Gtn−FA solution) by gentle pipetting to give homogeneous cell suspensions and added 125 μl of laccase stock solution (100 U/ml). After mixing the enzyme, the solution was incubated at 37 °C for 2 minutes and then transferred to a 96−well plate (BD Bioscience). The cells were cultured within the hydrogel matrices under standard culture conditions (37 °C and 5% CO_2) in high−glucose DMEM with 10% fetal bovine serum (FBS), 1% Penicillin−Streptomycin (PS, Invitrogen) and 1% *L*−glutamine (Invitrogen). The final concentration of cells, polymers, and laccase were 1.0−2.0 × 10^6 cells/ml, 3%, and 25 U/ml, respectively. The cancer cell morphology was observed by light microscopy (in phase−contrast mode) and fluorescence microscopy (BX60, Olympus, Tokyo, Japan).

3.2.4 **Primary Tumor Formation, DO Measurements and Encapsulation**

For primary tumor encapsulation, we generated mouse sarcomas through subcutaneous injection of 1.0 × 10^6 cells/ml of KIA into nude mice. After day 10 we isolated tumors and prepared tumor discs (diameter, 3.0 mm; thickness, 0.4 mm) by biopsy punching. The tumor specimens were encapsulated within the different thickness hydrogels (hypoxic, 2.5 mm thickness; nonhypoxic, 1.25 mm thickness). For tumor encapsulation, we first prepared 5 μl of the hydrogel pad (3 w/v% Gtn−HI) on a 96 well plate, and then placed the tumor specimens on the pad. The mixture of polymer and laccase solutions was applied to the wells, and entire hydrogel construct was cultured under standard cell culture conditions (37 °C and 5% CO_2) in either regular media (high glucose DMEM with 10% FBS, 1% PS, and 1% *L*−glutamine) for up to two weeks. The O_2 levels during the culture period were monitored using noninvasive O_2 sensors as described above. For quantification of 3D tumor invasion, we took 3−5 images of different regions within the hydrogels using confocal *z*−stack analysis (>200 μm

thickness) and measured the distance from the edge of tumor to the end of the tumor invading the hydrogel matrices using ImageJ software. To monitor real−time tumor invasion and migration, we encapsulated tumors generated from KIA-GFP cells.

3.2.5 **Non-invasive O_2 measurement during cell and tumor graft culture**

The DO levels were monitored non−invasively at the bottom of hydrogels using commercially available sensor patches (Presens, Regensburg, Germany), as previously established [139, 160]. _For DO measurement, the cell suspension (75 μl of polymer and cell suspension) and laccase solution (25 μl of 100 U/ml laccase stock solution) were mixed and incubated for 2 min, and then plated on the O_2 sensor attached to a 96−well plate (BD Bioscience). All measurements were performed under standard cell culture conditions (37 °C and 5% CO_2) in the culture media. To vary O_2 tension, we controlled the thickness of hydrogels in a volume−dependent manner. We generated three kinds of hydrogels with different minimum dissolved O_2 (DO_{min}) levels (defined as hypoxic gels, <1% O_2; hypoxic−nonhypoxic gel, 5−8% O_2; nonhypoxic gel, >8% O_2). For example, to generate hypoxic gels we plated 100 μl (2.5 mm thickness) of a mixture including polymer, cells, and laccase solutions into a well, whereas 50 μl (1.25 mm thickness) of the mixture was plated into the well for preparing nonhypoxic gels.

3.2.6 **Invasive O2 gradient measurements**

The O_2 levels *in vivo* were measured using Needle-Type Housing Fiber-Optic O_2 Microsensor (PreSens, Regensburg, Germany). These needle sensors were mounted on a micromanipulator with 10 μm precision (PreSens). Hydrogel-cell constructs were generated as detailed above. Tumors were generated as previously stated, and DO measurements were performed once tumors were visible. O_2 gradient measurements were

performed using the needle sensor and a micromanipulator (PreSens). The tumor diameter was measured using a caliper and the needle was placed at the center of the tumor and moved outward in 0.5 mm increments, recording a DO reading at each distance, until reaching the edge of the tumor. The volume of the tumor was calculated using the following equation:

$$V = \frac{1}{2} * L * W^2$$

where V is the volume of the tumor, L is the major axis, and W is the minor axis of the tumor [143]. The tumor O_2 measurements were averaged and the standard error mean was calculated for each distance from the center of the tumor.

This same technique was used to evaluate the O_2 gradient in the hydrogel at day 1,3,5 and 7 in the KIA encapsulated samples. It should be noted that *in vitro* invasive measurements might deviate a little from non-invasive measurements as the insertion of the needle can result in uncontrolled O_2 penetration into the hydrogel.

3.2.7 **Matrix degradation, migration assay, and drug treatment**

To assess effect of O_2 levels on matrix degradation, we incorporated 10 μg/ml of DQ™ gelatin (Invitrogen) into polymer solutions when preparing cell suspensions, and then mixed with the laccase solution as described above. After day 3, the hydrogels with DQ−gelatin was observed by the fluorescence microscopy (BX60, Olympus, Tokyo, Japan) and quantified by measuring the fluorescence intensity using a fluorescence spectrophotometer at wavelength of 495 nm excitation and 515 nm emission (Molecular Devices).

For the 3D cancer cell migration assay, we encapsulated KIA-GFP cells and tumor grafts in hydrogel to generate constructs with different O_2 levels as previously [139]. For non-

gradient hydrogel controls, constructs were formed and incubated at 1% oxygen for 3 days and then tracked in that chamber at day 3. Cells were tracked at day 3 using live-cell three-dimensional confocal microscopy (LSM 780, Carl Zeiss, Thornwood, NY, USA) equipped with a cell incubator (5% CO_2 and 37 °C). In order to properly optimize the experiment only cells that started in frame were included, with a shorter timeframe was used for the tumor encapsulated samples. The time-lapse and *z*−stack images (>200 μm thickness) were collected every 30 minutes up to 24 hours at five randomly selected positions. The images were analyzed using Imaris spot analysis (Imaris 8.1, Bitplane, South Windsor, CT, USA) software to track the time−dependent mobility. The 3D migration analysis was performed following the strategy developed by Wirtz and colleagues [144, 145]. A minimum of 100 individual cells at each point were tracked to generate x, y, and z coordinates at each time point. This data was then sorted to only include cells that were present at time zero. From this sorted data the time that the cells were in frame was calculated, and the most common time was used to pick cells for tracking analysis. This was done to maximize the sample size of cells that could be analyzed. Finally, velocity and speed profiles, mean squared displacements, and trajectory plots were calculated using code adapted from Wirtz et al [144, 145] for triplicate tracking trials (n=3) (Matlab, Mathworks Inc.). The statistical analysis was performed using MATLAB (Mathworks Inc.) to calculate the mean, standard deviation and standard error mean. A t-test was performed where appropriate to determine significance (GraphPad Prism 4.02). Graphed data is presented as average ±SD. Significance levels were set at: *P<0.05; ^P<0.01; #P<0.001[144, 145].

For minoxidil treatment, the cells were cultured in hypoxic hydrogels as stated above for three days. On the third day, 0.5 mM minoxidil (dissolved in KIA cell culture media) was added to the wells and the cells were tracked for 24 hours. Untreated cultures served as controls. Cell tracking and data analysis was performed as above.

3.2.8 **PLOD2 Western Blot**

Low-oxygen conditions were maintained in a Ruskinn in vivo$_2$ 400 hypoxia work station. Simultaneously, KIA Cells were treated with vehicle or 0.5 mM Minoxidil diluted in DMEM culture media (Sigma Aldrich) for 16 hours. Whole cell lysates were prepared in SDS/Tris pH 7.6 lysis buffer. Proteins were electrophoresed and separated by SDS-PAGE and transferred to nitrocellulose membranes and probed with the following antibodies: rabbit anti-GAPDH (Cell Signaling Inc.), and rabbit anti-PLOD2 (Proteintech).

3.2.9 **Rheological analysis**

To analyze matrix stiffness, we performed rheological analysis of the HI hydrogels using a rheometric fluid spectrometer (RFS3, TA Instruments, New Castle, DE) as we previously reported[139]. In the rheological experiments, tumor constructs cultured within HI hydrogels were plated in the instrument. We performed dynamic time sweep on the samples after day 3 in culture. We monitored the elastic modulus (*G'*) and viscous modulus (*G"*) at 10 percent of strain and a frequency of 0.1 Hz at 37 °C. A solvent trap wetted with deionized water was used to prevent sample evaporation.

3.2.10 **Gene Expression**

To assess gene expression, we performed quantitative real time RT−PCR as described previously. Total RNA was extracted from cancer cells encapsulated in hydrogels using TRIzol (Invitrogen), according to the manufacturer's instructions. In brief, we placed the hydrogel constructs into 500 μl of TRIzol and homogenized using a micro homogenizer. The suspension was centrifuged at 12,000 G for 15 minutes and the supernatant was separated. We then added 100 μl of chloroform to the solution and mixed manually for 20 seconds. The mixture was centrifuged at 12,000 G for 10 minutes and the supernatant was isolated. The solution was mixed with 250 μl isopropyl alcohol and kept at −4 °C for 1 hour. The precipitates were separated by centrifugation at 7,500 G for 5 minutes and then washed using 70% ethyl alcohol (EtOH). Total RNA was quantified using an ultraviolet (UV) spectrometer and validated by lack of DNA contamination. One microgram of RNA was transcribed using reverse transcriptase M−MLV and oligo(dT) primers (both from Promega, Madison, WI), according to the manufacturer's instructions. We used TaqMan Universal PCR MasterMix and Gene Expression Assay (Applied Biosystems, Foster City, CA), according to the manufacturer's instructions for *LOX, PLOD2, col1A1,* and *β−actin*.

3.2.11 **Histological Analysis**

For histological analysis, hydrogel constructs or tumors were harvested and fixed using 3.7% paraformaldehyde and then dehydrated in graded EtOH (80−100%). We then embedded the samples in paraffin blocks and serially sectioned them using a microtome (5 μm). The slides were stained with either haematoxylin or eosin (H&E) or underwent

immunohistochemistry for HIF−1α as previously described [140]. For quantification of HIF−1α positive cells in tumor sections, cells expressing nuclear HIF−1α were counted manually from 40x images (n=8). The total number of cells in the images were counted and percent positive cells were calculated. The standard deviation and t-test were performed on the data to determine significance (GraphPad Prism 4.02). Graphed data is presented as average ±SD. Significance levels were set at: $P<0.05$; $^{**}P<0.01$; $^{***}P<0.001$.

3.2.12 **Immunoflorescence analysis**

Hydrogels were fixed using 3.7% paraformaldehyde and incubated at room temperature for 1 hour. For staining the cells were permabolized with 0.05% Triton-X for 30 minutes, washed with PBS and incubated with primary antibodies over night. The primary antibody used with collagen 1 or HIF−1α (Novous Biologicals, Littleton, CO). Certain samples were rinsed with PBS and incubated with Alexa Fluor 546 (1:500; Invitrogen) for 1 hour, followed by incubation with Alexa Fluor 488 Phalloidin (1:40; Invitrogen) for 30 minutes and with 4-6-diamidino-2- phenylindole, DAPI, (1:1000; Roche Diagnostics) for 10 minutes. The labeled cells were examined using fluorescence microscopy (LSM 780, Carl Zeiss, Thornwood, NY, USA). Collagen fluorescence intensity was analyzed using ImageJ (ImageJ, National Institutes of Health, Bethesda, MD).

3.2.13 **Statistical analysis**

All experiments were performed in triplicate for at least 3 biological replicates. We performed RT-PCR analysis in triplicate with duplicate readings. We performed

statistical analysis using GraphPad Prism 4.02 (GraphPad Software Inc., La Jolla, CA). For all analyses other than the live migration (which its statistics is detailed above), the standard deviation and t-test were performed on the data to determine significance (GraphPad Prism 4.02). Graphed data is presented as average ±SD. Significance levels were set at: $P<0.05$; $^{**}P<0.01$; $^{***}P<0.001$. All graphical data were reported.

3.3 *Results and Discussion*

3.3.1 **Primary sarcoma grafts invade hypoxic hydrogels**

To ascertain the physiological range of O_2 gradients in the developing sarcoma tumor, we began by measuring dissolved O_2 (DO) levels during the growth of primary mouse sarcoma tumors. The primary sarcoma tumors were generated in nude mice using murine sarcoma cells derived from *Kras*$^{G12D/+}$; *Ink4a/Arf*$^{fl/fl}$ tumors (KIA[161]) as described in previous studies [140]. O_2 gradient measurements during growth of subcutaneous primary sarcomas showed that in large tumors (>300mm^3) about 50% of the tumor mass is hypoxic (≤0.1% pO_2). Smaller tumors exhibit hypoxic gradients throughout the tumor mass ranging from 0.1% pO_2 at the center, to >6% pO_2 in the outer layer bordering the edge of the tumor (**Figure 3-1A**). Histological analysis further revealed the severe hypoxic tumor core with cells expressing HIF–1α localized to the nuclei in the larger tumor, while weaker and more diffused HIF–1α signal was observed throughout the entire smaller tumors (**Figure 3-1B-C; Supplementary Figure 3-1**). Previously, we have established O_2-controlling hydrogels and found that after hydrogel formation, the DO levels at the bottom of hydrogels decreased as gel thickness increased due to oxygen diffusion limitation, resulting in a broad range of O_2 tensions within the gel matrices [139]. Based on the oxygen gradient found in the xenograft tumors we

sought to use the O_2-controllable hydrogel system to provide a more physiologically relevant 3D microenvironment to study cell migration. Using the hypoxic hydrogel system we recreated the hypoxic DO conditions found in the subcutaneous *in vivo* tumors and evaluated the role of O_2 in 3D tumor cell migration assay. Tumor biopsy punches from smaller tumors were cut into 8mm sections and grafted into the hypoxic and nonhypoxic hydrogels (**Figure 3-1D**). Using noninvasive DO measurements at the bottom of the hydrogels, we found that DO levels in the hypoxic hydrogels reached <5% pO_2 within initial 30 min and remained there during the entire week of measurements. Nonhypoxic hydrogels exhibited a higher level of O_2 (>5% partial pressure of O_2) during this culture period (**Figure 3-1E**). The tumor engrafted within hypoxic matrix demonstrated increased invasion compared with tumors engrafted within nonhypoxic matrix. Specifically, tumors in hypoxic matrix invaded further into the hydrogel and away from the primary graft (after 1 week, 610 ± 210 μm) compared to those encapsulated in nonhypoxic gels (after 1 week, 410 ± 130 μm) (**Figure 3-1F**). Moreover, migrating cells exiting tumor grafts in the hypoxic hydrogel deposited new collagen compared to nonhypoxic hydrogels (**Figure 3-1G**), consistent with our previous findings [140]

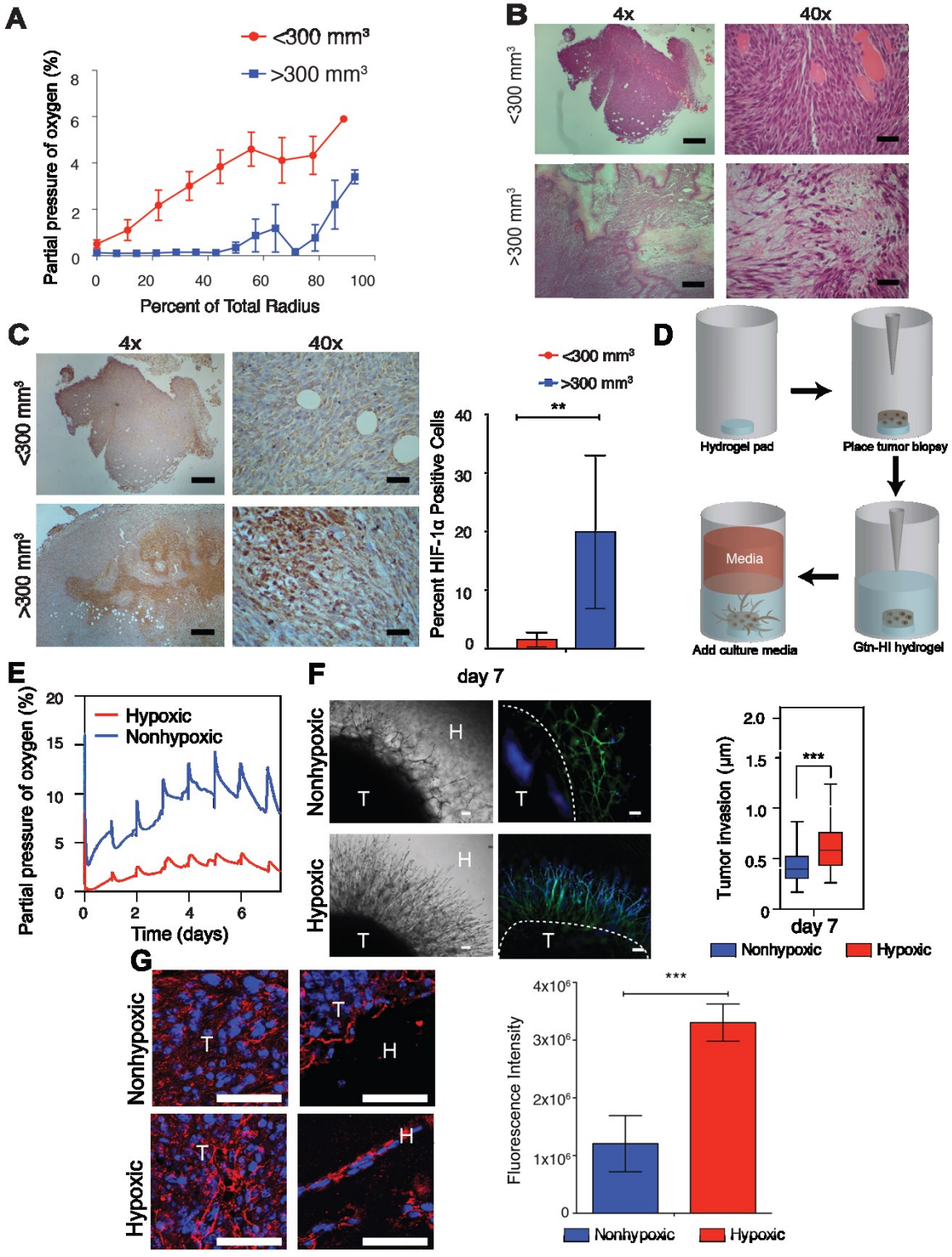

Figure 3-1: Enhanced invasion of sarcoma tumor grafts in hypoxic hydrogels. (A) *In situ* DO measurements in KIA tumors. (B) H&E stains and (C) HIF1–α stains (left) and quantification (right) of small and large tumors. Scale bars, 200 μm for the 4x images and 20 μm for the 40x images. (D) Schematic illustration of tumor

encapsulation within HI hydrogel matrix. (E) DO levels of HI hydrogels encapsulated with tumor biopsy in hypoxic and nonhypoxic matrixes up to day 7 in culture (F) Left: Light microscope (*left*) and fluorescence microscope (*right*) images of sarcoma tumors encapsulated within nonhypoxic and hypoxic matrices (phalloidin in green; nuclei in blue). H, hydrogels; T, tumors. Scale bars, 100 μm. Right: Quantitative analysis of the sarcoma tumor invasion into hydrogel matrix, (G) Immunofluorescence staining and quantification of collagen deposition by tumor grafts cultured for 7 days (collagen in red; nuclei in blue). Scale bars, 25 μm. Significance levels were set at $^{*}P<0.05$, $^{**}P<0.01$ and $^{***}P<0.001$.

3.3.2 Cell migration from sarcoma grafts is regulated by O_2 gradients

To further investigate the effect of O_2 gradients on sarcoma tumor migration, we performed real-time confocal analysis. Tumors generated from green fluorescent protein (GFP) positive KIA cells were engrafted in hypoxic and nonhypoxic hydrogels and imaged on day 3 when we first detected cell invasion into the hydrogel (**Figure 3-2A**). We then analyzed cell migration on day 3, when we could first detect cell invasion from the tumor to the hydrogel. We observed dynamic cell movement in the hypoxic constructs compared to the nonhypoxic constructs with more cells migrating out of the grafts under hypoxic conditions (**Figure 3-2B and Supplementary Figure 3-2**). Cell velocity analysis did not indicate specific directionality of migration with most cells moving in the x and y planes, suggesting a random migration path independent of O_2 tension (**Supplementary Figure 3-3**). However, we found a higher migration speed in hypoxic grafts compared to nonhypoxic grafts (**Figure 3-2C**). Examining mean square displacement (MSD) in the three planes, we found that cells migrating in the hypoxic gradients move to larger distances compared to the nonhypoxic gradients with significantly longer distance in the z-direction **(Figure 3-2D**) suggesting that while cells typically migrated in the x and y directions, those that migrated in the z-direction

exhibited higher persistence. Overall, these data show that hypoxic gradient promotes tumor cell migration.

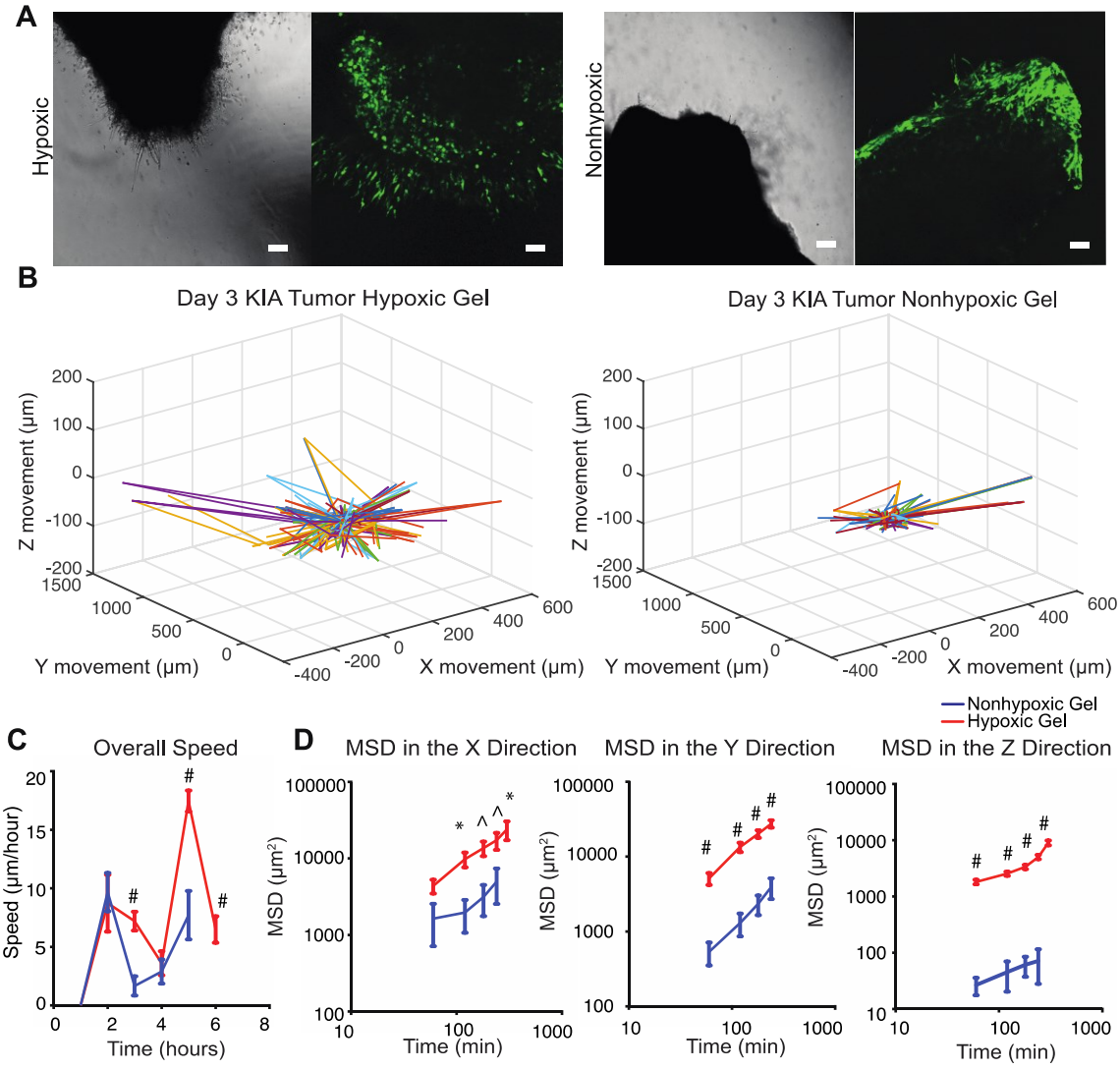

Figure 3-2: Hypoxia promote primary sarcoma migration
(A) Light microscope (*left*) and fluorescence microscope (*right*) images of day 3 images of KIA-GFP sarcoma tumors encapsulated within nonhypoxic and hypoxic matrices. Migrating GFP cells were tracked to determine (B) Three-dimensional trajectories of tracked cells (representative trajectories) (C) Overall speed, and (D) Mean square displacement (MSD) in the x, y, and z directions. Plots were created using position of KIA-GFP cells in the hydrogels. Significance levels were set at $^{*}P<0.05$, $^{\wedge}P<0.01$ and $^{\#}P<0.001$.

3.3.3 **Sarcoma cells remodel collagen in hypoxic hydrogels**

While the tumor graft model provides vital information, the inherited heterogeneity of the system limited the mechanistic insights that such system can provide. To more accurately model the effect of DO gradients on sarcoma cell invasion/ migration within a complex tumor microenvironment, we next examined individual sarcoma cells embedded in the HI hydrogel [139]. Non-invasive measurements of DO at the bottom of the hydrogel confirmed that the hypoxic matrix maintains low O_2 levels during the 7 days of culture compared to nonhypoxic matrix (**Figure 3-3A**). Notable, by day 7 in culture oxygen levels have decreased to ~0.5%, likely to due to expansion of the cell number over the longer culture period and the associated cellular oxygen consumption [162]. An important feature of this culture system is the ability to maintain the hypoxic gradient environment without exposure to high oxygen levels thus minimizing the introduction of reactive oxygen species (ROS). This, alongside with the ability to perform live-imaging of the cells while monitoring DO levels present a unique opportunity to link cellular responses to DO gradients. Growing evidence suggests that ECM remodeling is critical in sarcoma migration and metastasis. In particular, proteolytic degradation as well as abnormal collagen deposition and modification within hypoxic tumor microenvironments have been implicated as important parameters that enhance tumor invasion and metastasis [163-165]. The gelatin-based HI hydrogels provide matrix adhesion and degradation sites similar to those in the tumor microenvironment, yet are collagen-free to prevent confounding results. We first tested whether sarcoma cells embedded in hypoxic hydrogel remodel the matrix material. We examined the proteolytic degradation of the HI gelatin matrices using DQ^{TM} gelatin that emits green fluorescence

when degraded by a protease secreted by the cells.[166, 167] Interestingly, we observed higher fluorescence intensity in the cells cultured within the hypoxic microenvironments (480 RFU) compared to nonhypoxic matrix (50 RFU) (**Figure 3-3B**). Rheological analysis further confirmed the softening of the hypoxic matrix (young's modulus of 20 Pa) compared to nonhypoxic matrix (young's modulus of 45 Pa) within 3 days of culture (**Figure 3-3C**). The gelatin-based HI hydrogels further enabled us to examine whether sarcoma cells modify collagen in the hypoxic matrix. We next examined the upstream effect of HIF−1α activation on relevant genes on days 3 and 7. While no change in gene expression was detected on day 3 of culture, we observed an upregulation of Col1A1, LOX, and PLOD2 expression after 7 days of culture in the hypoxic hydrogel compared to the nonhypoxic hydrogel (**Figure 3-3D**). Moreover, at this time point, we detected collagen expression and deposition (**Figure 3-3E**) as well as HIF−1α expression (**Supplementary Figure 3-4)** by the sarcoma cells in the hypoxic hydrogel. To determine whether ECM remodeling is regulated by the HIF−1α in the hypoxic matrix, we used short hairpin RNA (shRNA). We detected significant down regulation of collagen modifying genes, Col1A1, LOX, and PLOD2 when HIF−1α expression was inhibited (**Figure 3-3F**), resulting in less collagen deposition in hypoxic hydrogel encapsulated cells compared to controls (**Figure 3-3G**). Overall, these results demonstrate that the 3D hypoxic hydrogel, regulates sarcoma matrix remodeling through hypoxic induction of HIF−1α expression. These results are consistent with various sarcoma studies *in viv*o [140, 168, 169], suggesting that the HI hydrogels are an appropriate 3D model with the necessary biological attributes to study sarcoma cell invasion and migration.

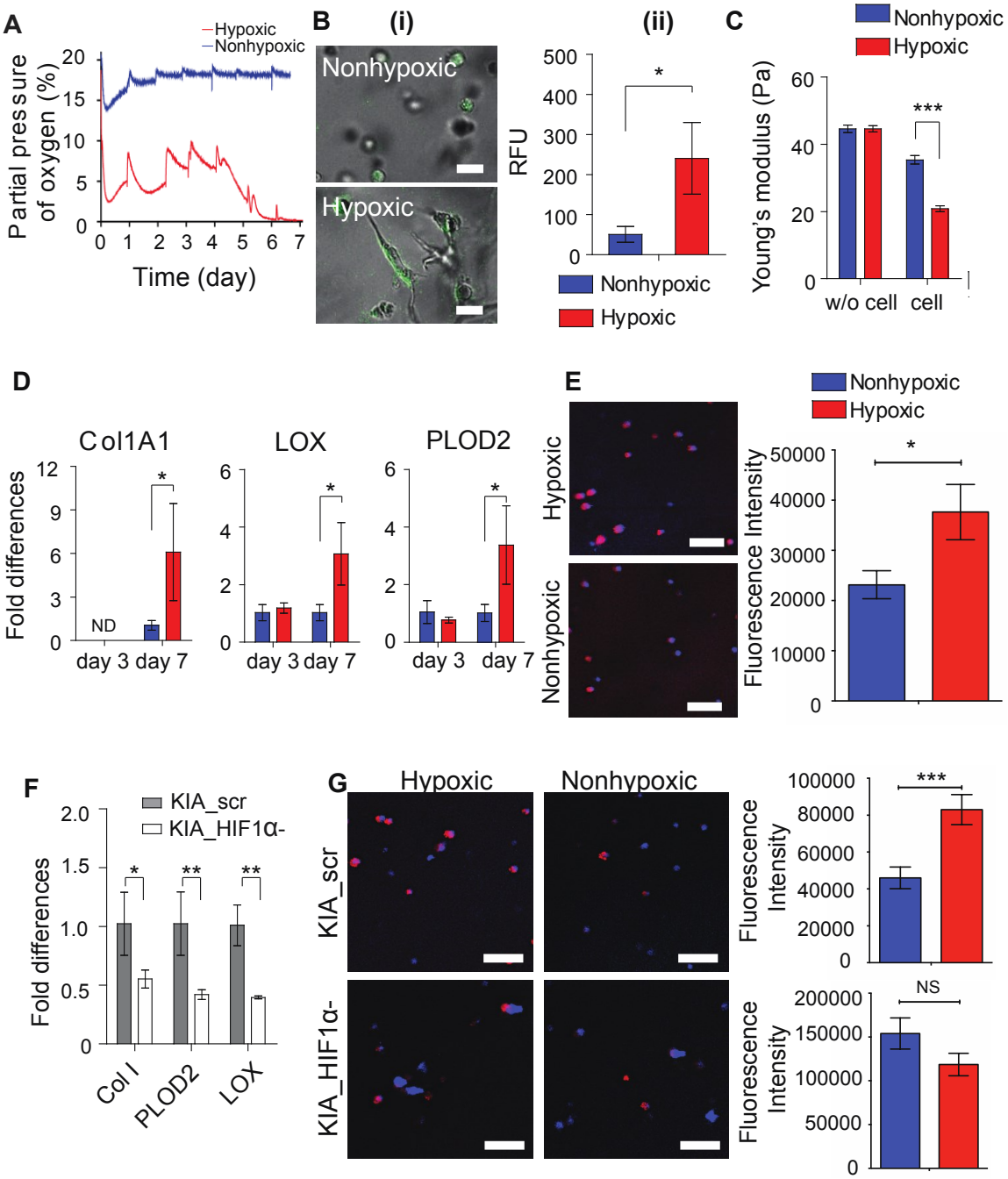

Figure 3-3 Sarcoma cells remodel the hypoxic hydrogel.
(A) Non-invasive DO readings at the bottom of the hypoxic and nonhypoxic hydrogel-sarcoma cell constructs. (B) Sarcoma cells encapsulated within HI hydrogels incorporating DQ™ gelatin for 3 days: (i) Representative fluorescence microscopy images. Scale bars, 25 μm and (i) Quantitative analysis of relative fluorescence intensity (RFU). (C) Young's modulus (Pa) of the hypoxic and nonhypoxic hydrogels on day 0 and after 3 days of culture. (D) Real–time RT–PCR analysis of collagen modification genes. (E) Immunofluorescence staining and analysis of collagen deposition by the encapsulated cells (collagen in red; nuclei in

blue). Scale bars, 50 µm. The effect of HIF1–α suppression in encapsulated sarcoma cells (KIA_scr, a control; KIA_HIF–1α(–), HIF knock down) after 7 days in culture was analyzed including: (F) collagen modification gene expression and (G) collagen deposition and quantification (collagen in red; nuclei in blue). Scale bars, 50 µm. Graphical results shown as the average value ± s.d. Significance levels were set at $^{*}P<0.05$, $^{**}P<0.01$ and $^{***}P<0.001$.

3.3.4 O_2 gradients modulate the speed, distance, and directional bias of sarcoma cell motility

As we previously shown, the HI-hydrogel system is designed to create an O_2 upward gradient, wherein DO levels increase toward the interface between the construct and O_2 saturated culture media [139]. Encapsulation of individual cell suspension would provide us the opportunity to document single-cell movement in relation to the O_2 gradient (**Figure 3-4Ai**). As these constructs are cultured in air-oxygenated media, hypoxic and nonhypoxic upward gradients are maintained in each of the gel type [139]. Invasive DO measurements validated hypoxic and non-hypoxic gradients in the hydrogel-cell constructs (**Figure 3-4Aii and Supplementary Figure 3-5**). These results confirm that we are able to successfully mimic the gradients seen in the primary tumor *in vivo*. Thus, we next examined how sarcoma cell motility is regulated by the O_2 gradients in the 3D hypoxic and nonhypoxic gradients. We encapsulated KIA-GFP in the HI hydrogels and analyzed movement on day 3 using real-time 3D cell tracking. Upon examining the 3D trajectory profiles of the KIA-GFP encapsulated cells, we observed greater overall cell movement in the hypoxic gradients compared to the nonhypoxic gels **(Figure 3-4B and Supplementary Figure 3-6)**. We also found that cells in the hypoxic gradient gels are moving faster than those in the nonhypoxic gels. This holds true for the velocity profiles in the x, y, and z directions as well as the overall speed of the cells moving through the gel **(Figure 3-4C-D)**. Interestingly, we found that cells also moved in the z-

direction, which has not been reported before. Importantly, cell velocity in the z-direction was primarily upwards, in the direction of increased O_2 tension **(Figure 3-4D)**. We further computed and analyzed the MSD in the three planes. **(Figure 3-4E)**. Here too, O_2 gradient seem to affect cell motility as indicated by the MSD in the z-direction. Cells exposed to the hypoxic gradients cells are traveling over larger distances compared to those in the nonhypoxic gradients **(Figure 3-4E).** Interestingly, non-gradient hypoxic constructs (ie- hydrogel constructs cultured in hypoxic conditions) showed slower cell movement and a lower mean squared displacement compared with hypoxic gradient constructs (**Supplementary Figure 3-7).** Overall, this data shows that increased DO levels enhance the speed, distance and direction of sarcoma cell movement.

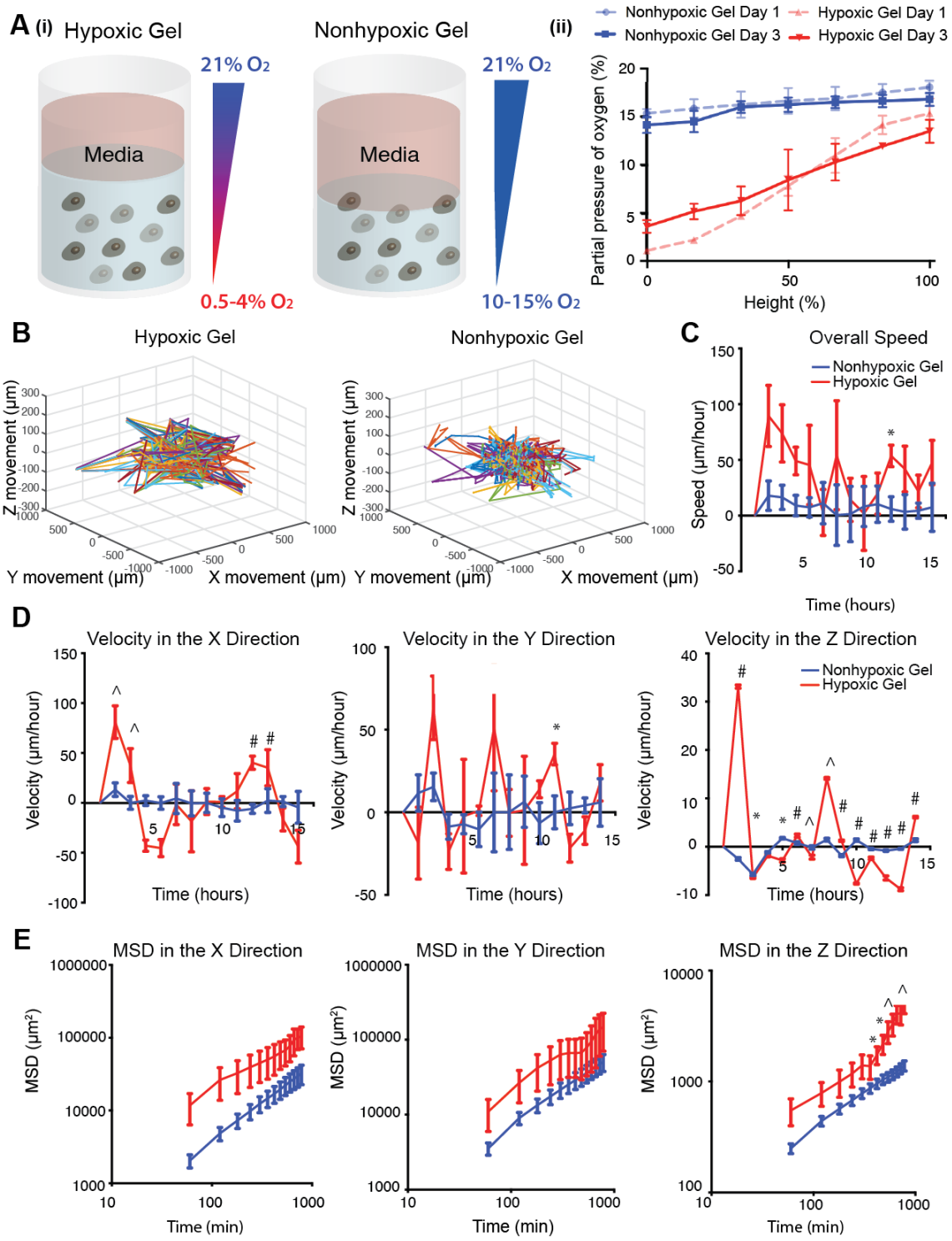

Figure 3-4: Efficient sarcoma cell migration in hypoxic gradients
(A) *(i)*- Illustration of hypoxic and nonhypoxic O_2 gradient in HI hydrogels. *(ii)*- Invasive DO readings showing gradients in the HI hydrogels on Day 1 and 3. KIA-GFP cells were tracked on day 3 in hypoxic and nonhypoxic hydrogel to determine (B) Three-dimensional trajectories of tracked cells (representative trajectories), (C) Overall speed (D) Velocity in the x, y, and z directions; and (E) Mean square

displacement (MSD) in the x, y, and z directions. Plots were created using position of KIA-GFP cells in the hydrogels. Significance levels were set at $^{*}P<0.05$, $^{\wedge}P<0.01$ and $^{\#}P<0.001$.

3.3.5 Inhibiting 3D hypoxic gradient migration

We previously demonstrated that PLOD2 promotes metastasis in a hypoxia and HIF–1α dependent manner in an *in vivo* model of UPS [140]. To examine whether the oxygen-controllable hydrogel faithfully represents the intratumoral hypoxic environment, we examined the effect of minoxidil, a pharmacologic inhibitor of PLOD2 expression [170], on sarcoma cell migration. Minoxidil treatment (0.5 mmol/L) for 12 hours of sarcoma cells encapsulated in the hypoxic hydrogels, significantly reduced KIA cell movement (**Figure 3-5A and Supplementary Figure 3-8**) concomitant with reduced overall cell speed as well as velocity and MSD in the x.y.and z directions (**Figure 3-5B-D**). Minoxidil treatment of sarcoma cells encapsulated in the nonhypoxic hydrogels did not significantly affect cell migration in the X and Y directions, with slight inhibition of migration in the z-direction (**Supplementary Figure 3-9**). Examining matrix remodeling, we found that minoxidil treatment reduced collagen deposition (**Figure 3-5E**) and inhibited the proteolytic degradation of the hypoxic matrices (**Figure 3-5F**). As expected, we found that hypoxia-induced PLOD2 expression is inhibited with Minoxidil treatment (**Figure 3-5G**). Together, this data shows that hypoxia gradients determine the direction and speed of sarcoma cell migration in a HIF1/PLOD2 dependent manner. Importantly, these findings also highlight the utility of hydrogel encapsulation assays for the identification of novel therapeutic targets and inhibitors for the treatment of metastatic sarcoma and potentially other cancers as well.

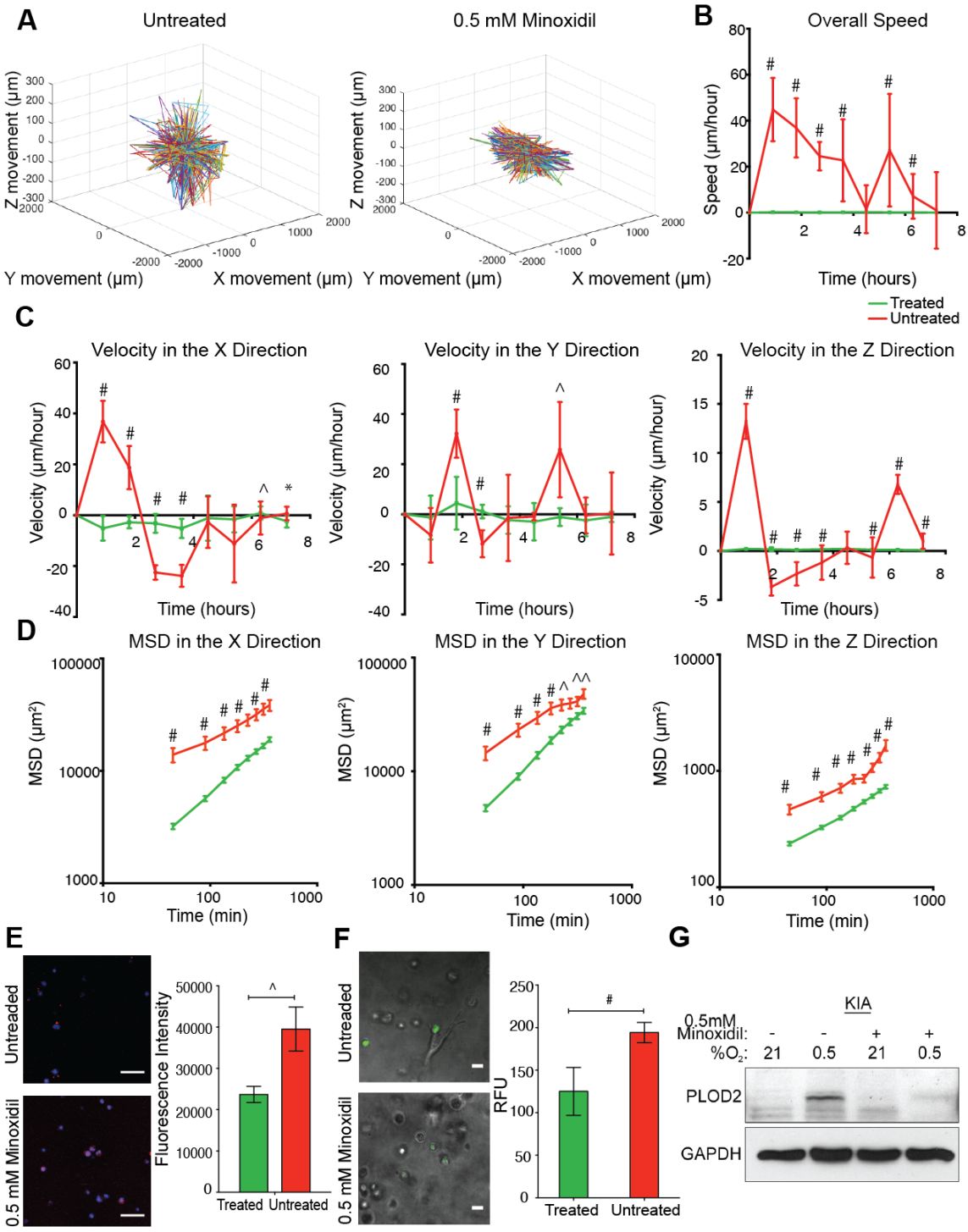

Figure 3-5: Minoxidil inhibit sarcoma cell migration and matrix remodeling in hypoxic hydrogel.
KIA-GFP cells were tracked on day 3 in hypoxic treated and untreated hydrogel to determine (A) Three-dimensional trajectories of tracked cells (representative trajectories), (B) Overall speed (C) Velocity in the x, y, and z directions; and (D) Mean square displacement (MSD) in the x, y, and z directions. Plots were created

using position of KIA-GFP cells in the hydrogels. (E) Collagen deposition and quantification (collagen in red; nuclei in blue). Scale bars, 50 µm. (F) Proteolytic degradation of HI hydrogels incorporating DQ™ gelatin for 3 days: (i) Representative fluorescence microscopy images. Scale bars, 20 µm and (ii) Quantitative analysis of relative fluorescence intensity (RFU).(G) Western blot analyses for PLOD2 in KIA cells cultured in hypoxic conditions with and without minoxidil treatment. Significance levels were set at $^{*}P<0.05$, $^{\wedge}P<0.01$ and $^{\#}P<0.001$.

3.4 Conclusions

Leveraging our novel O_2 controlling hydrogel, we generated a 3D *in vitro* model that enables us to analyze cancer cell responses to O_2 gradients and the effect of small molecule inhibitors. Using this approach, the current study presents a new concept in which O_2 acts as a 3D physico-tactic agent during early stages of sarcoma tumor invasion. We found that an O_2 gradient is present in early stages of sarcoma development and that during this stage, cells respond to the hypoxic gradient by aggressively invading the matrix, followed by fast and long-distance migration. Moreover, we demonstrated that in hypoxic gradients individual sarcoma cells not only migrate faster and over a longer distance while remodeling the matrix, they also migrate in the direction of increased O_2 tension. Finally, we showed that treatment with minoxidil inhibits the migration and matrix remodeling in the hypoxic gradient. These findings are important for the understanding of the metastatic process and establishing the 3D *in vitro* model as a platform for testing therapeutic targets and interventions for the treatment of cancer.

3.5 Supplementary Materials

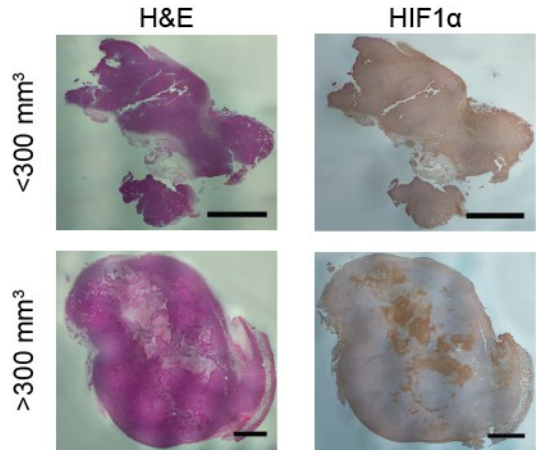

Supplementary Figure 3-1: Primary mouse sarcoma tumors.
Whole tumor showed using tiled micrographs of H&E stains and (left) HIF1α stains (right) of small and large tumors. Scale bars, 1 mm

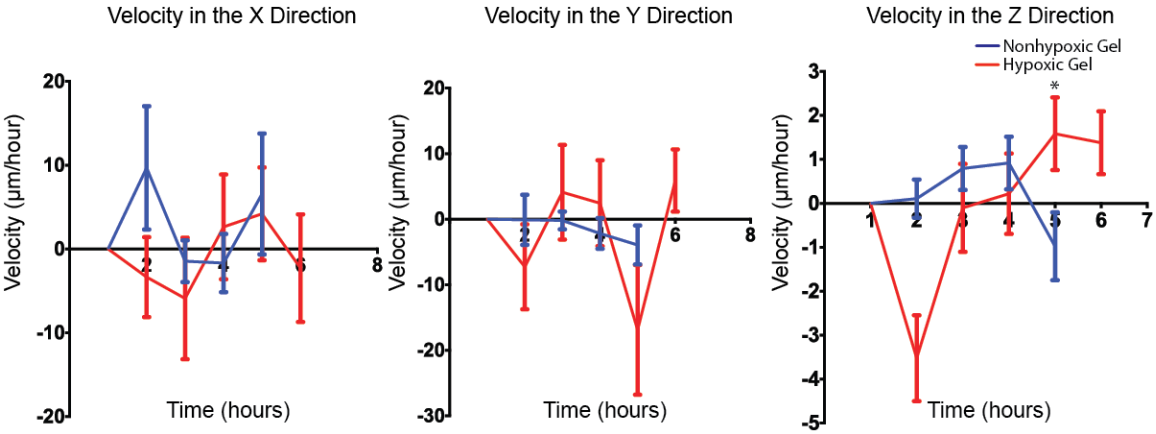

Supplementary Figure 3-2: Primary sarcoma tumor migration velocity.
KIA-GFP sarcoma tumors were encapsulated within nonhypoxic and hypoxic matrices. Day 3 migrating GFP cells were tracked to determine velocity in the x,y, and z directions.

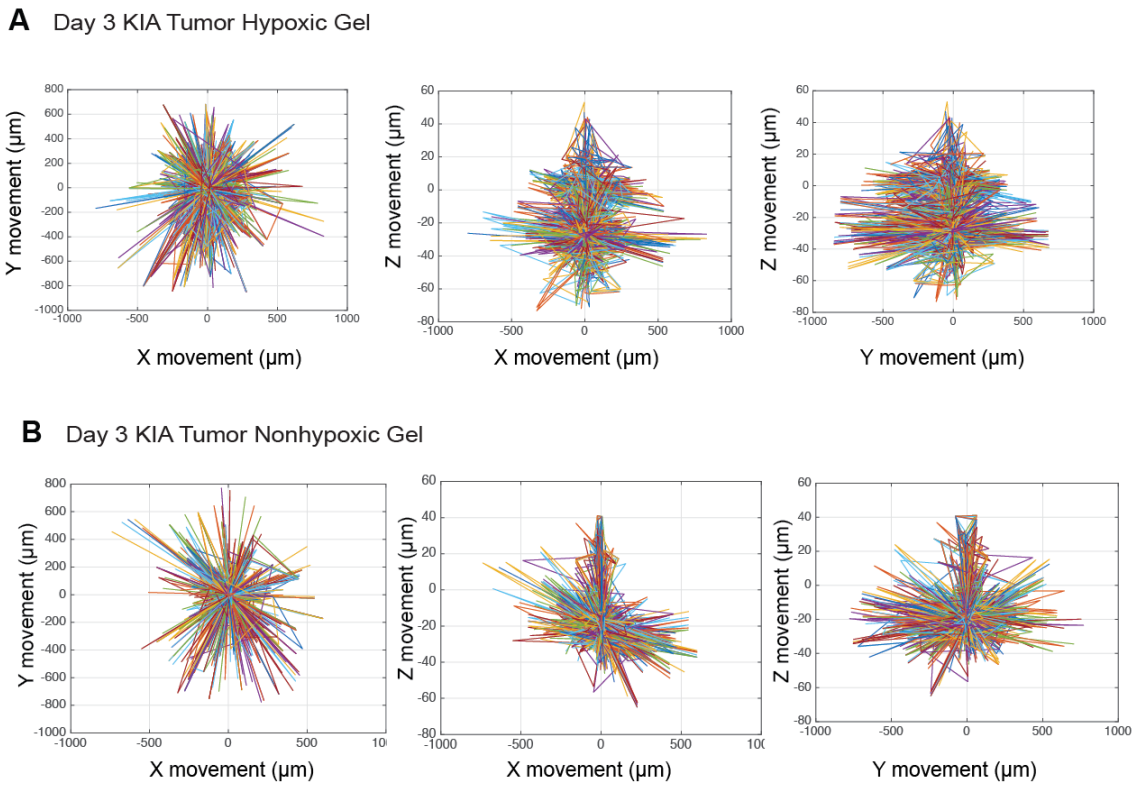

Supplementary Figure 3-3: Primary sarcoma migration trajectories.
2D Trajectories of tracked cells in (A) hypoxic and (B) non-hypoxic hydrogels.

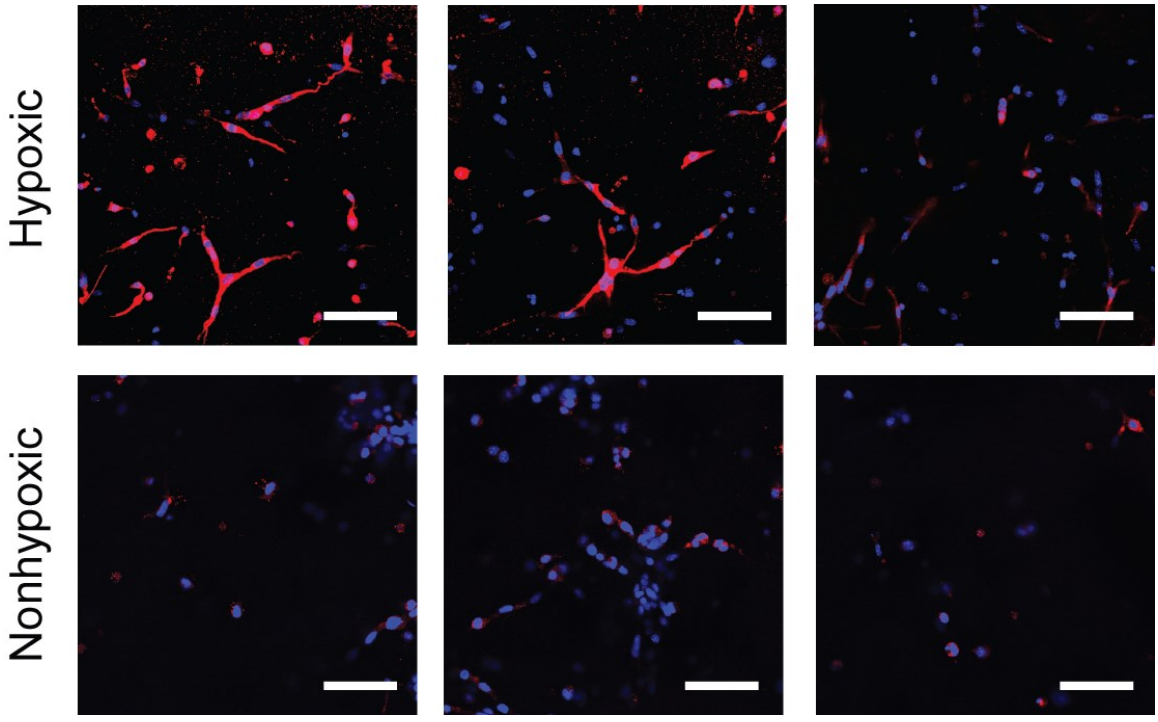

Supplementary Figure 3-4: HIF1α expression.

Representative immunofluorescence staining of HIF1α expression by the encapsulated cells (HIF1α in red; nuclei in blue). Note the abundant nuclear staining and cytoplasmic staining as it relates to rapid protein turnover in the hypoxic hydrogels. Scale bars, 25 µm.

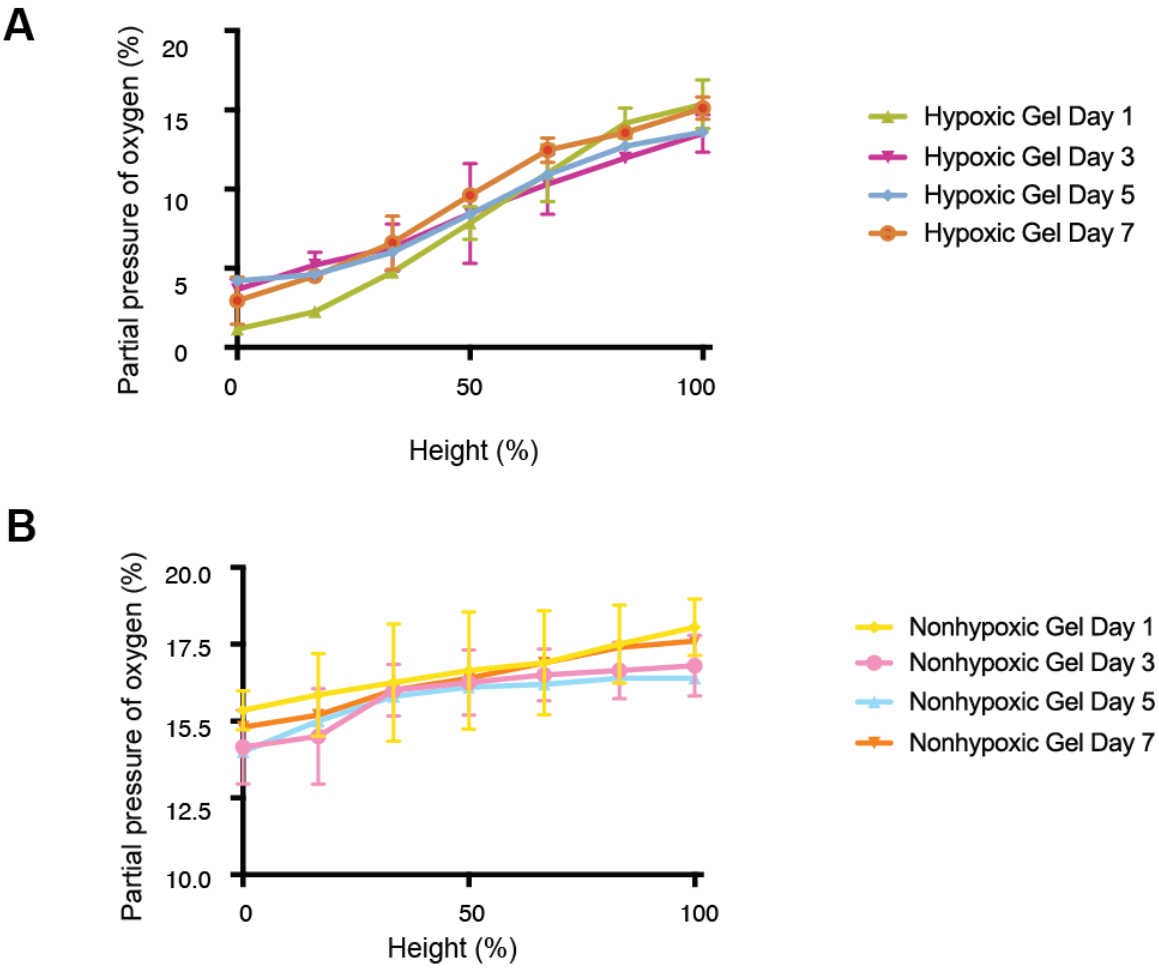

Supplementary Figure 3-5: DO gradient measurements.
Invasive DO readings in the HI hydrogels on Day 1,3,5 and 7.

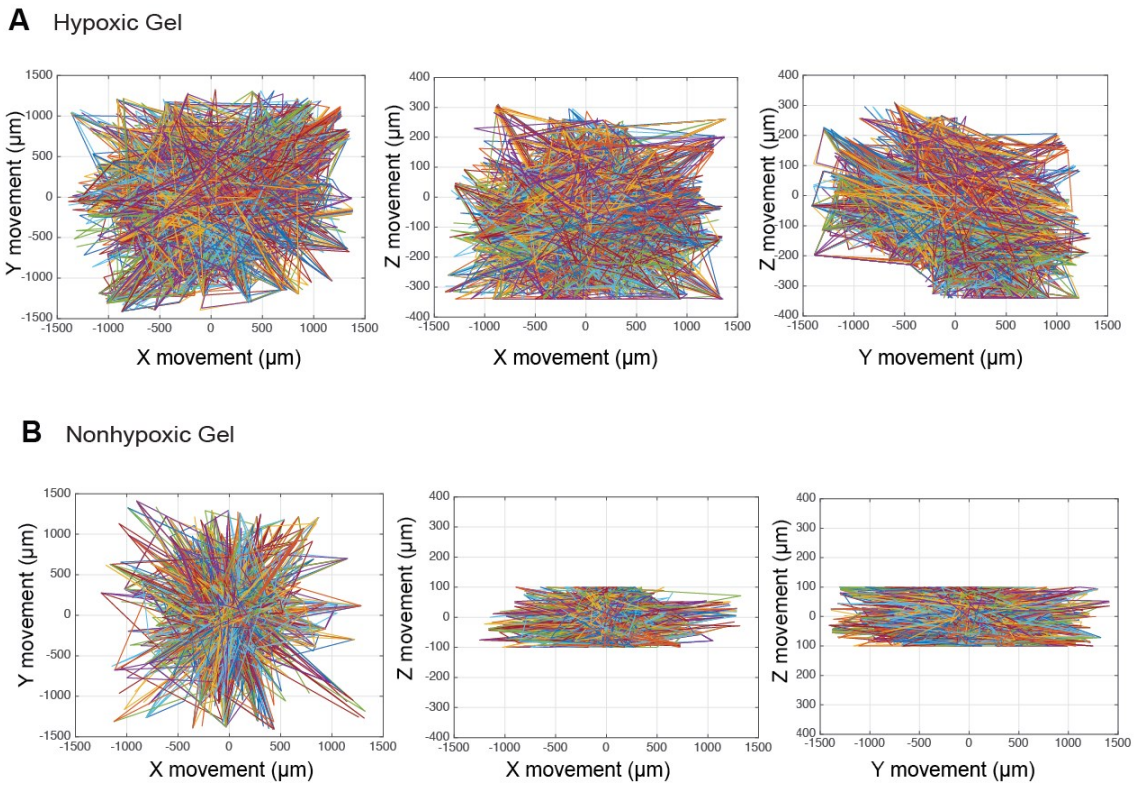

Supplementary Figure 3-6: Sarcoma cell migration trajectories.
2D Trajectories of tracked cells in (A) hypoxic and (B) non-hypoxic hydrogels.

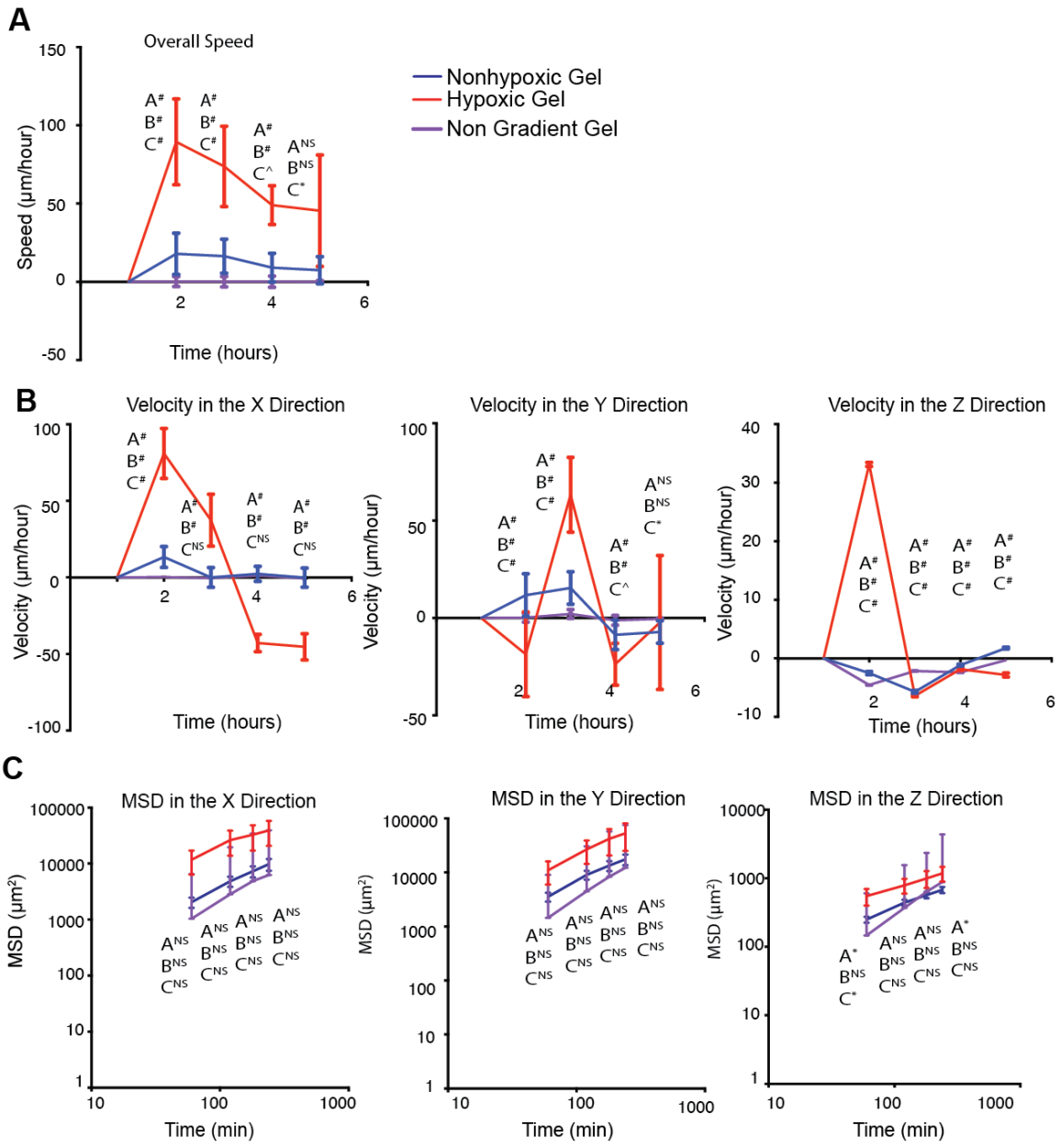

Supplementary Figure 3-7: Sarcoma migration in non-gradient gels.
KIA-GFP cells were tracked on day 3 in non-gradient gels and compared to the cell migration in gradient hypoxic and non-hypoxic gels. (A) Overall speed (C) Velocity in the x, y, and z directions; and (D) Mean square displacement (MSD) in the x, y, and z directions. Plots were created using position of KIA-GFP cells in the hydrogels.

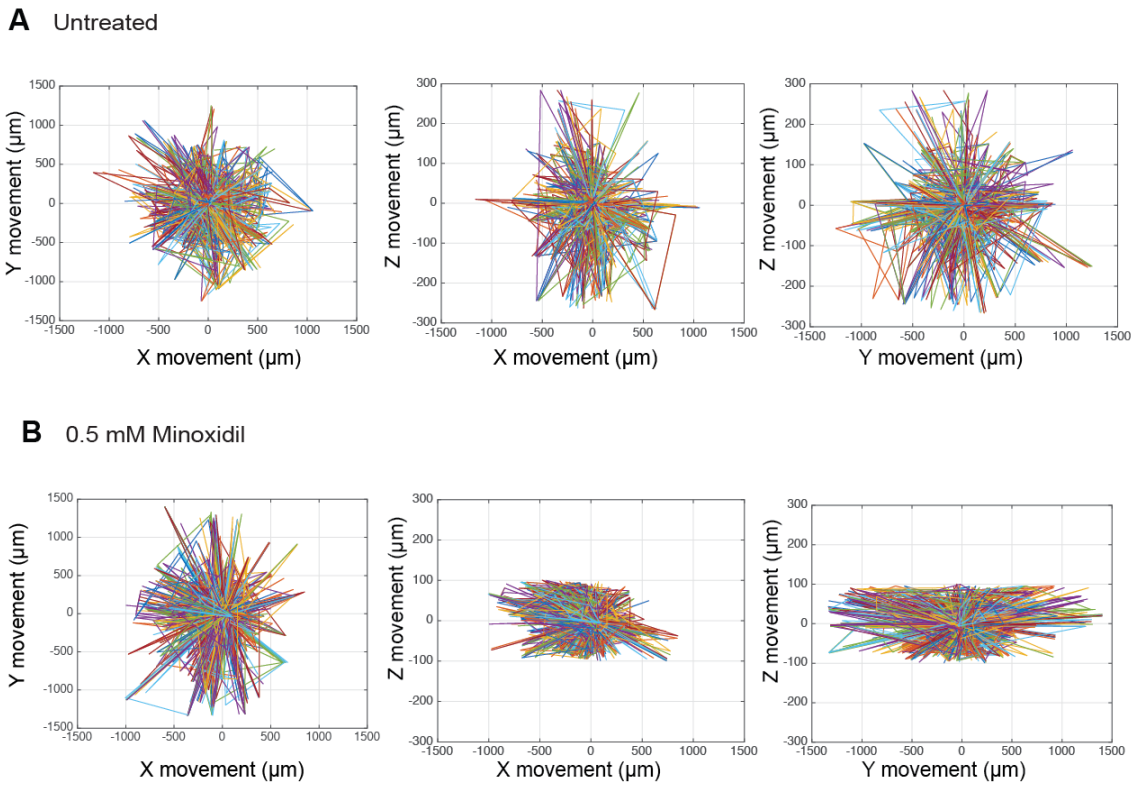

Supplementary Figure 3-8: Minoxidil treatment effect on sarcoma cell migration trajectories.
2D Trajectories of tracked cells in (A) untreaded hydrogels and (B) hydrogels treaded with 0.5 mM minoxidil.

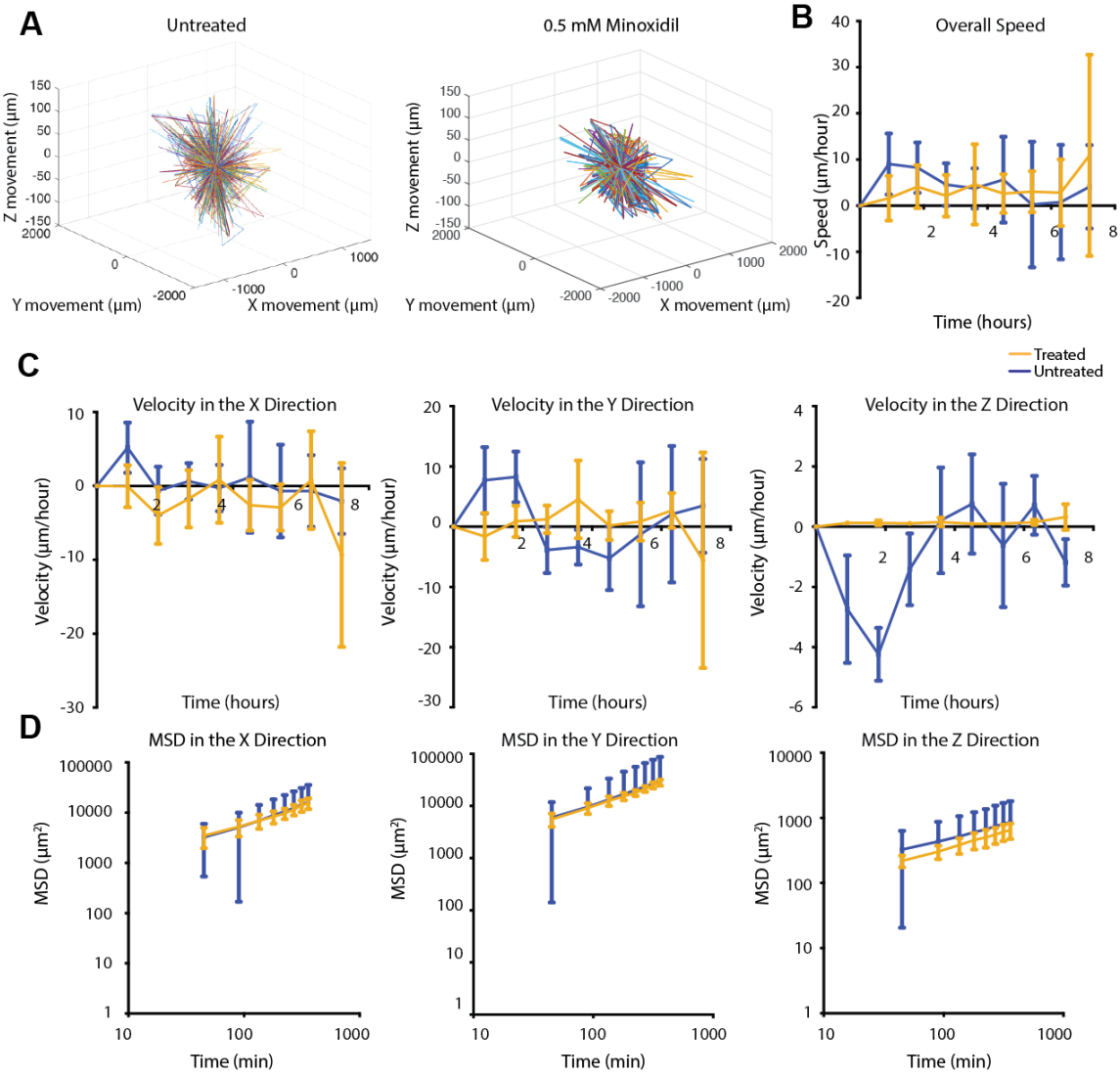

Supplementary Figure 3-9: Minoxidil treatment effect on sarcoma cell migration in nonhypoxic hydrogel.
KIA-GFP cells were tracked on day 3 in nonhypoxic treated and untreated hydrogel to determine (A) Three-dimensional trajectories of tracked cells (representative trajectories), (B) Overall speed (C) Velocity in the x, y, and z directions; and (D) Mean square displacement (MSD) in the x, y, and z directions. Plots were created using position of KIA-GFP cells in the hydrogels.

4 *Collagen Fiber Architecture Regulates Hypoxic Sarcoma Cell Migration.*

4.1 *Introduction*

The complex tumor microenvironment includes a variety of components including stromal cells, blood and lymphatic vessels, and the extracellular matrix (ECM). Each of these factors can generate non-uniform mechanical and physico-chemical gradients within a tumor. A prominent physico-chemical gradient in the tumor microenvironment is intratumoral hypoxia. Intratumoral hypoxia occurs when the oxygen partial pressure in the tissue drops to below 5%[171]. Hypoxia can trigger the upregulation of collagen modifiers [40] as well as a variety of cellular interactions and the recruitment of blood vessels[172]. In soft tissue sarcomas, hypoxic gradients lead to an increased metastatic potential and greatly decrease patient survival rates [40, 59].

Several properties of the ECM, such as elastic modulus and stress relaxation time, have been shown to regulate cellular responses[71] including cell motility[72], mesenchymal stem cell differentiation [66], and the cell's ECM sensing capability [73]. These properties are drastically different in different organs [173]. In the tumor ECM, the increase in collagen fiber density has been shown to promote human fibro-sarcoma migration speeds via beta-1-integrin [174]. Recently Ogawa et al have shown an abundance of collagen present in spontaneous formation of soft tissue sarcomas[175]. In

addition, collagen crosslinkers such as lysyl oxidase (LOX) and procollagen-lysine, 2-oxoglutarate 5-dioxygenase (PLOD2) have been shown to lead to a higher metastatic potential of sarcomic tumors [40, 59].

Traditional two-dimensional (2D) cell culture platforms in which cells are attached to the culture surface and exposed to atmospheric air have limited physiological relevance. The over simplification of these platforms has led to the development of three-dimensional (3D) platforms that mimic the tumor microenvironment *in vitro*. Such 3D platforms can aid in the understanding of tumor cell and microenvironment interactions. However, in order to study cell motility within a 3D ECM, there is a need to design biomaterials where such properties like crosslinking density[176], pore size[177, 178], and fiber density[142, 174] can be controlled. Furthermore, the combined effects of ECM properties and chemotactic gradients have added further complexity to the problem, with the underlying mechanism poorly understood. For example, most current approaches either overlook the gradients generated in the tumor microenvironment or are unable to decouple matrix properties from chemotactic gradients. Hydrogel biomaterials, due to their unique viscoelastic characteristics[179], may offer opportunities to address some of these limitations and can uncover the important biological responses.

In this study we aim to understand how hypoxic gradients affect sarcoma cell migration in a hydrogel-based, collagen-rich, fibrous ECM platform. In the collagen hydrogel platform, collagen fiber density is controlled by altering pre-incubation periods of collagen solution prior to polymerization. Oxygen gradients are modulated by controlling the passive diffusion of atmospheric (~21%) O_2 (via modifying hydrogel thickness) and O_2 consumption by the encapsulated cells. Using this platform we

demonstrated for the first time the synergistic effect of oxygen gradients and collagen-rich matrix properties on sarcoma cell migration. Using a mouse undifferentiated pleomorphic sarcoma (KIA cells) line, we found that hydrogels with denser collagen fibers have a shorter stress relaxation time and larger pore sizes that lead to an increased speed of sarcoma cell motility. We further demonstrated the additive effect of hypoxic gradients on increasing sarcoma cell migration by comparing the mean squared displacements (MSD) of cells in hypoxic-gradient and nonhypoxic hydrogel matrices.

4.2 *Materials and Methods*

4.2.1 **Collagen Gel Preparation**

The collagen gel synthesis protocol was adapted from previously established protocols [118, 141, 142]. In order to make 1 mL of 3 mg/mL collagen solution, we first mixed 35.96 μL of M199 10x media (Thermo Fisher Scientific) with 11.51 μL of 1M NaOH. This solution was mixed until it turned dark pink. Next we used acid soluble rat tail collagen I at 9.61 mg/mL (Corning #354249). A total of 312 μL of collagen was added to the dark pink solution and mixed thoroughly. 640.35 mL of M199 1x media (Thermo Fisher Scientific) was then mixed with the solution to create our final collagen gel solution. The solution was then incubated for 30 minutes on ice to create a low fiber density solution and 2 hours on ice to create a high fiber density solution.

4.2.2 **Cancer Cell Encapsulation and Culture with Hypoxic and Nonhypoxic collagen gels**

KIA was derived from a genetic murine model of sarcoma, LSL-KrasG12D/+; Ink4a/Arffl/fl as established previously [40], KIA-GFP was expanded under standard culture conditions (37°C and 5% CO_2) in high glucose DMEM with 10% FBS, 1%

penicillin/streptomycin (PS; Invitrogen). For cancer cell encapsulation, we first prepared cell pellets of KIA and KIA-GFP cells (7.5 x 10^5 cells) in a 1.5 mL eppendorf tube. We then mixed the pellet with 0.5 mL of collagen solution by gentle pipetting to give a homogenous cell suspension. After mixing, the solution is pipetted into a 96 well plate (BD Bioscience) and incubated for 30 minutes at 37°C. The nonhypoxic gels were created with 50 μL of collagen while the hypoxic gels were made from 100 μL of collagen solution. The cells were then cultured within the hydrogel matrices under standard culture conditions in DMEM (Dow Corning) with 10% heat-inactivated fetal bovine serum (Gibco) and 1% penicillin streptomycin. 200 μL of media was used to culture the hypoxic gels and 100 μL was used to culture the nonhypoxic gels.

4.2.3 **Noninvasive and Invasive Oxygen Measurments**

The dissolved oxygen (DO) levels were monitored noninvasively and invasively as previously performed[59]. We used a commercially available sensor patch (PreSens) for the non-invasive measurements and a Needle-Type Housing Fiber-Optic Oxygen Microsensor (PreSens) for invasive measurements. Hydrogel cell constructs were created as stated above, and DO measurements were performed on day 3 of cell culture.

4.2.4 **Oxygen Modeling**

The Oxygen Modeling was performed using a previously established method [59]. COMSOL Multiphysics (Burlington, Vermont), a commercial finite element modeling software was used to evaluate the oxygen concentration in the hypoxic and nonhypoxic/atmospheric hydrogels. The values, parameters, and equations are ones reported in papers from Gerecht and colleagues [180-182]. Fick's first law was used to model the oxygen diffusion in the gel[183]:

$$J = D\nabla C + R \qquad \text{(Equation 1)}$$

where J is the flux of oxygen in the system, ∇C is the change in concentration in the x, y, and z direction, and R is the cell consumption rate, which is dependent on cell type and cell density. The model was verified experimentally.

4.2.5 **Matrix Degreadation and Migration Assays**

DFU To assess the effect of fiber density and oxygen levels on matrix degradation, we incorporated 10 μg/mL of DQ Collagen (Invitrogen) into polymer solutions when preparing cell suspension as described above. After day 3, the hydrogels with DQ-Collagen were observed by fluorescence microscopy (Axio Observer Z1, Zeiss) and quantified by measuring the fluorescence intensity using a fluorescence spectrophotometer at a wavelength of 495 nm excitation and 515 nm emission (Molecular Devices).

For the 3D cancer cell migration assay, we used a previously developed method [59]. Briefly, we encapsulated KIA-GFP cells in hydrogel constructs with different oxygen levels. Cells were tracked at day 3 using live-cell 3D confocal microscopy (LSM 780; Carl Zeiss) equipped with a cell incubator (37°C and 5% CO_2). To optimize the experiment properly, only cells that start in-frame were included in the experiment. The time-lapse and z-stack images (>200-μm thickness) were collected every 30 min up to 24 h at 5 randomly selected positions. The images were then analyzed using Imaris spot analysis software (Imaris 8.2; Bitplane) to track time-dependent mobility. The 3D migration analysis was then analyzed using a previously developed strategy[59, 144,

145]. A minimum of 100 individual cells at each point were tracked to generate x, y, and z coordinates at each time point. This data was then sorted to include only cells that were present at time 0. From this sorted data, the time that the cells were in-frame was calculated, and the most common time was used to select cells for tracking analysis. By choosing the time frame with the most visible cells we could maximize the sample size of cells that could be analyzed. Finally, velocity and speed profiles, MSDs, and trajectory plots were calculated using code adapted from previously established methods [59, 144, 145] for triplicate tracking trials (n = 3). Statistical analysis was performed using MATLAB (Mathworks, Inc.) to calculate the mean, SD, and SE of the mean. A t-test was performed where appropriate to determine significance (GraphPad Prism 4.02; GraphPad Software, Inc.). Graphed data are presented as average ± SD. Significance levels were set at $*P < 0.05$.

4.2.6 **Reflective Imaging of Collagen Fibers**

During To visualize collagen fibers within a 3D collagen gel reflection confocal images were collected using LSM 780 (Zeiss) microscopes. The microscopes are equipped with a 40x oil-immersion objective (Zeiss). For reflection imaging, the microscope was configured to capture 405 nm light reflected during illumination with the 405 nm lasers. Reflection microscopy was used for live samples, fiber dimensions and pore-size analyses (see below).

4.2.7 **Collagen Fiber Density, Orientation, and Cell Aspect Ratio Analysis**

Collagen fiber density and orientation was adapted from a previously developed method using MATLAB (Mathworks)[184]. Collagen fiber width and length were analyzed using a previously established method[185]. The software segments the image

and then calculates intensity gradients within subregions of images and uses them to track the overall directions of individual. In order to study cell aspect ratio, code was developed to fit an ellipse around the cell. The aspect ratio in our sample is a ratio of the major to minor axis, in which a perfectly circular cell would have an aspect ratio of one.

4.2.8 **Collagen Gel Morphology and Pore Size Analysis**

For pore size analysis at the nano-scale scanning electron microscopy (SEM) imaging was performed using a Hitachi S4700 Scanning Electron Microscope equipped with a cold field emission gun operated at 5 kV. Collagen samples were first fixed with a routine morphology fixative solution containing 3.0% formaldehyde (Electron Microscopy Sciences, 19200), 1.5% glutaraldehyde (Electron Microscopy Sciences, 16120), 2.5% sucrose (Sigma, S7903), 5 mM calcium chloride (Sigma-Aldrich, C1016), 5 mM magnesium chloride (Sigma,M8266), and 100 mM sodium cacodylate, (pH 7.4) at room temperature for 1 hr. Then, the samples were washed three times with 0.1 M sodium cacodylate (Electron Microscopy Sciences,12,300) and 2.5% sucrose (pH 7.4). This was followed by quick rinses in deionized water (Milli-Q System) and then 50% cold ethanol. After that a series of cold ethanol (Sigma Aldrich, 459836) (70, 90, and 100%) washes was performed to further dehydrate the sample. After dehydration, the samples were washed three times with 100% ethanol at room temperature. Once all samples had been fixed, they were supercritically dried using a Samdri-795 supercritical point dryer (Tousimis Research Corporation) for 3 hours.

To reduce surface charge, prior to SEM imaging, all surfaces were coated with approximately 12 nm of iridium using a Quorum Q150T ES Sputter Coater. Prepared collagen samples were imaged under 5 kV.

For pore size analysis at the micro-scale reflection imaging techniques were used as stated above. Images were taken at the bottom, middle, and top of the hydrogels in order to visual the micron scale pores.

All pore size analysis was performed using an l ImageJ macro adapted from strategies that have previously been used[185, 186]. The script was able to threshold the image and then calculate the areas of the gaps between fibers within the image. Those gaps were treated as representing the pores in the samples.

4.2.9 **Rheological and Stress Relaxation Analysis**

To analyze matrix stiffness, we performed a rheological analysis of the collagen hydrogels using a RFS3 rheometric fluid spectrometer from TA Instruments as we previously reported [59, 181]. A time sweep was performed on different fiber density hydrogels to monitor the storage modulus (G') and loss modulus (G'') at 10% strain and a frequency of 0.1 HZ at 37°C. A solvent trap wetter with DI water was used to prevent sample evaporation.

Stress relaxation experiments were performed on RSAG2 dynamic mechanical analyzer from TA instruments. The initial elastic moduli and stress relaxation properties of collagen gels were measured from compression tests of the gel disks (6 mm in diameter, 2 mm thick, equilibrated in PBS for 24 h) (**Supplementary Figure 4-1**). The gel disks were compressed to 10% strain. Stress relaxation under shear mode was performed on an AR1500 EX rheometer from TA instruments. Collagen gel disks of 6 mm in size were used to perform the stress relaxation tests at 0.5% strain for 5 minutes. As previously performed (5), single element Maxwell model was used to fit the stress

relaxation data in order to compare the time decay constants for different conditions (**Supplementary Figure 4-2**).

4.2.10 **Thermogravimetric Analaysis**

Water content of all samples was analyzed by Thermal Gravimetric Analysis (TGA) using the TA Instrument Q5000. Samples with masses of approximately 30 mg were analyzed for weight loss under N_2 purge from 25°C to 650°C at a heating rate of 20°C/min. The data was analyzed using TA Universal Analysis 2000 Software.

4.2.11 **Statistic Analysis**

Statistical analysis was performed using MATLAB (Mathworks, Inc.) or GraphPad (Prism 4.02; GraphPad Software, Inc.) to calculate the mean, SD, and SE of the mean. T-tests and one way ANOVA were performed where appropriate to determine significance (GraphPad Prism 4.02; GraphPad Software, Inc.). All experiments were performed in triplicate. Graphed data are presented as averages ± SD. Significance levels are set at *P < 0.05.

4.3 ***Results and Discussion***

4.3.1 **Design of Hypoxic Collagen Gel**

Type I collagen gel has been previously used as a platform to study cancer cell migration [187-189]. As collagen is the most abundant ECM component in the body, it is critical to better understand how collagen matrix properties affect cancer cell migration with and without hypoxic gradients. With our recent findings of increased sarcoma cell migration in hypoxic gradient hydrogels [59, 190], we set out to study how the fibrous structure of the matrix further modulates sarcoma cell migration. To create a hypoxic

hydrogel, a better understanding of our system parameters needed to be established. The parameters included the diffusion coefficient of our material, boundary conditions, and cell oxygen consumption rate. We chose collagen as our matrix due to its fibrous structure and a relatively low oxygen diffusion coefficient [191]. It has also been shown that collagen fiber density, its post-translational modification, deposition, and degradation all can lead to sarcoma cell migration[32, 40, 59, 192]. Next, we had to choose a material for the hydrogel to be polymerized in that would allow for close control of the oxygen diffusion into the system. By choosing polystyrene, which has a very low diffusion coefficient[193], we could create an impermeable barrier on the sides and bottom of the hydrogel placed within this common cell culture Petri-dish, thus allowing diffusion of oxygen and nutrient from the culture media on the top of the hydrogel. Lastly, the oxygen consumption rate needed to be modulated to balance the diffusion of oxygen into the system from the media. This oxygen consumption rate is dependent on the concentration of the encapsulated cells in the hydrogel. Using these parameters we modelled the system using the Fick's first law, creating an oxygen gradient in the upward direction of the hydrogel. To verify the oxygen concentration in the system, KIA-GFP cells were encapsulated in the hypoxic and nonhypoxic collagen gels (**Figure 4-1A**). Using reflective microscopy, we verified viability of KIA-GFP cells in the fibrous gel constructs (**Figure 4-1B**). We measured dissolved oxygen (DO) concentration using a non-invasive sensor at the bottom of the hydrogel and found the oxygen concentration was at 0.5-2%. We were able to maintain these hypoxic and nonhypoxic oxygen levels for 3 days (**Figure 4-1C**). With this data we built a model using COMSOL Multiphysics, simulating oxygen concentration in the hypoxic and nonhypoxic collagen gels (**Figure 4-**

1D).

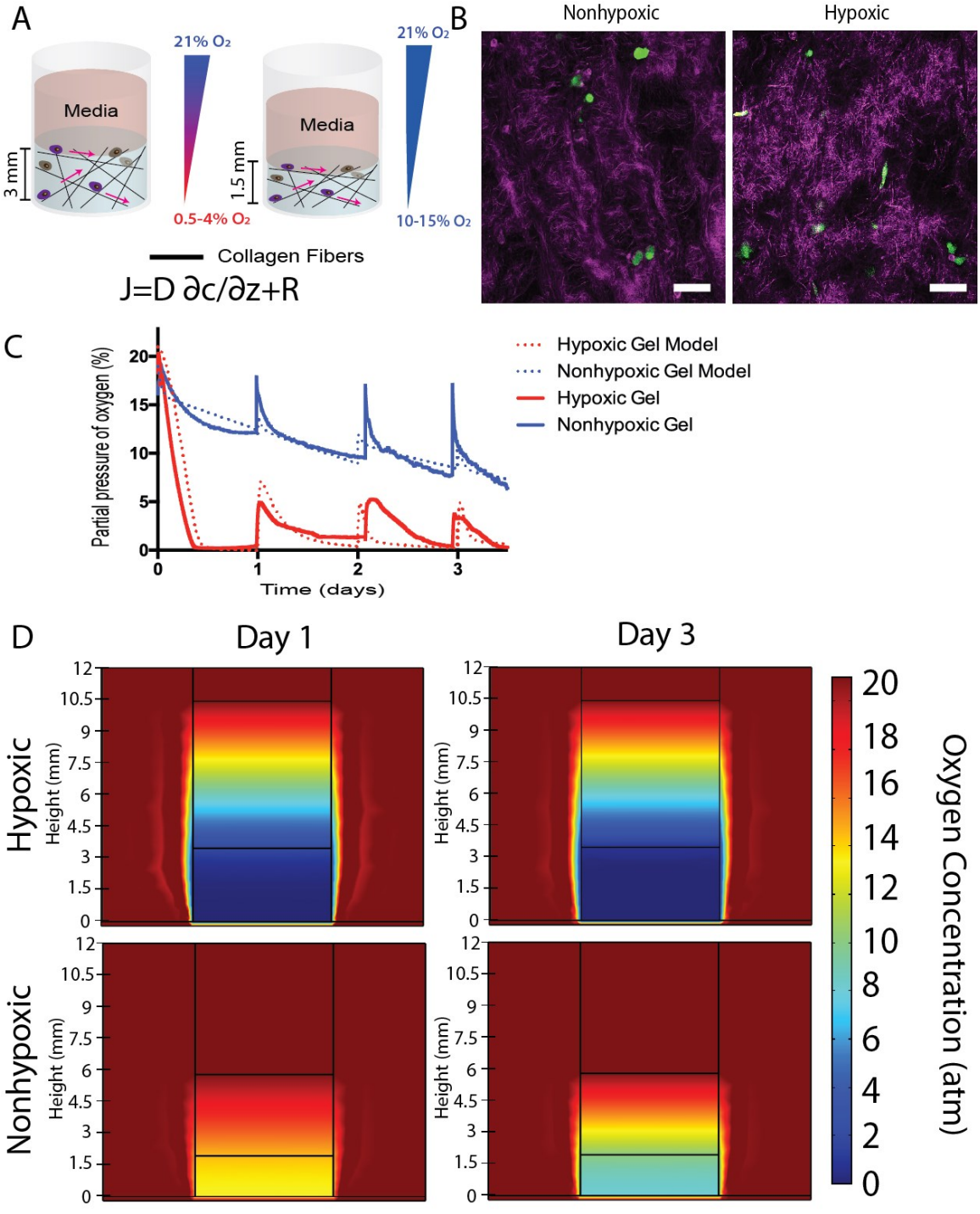

Figure 4-1: Establishment of Hypoxic Collagen Hydrogel
(A) Illustration of hypoxic and nonhypoxic fibrous collagen hydrogels. In order to create oxygen gradient the height of the hydrogel- cell constructs was altered. To generate these gels the hypoxic gradient was optimized using Fick's first law, where

D is the diffusion coefficient of the polymer, dc/dz is the change in concentration per change in height, and R is the cell consumption rate. (B) Cells encapsulated in the gels are shown using KIA-GFP cells and reflective imaging to visualize the collagen fibers. The images were taken at the bottom 300 μm of the gel.(C) Non-invasive DO readings at the bottom of the hypoxic and nonhypoxic hydrogel-sarcoma cell constructs, and compared to the mathematical model. (D) COMSOL was used to model the oxygen concentration in the hypoxic and nonhypoxic hydrogels.

4.3.2 Modulating Collagen Fiber Density Independently of Oxygen Tension

In addition to establishing the oxygen gradient, the ability to control material properties independently from oxygen concentration is key to elucidating the interplay between hypoxia and the ECM. Due to this design criteria, a method developed by Nguyen-Ngoc et al [194] was chosen to control fiber density independently from collagen concentration. The benefit of a constant collagen concentration is the ability to keep the availability of cell binding domains constant, independent from collagen fiber density. This method includes preparation of the type I collagen solution followed by its incubation at 4º C for various time intervals. This low temperature incubation period allows collagen fibers to aggregate without crosslinking, resulting in a slower and better controlled fiber assembly (**Figure 4-2**)[195, 196].

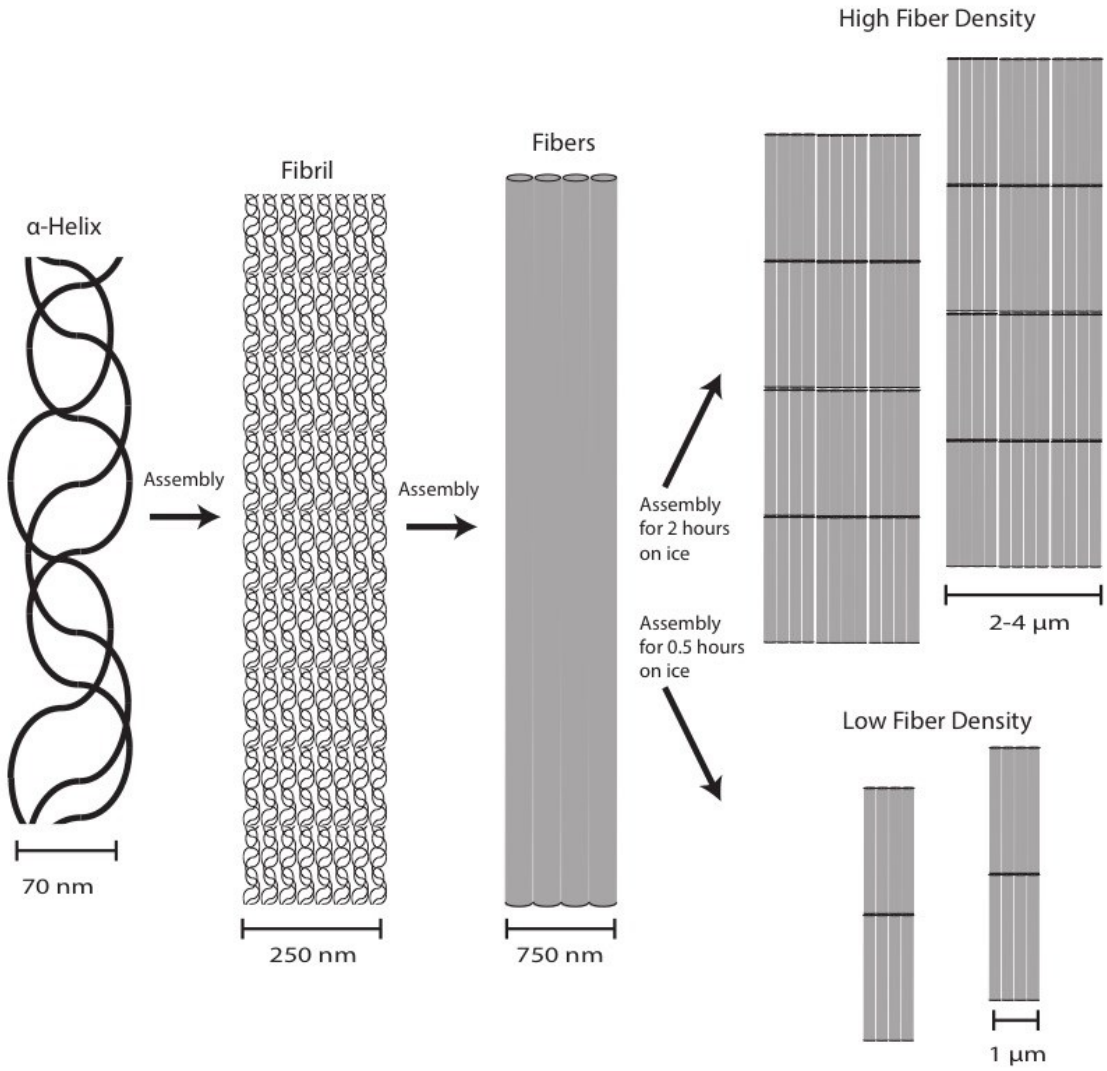

Figure 4-2: Collagen Fiber Formation
Schematic showing Collagen fibers aggregate from α-Helix to form fibrils. These fibrils aggregate to form larger fibers. Under various low-temperature incubation periods, these fibers aggregate to different degrees allowing for the formation of high and low density hydrogels. Drawing not to scale.

Using this protocol, fiber density could be modulated by incubating the collagen solution for 30 minutes to create a low fiber density gel and 2 hours to create a high fiber density gel (**Figure 4-3A**). The density of these collagen fibers per μm^2 was quantified using a MATLAB script (**Figure 4-3A**)[184]. In order to verify that fiber density could be independently controlled from oxygen concentration, an invasive DO measurement was

performed to verify the oxygen concentration along the height of the gel on day 1 and 3 of culture with KIA cells. From these measurements DO tension in the low and high fiber density hypoxic gels ranged from 1-15%, while the nonhypoxic gels ranged from 10-15%. These measurements show no dependence of oxygen tension on collagen fiber density (**Figure 4-3B**).

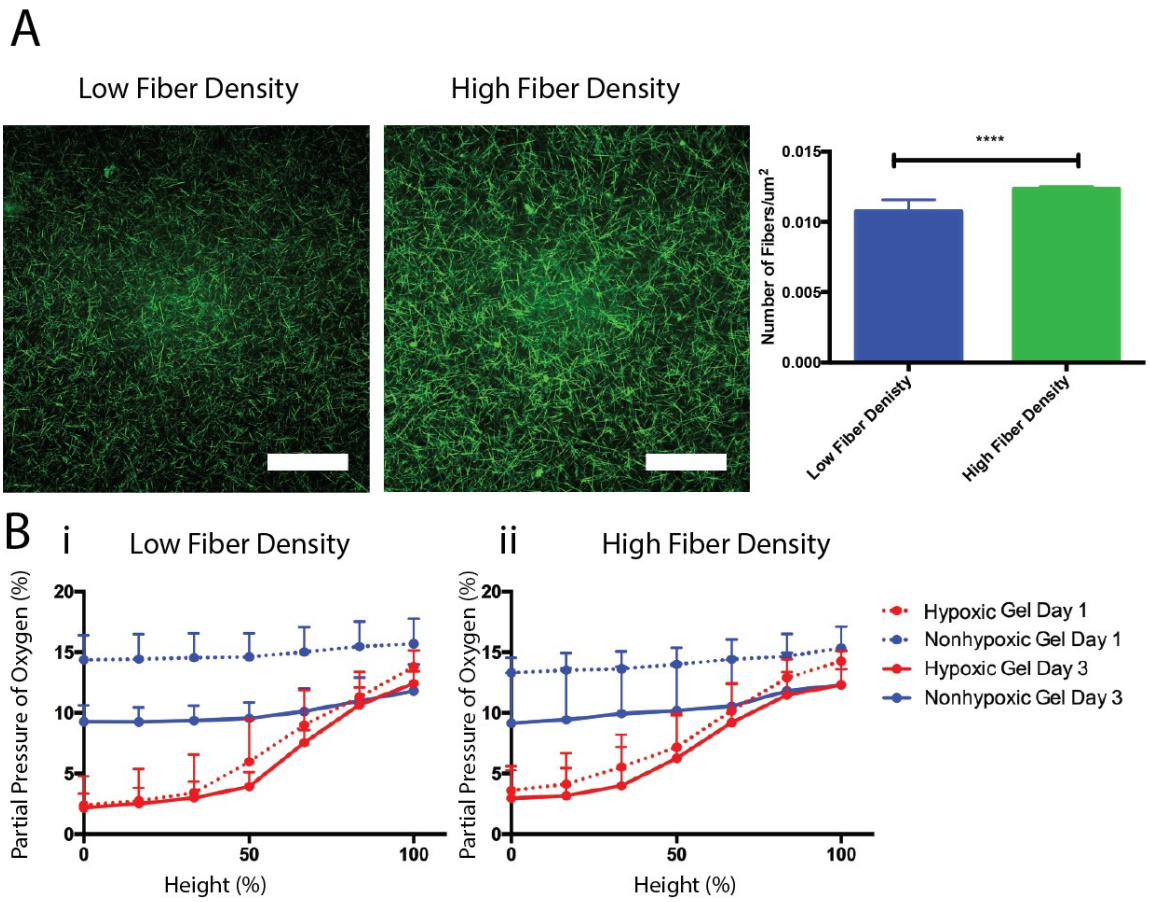

Figure 4-3: Decoupling Fiber Density and Oxygen Gradient
(A) Collagen fiber density can be varied via pre-incubation of collagen solution on ice prior to polymerization to create low and high density fiber concentrations: (left) SHG images (collagen fibers in green) and (right) fibers quantification (B) Invasive DO readings within different regions of the hydrogel showing gradients in the (i) low and (ii) high fiber density collagen hydrogels on Day 1 and 3. Scale bars, 25 µm. Significance levels were set at ****P<0.0001. Scale bar 50 µm.

4.3.3 **Mechanical Properties of Different Fiber Densities**

To better understand the new hypoxic fibrous collagen gel system, we studied their mechanical properties. First, we analyzed the composition of collagen hydrogels by TGA. Based on the TGA analysis, the moisture level was found to be approximately 98.5% and was independent of the sample gelation time (**Supplementary Figure 4-3**). This result shows that the hydrogels have a collagen level of about 1.5% by weight.

In addition to the moisture content, we analyzed the material properties of the collagen gel system. Using reflective microscopy, we first analyzed the fiber thickness and length. The higher fiber density collagen gel was found to have wider and longer fibers then the low fiber density collagen gel (**Supplementary Figure 4-4A-B**). We next analyzed pore area at micron-scale using reflective microscopy, and found an insignificant difference in the pore area (**Supplementary Figure 4-4C-E**). Pore area at nano-scale was quantified using a custom ImageJ macro of SEM images. Interestingly, we found that a larger pore area in the higher fiber density collagen gels (**Supplementary Figure 4-5**). These larger pores are due to fiber aggregation in the gel that seems to reduce the crosslinking density. This approach thus, allows us to increase the collagen pore size at nano-level length scale without altering the number of cell-binding sites, since the collagen concentration is the same. Next, we evaluated the elastic moduli of both high-density and low-density fiber hydrogels, and observed no difference between the two hydrogels (**Figure 4-4A**). Finally, we evaluated the stress relaxation of the material and found the decrease in stress relaxation time of the material is closely related to fiber density (**Figure 4-4B-C**). This decrease in stress relaxation time is most likely due to the larger pore sizes and lower crosslinking density in the high fiber density

collagen gel. We speculate this occurs from the collagen α-helix aggregation to create larger fibers, thus leaving less available monomer for crosslinking. In addition, the stress relaxation time is on the same order of magnitude of cell sensing. Wottawah et al. have shown rapid structural changes on the order of magnitude of minutes in 3T3 fibroblasts in response to mechanical stimulus of laser beams probing for the stress relaxation time of the cellular membrane [197]. This quick response to mechano-transduction is further elaborated by Chaudhuri et al which have shown the effect of stress relaxation in regulating cell spreading via a yes-associated protein (YAP) [198] and the effect of stress relaxation as a key mechanism affecting cell-ECM interactions mediated by adhesion-ligand binding, actomyosin and contractility[66]. With the structural and mechanical properties of the hydrogel established, we next examined the effect of the above parameters on sarcoma cell migration.

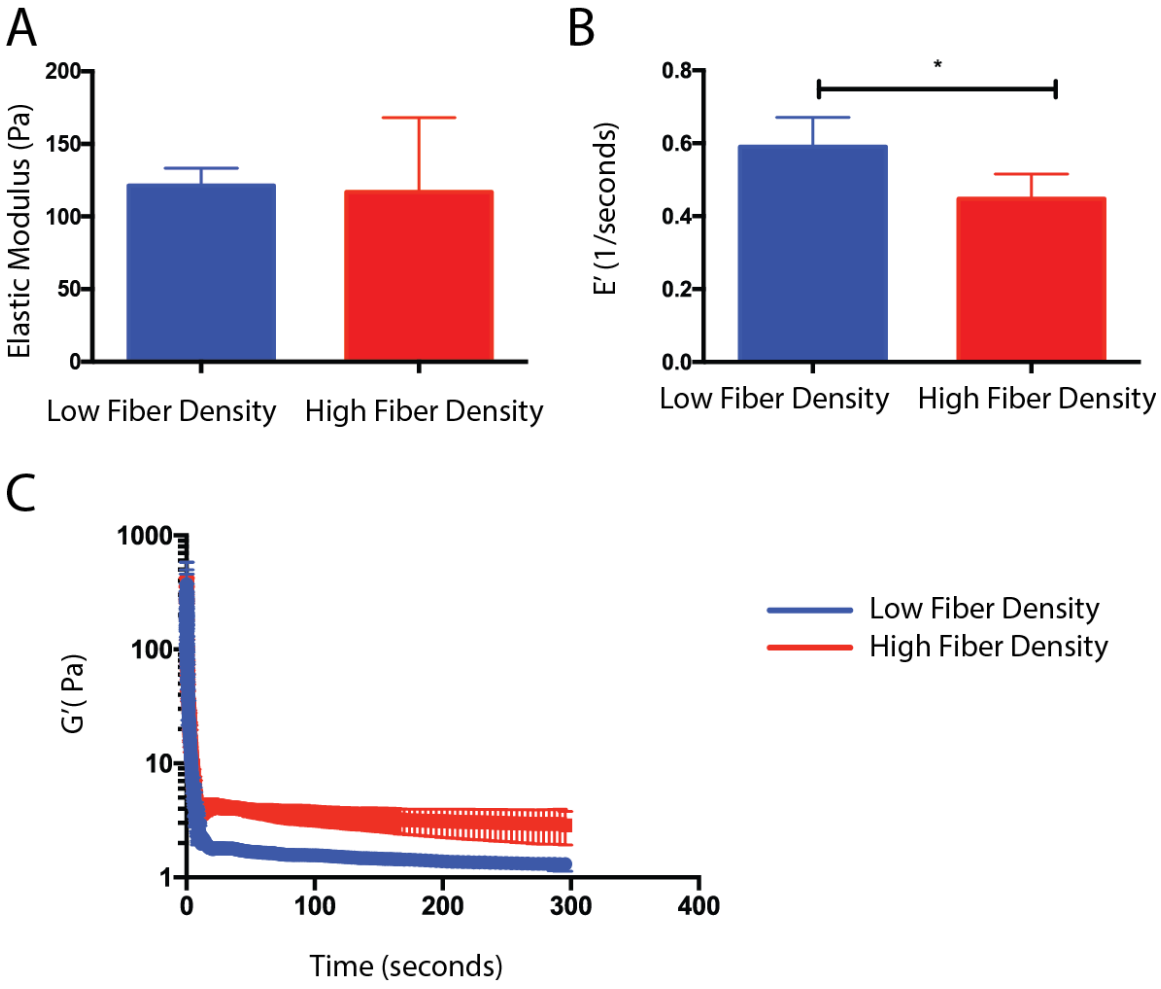

Figure 4-4: Analysis of Material Properties of Fibrous Collagen Gels.
(A) Young's Modulus of the collagen hypoxic hydrogels. (B) With the same elastic modulus, the stress relaxation time can be modulated and kept at the same time frame as cells. (C) A representative trial of the rheological shear test used to determine the stress relaxation time. Scale bars, 2 µm. Significance levels were set at *P<0.05.

4.3.4 Sarcoma Cell Migration in Nonhypoxic Collagen Gels at Low and High Fiber Concentrations

With this platform established, we sought to further investigate the effect of O_2 gradients and mechanical properties on sarcoma cell migration in varying collagen fiber densities. To do this we performed real-time 3D cell tracking using confocal microscopy. KIA-GFP

cells were encapsulated in the nonhypoxic low and high fiber density gels. Using reflective images, we analyzed collagen fibers after the cells were cultured in the hydrogels for three days. First, using the MATLAB code, we were able to determine the orientation of individual fibers in the gel (**Figure 4-5A**). We defined aligned collagen fibers as fibers that were within a 5% angle from the mean angle of the images. We observed that following 3 days of culture, there were more aligned collagen fibers in the high fiber density nonhypoxic hydrogels compared to the low density nonhypoxic hydrogels (**Figure 4-5B**). Using those same images, the aspect ratio of the cells was also analyzed. We found that the KIA-GFP cells are more elongated in the low fiber density nonhypoxic collagen gels and more circular in the high fiber density nonhypoxic collagen gels (**Figure 4-5C**). We could not detect differences in the elastic modulus between the two nonhypoxic gels (**Figure 4-5D**).

To better understand these differences in fiber alignment and cell morphology in the different gels, we next sought to compare collagen degradation and live cell movement in the nonhypoxic, low and high fiber density gels. We begun by study the protease activity of the encapsulated cells using DQ collagen assay [199]. We found that there was no difference in protease activity in the low and high fiber density nonhypoxic gels (**Figure 4-5E**). We observed no difference in the migration speeds between the two nonhypoxic gels (**Figure 4-5F**). Insignificant differences in instantaneous cell velocities in the x, y, and z directions were observed between the two nonhypoxic gels (**Figure 5G**). By analyzing the mean squared displacement (MSD) in the three planes, we noticed no significant difference in the MSD between the two hydrogels (**Figure 4-5H**). Once the

baseline values had been established in the system we next sought out to compare these observations with GFP-KIA cells encapsulated in the hypoxic collagen gels.

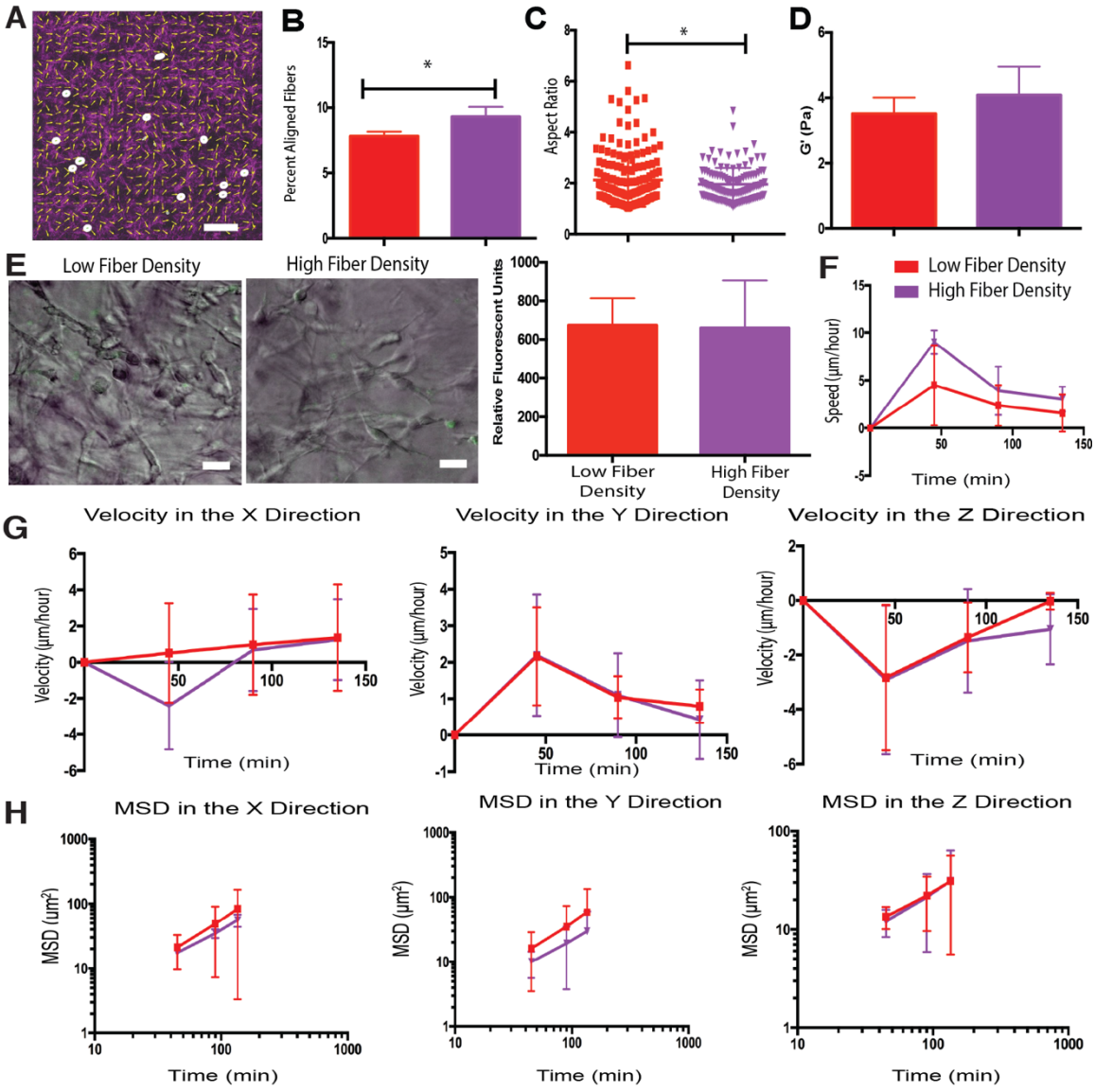

Figure 4-5: Sarcoma Cell Migration in Atmospheric Gradients
(A) A representative reflective microscopy image showing use of Matlab code to analyze fiber alignment and cell aspect ratio. To calculate the aspect ratio, white circles were drawn around the cells, green. The aspect ratio was then calculated from the major and minor axis of the ellipse. To calculate the fiber angle, yellow arrows were drawn along the fibers (in pink), and the angle of the arrows was determined. (B) Collagen fiber alignment and (C) cell elongation (aspect ratio) in the two fiber density nonhypoxic constructs after 3 days in culture. (D) Elastic modulus of low and high fiber density nonhypoxic gels. (E) Proteolytic degradation of the two fiber density nonhypoxic constructs incorporating DQ Collagen for 3

days in culture. (F) Overall speed, and (G) Velocity, and (H) Mean square displacement (MSD) in the x, y, and z directions. Plots were created using position of KIA-GFP cells in the hydrogels on day 3. Scale bars, 25 μm. Significance levels were set at *P<0.05.

4.3.5 Syngersitc effect of sarcoma cell migration of oxygen and fiber density

We have previously demonstrated that sarcoma cells migrate faster in hypoxic gradients [59]. Here, we sought to observe the effects of collagen fiber density and viscoelastic properties on hypoxic sarcoma cell migration. In order to perform the single cell analysis, KIA-GFP cells were encapsulated in hypoxic gradient gels at varying collagen fiber concentrations. To control these gradients, an air-oxygenated medium was used to create an oxygen gradient in the upward direction of the hydrogel. Using similar fiber analysis as above, we observed that, following 3 days of culture, there were more aligned fibers in the lower density hypoxic hydrogel compared to the higher density hypoxic hydrogel (**Figure 4-6A**). This is the opposite of what we observed in the nonhypoxic hydrogels (**See Figure 4-5B**). Interestingly, cells in the higher fiber density hypoxic collagen hydrogel were more elongated with larger aspect ratio, compared to the spherical cells in low fiber density hypoxic collagen hydrogels (**Figure 4-6B**). This trend is also opposite of the nonhypoxic collagen hydrogels. Similarly to the nonhypoxic collagen hydrogels, we could not detect differences in the elastic modulus between the two hypoxic gels (**Figure 4-6C**).

Using the same approach above, we also explored sarcoma cell protease activity and migration in the hypoxic collagen hydrogel. There was a stark increase in protease activity in the higher fiber density hypoxic gels compared to the low fiber density hypoxic gels (**Figure 4-6D**). We found that sarcoma cell encapsulated in the higher fiber density hypoxic gel had a faster migration speed than in the lower fiber density hypoxic

gel (**Figure 4-6E**). There was an insignificant difference in instantaneous cell velocities in the x, y, and z directions (**Figure 4-6F**). In addition to the increase in cell speed, we observed an increase in the MSD of the KIA-GFP cells in the x, y, and z direction, with persistent movement in the more fibrous gels (**Figure v6G**). The increase in migration speed and persistence may explain the difference in fiber alignment and cell elongation in the hypoxic collage gels after 3 days of culture.

Comparing the low fiber density collagen gels, we find higher speed and persistent migration of KIA cells in the hypoxic gradients (**Supplementary Figure 4-6**). Comparing the high fiber density collagen gels, we find that KIA cell migrating more persistently in the hypoxic hydrogels compared with the nonhypoxic hydrogel (**Supplementary Figure 4-7**). Example trajectories of the cells moving in the various conditions (**Supplementary Figure 4-8**) helped demonstrate that higher fiber density hypoxic gel had the most impact on KIA cell migration (**Supplementary Table 4-1**). We also observed that in the hypoxic gradients, matrix fiber alignment is corresponding to slower cell migration (and their low aspect ratio), while no fiber alignment is observed with rapid cell migration. The fibers in the high fiber desnity gel were wider and longer which could explain why these fibers were less aligned due to their increase in size. Compared with previous results [59], we found that the KIA cells migrated slightly slower in the hypoxic collagen gels than in the hypoxic gelatin gels. As the hypoxic gradients are similar in both of these system cultures, we speculate that the slower movement is most likely due to the more fibrous structure of the collagen hydrogels. Overall, this data shows that cell migration persistence increases in hypoxic gels and with

increasing fiber density. We could not detect difference in the direction of movement between the low and high fiber density hypoxic gels.

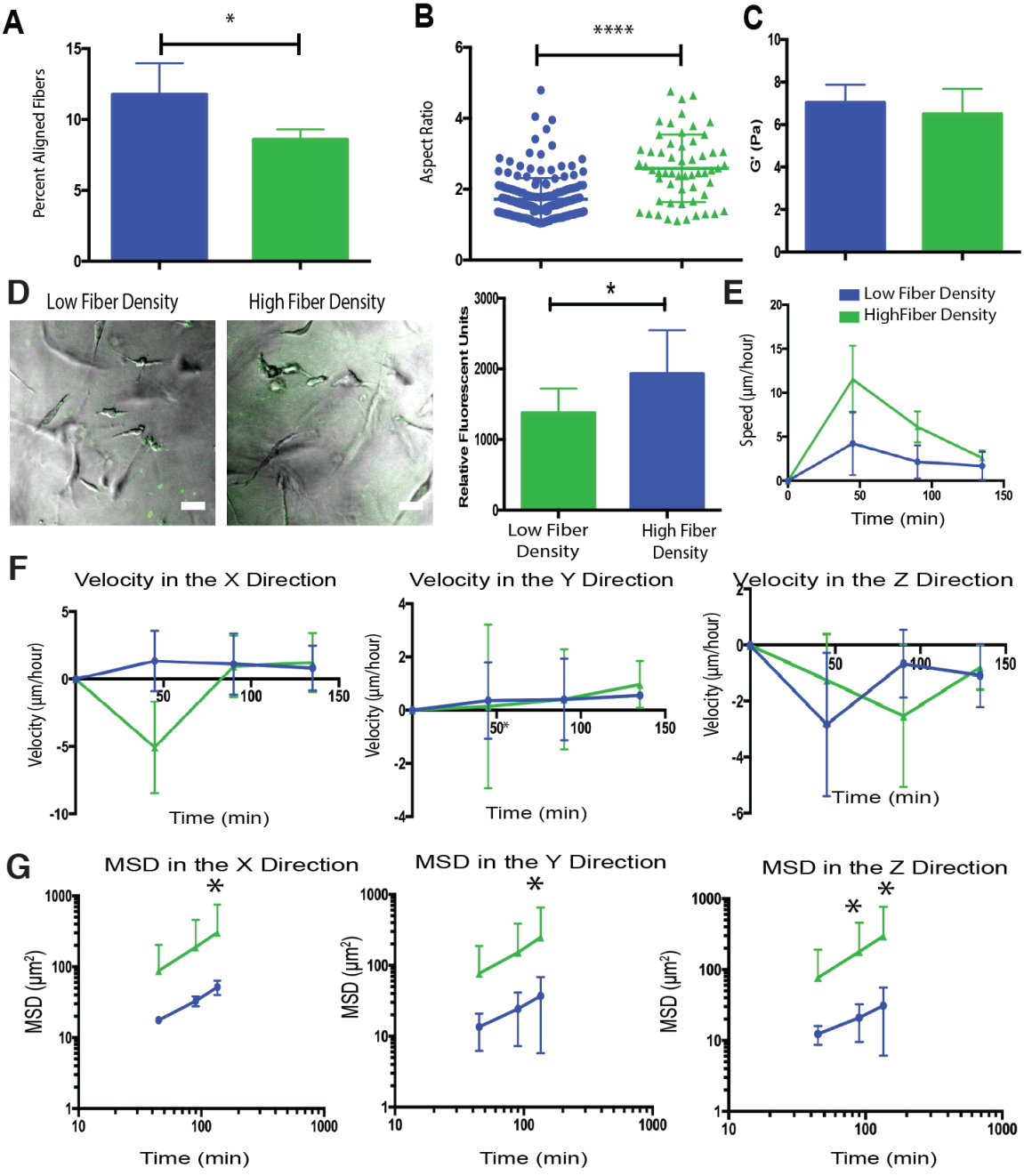

Figure 4-6: Collagen Hypoxic Gel Fiber Density Influences Cell Migration (A) Collagen fiber alignment and (B) cell elongation (aspect ratio) in the two fiber density hypoxic constructs after 3 days in culture. (C) Elastic modulus of low and high fiber density hypoxic gels. (D) Proteolytic degradation of the two fiber density hypoxic constructs incorporating DQ Collagen for 3 days in culture. (E) Overall speed (F) Velocity in the x, y, and z directions; and (G) Mean square displacement

(MSD) in the x, y, and z directions. Plots were created using position of KIA-GFP cells in the hydrogels on day 3. Significance levels were set at *P<0.05 and ****P<0.0001.

4.4 *Conclusion*

Previous studies have shown the effect of fiber density [142, 200] and oxygen gradients independently on cancer cell migration[59]. Specifically, pathologically, it has previously been shown that collagen fiber density leads to an increase in lymph node positive breast cancers metastasis [201], while in sarcomas it has been shown to lead to an increase in metastatic potential [40]. Here we elucidate the effects of these cues, by engineering collagen gels to control collagen fiber density and its corresponding stress relaxation characteristics, as well as oxygen tension. We found that an increase in collagen fiber density enhanced sarcoma cell migration only in hypoxic gradients. In agreement with Wottawah et al. who demonstrated cellular responses to mechanical stress on the order of magnitude of minutes [197], we show a 3D culture system with a similar time to cellular response, most likely mediated by stress relaxation time. Given this cellular-applicable stress relaxation time and the fact that the differences in pore size are at a smaller length scale than that of the cells, we suggest that an increase in fiber density in addition to hypoxic gradients increase sarcoma cell migration. Since the cells are migrating faster and to longer distances in the hypoxic high fiber density gels, they spend less time modifying the matrix (fiber alignment) and more time moving (cell elongation) compared to hypoxic low fiber density gels. The insights into the stress relaxation in the higher fiber desnity gel should be further explored to better understand the effects. The collagen gel platform could be further utilized to study different forms of

migration seen in a variety of cancer cells such as amoeboid, single or multicellular dissemination[202].

4.5 *Supplementary Information*

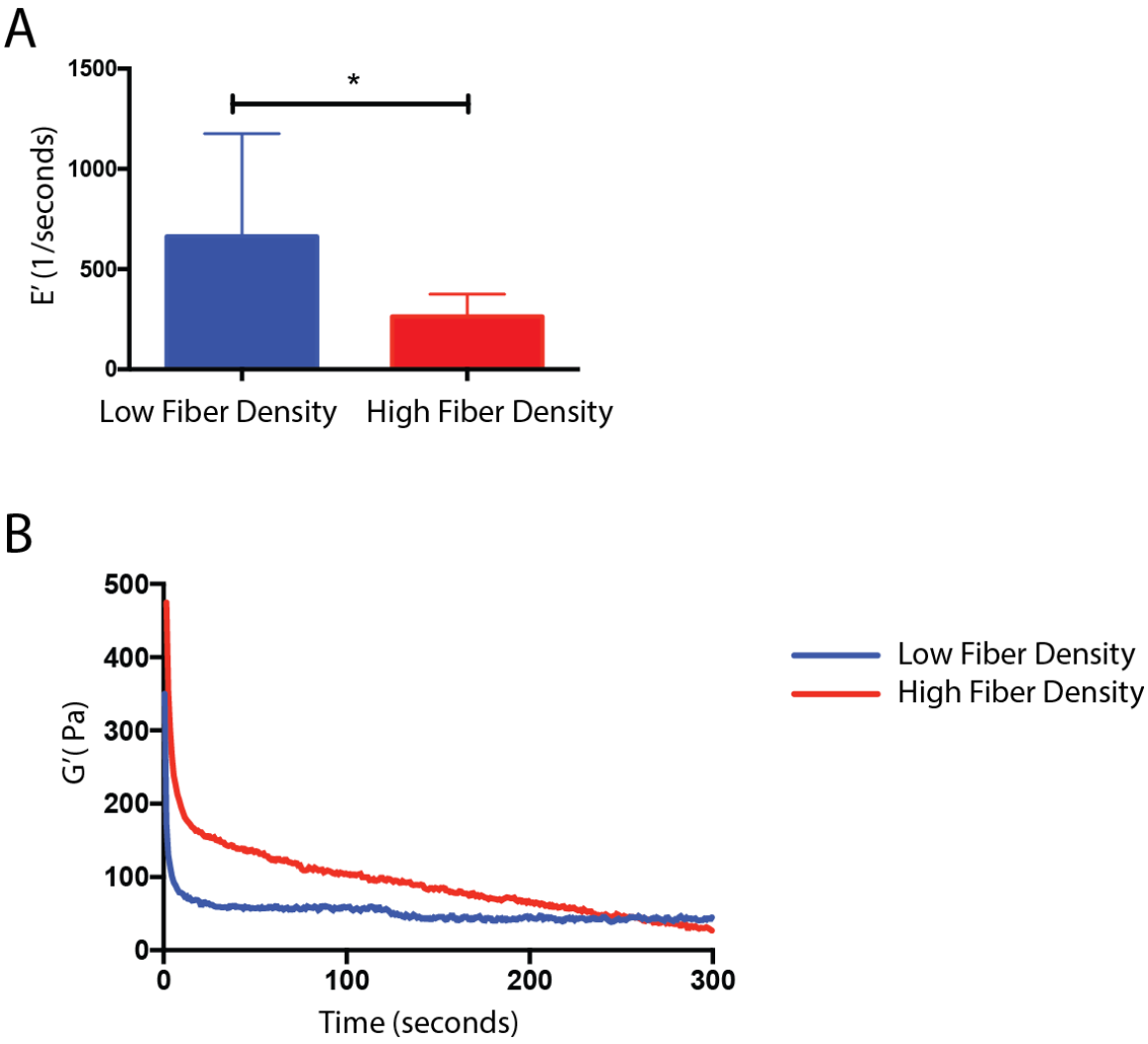

Supplementary Figure 4-1 Compression stress relaxation of the low and high fiber density hydrogels.
(A) The stress relaxation determined from compression testing of hydrogels. (B) A representative trial of the rheological compression test used to determine the stress relaxation time. Scale bars, 2 μm. Significance levels were set at *P<0.05.

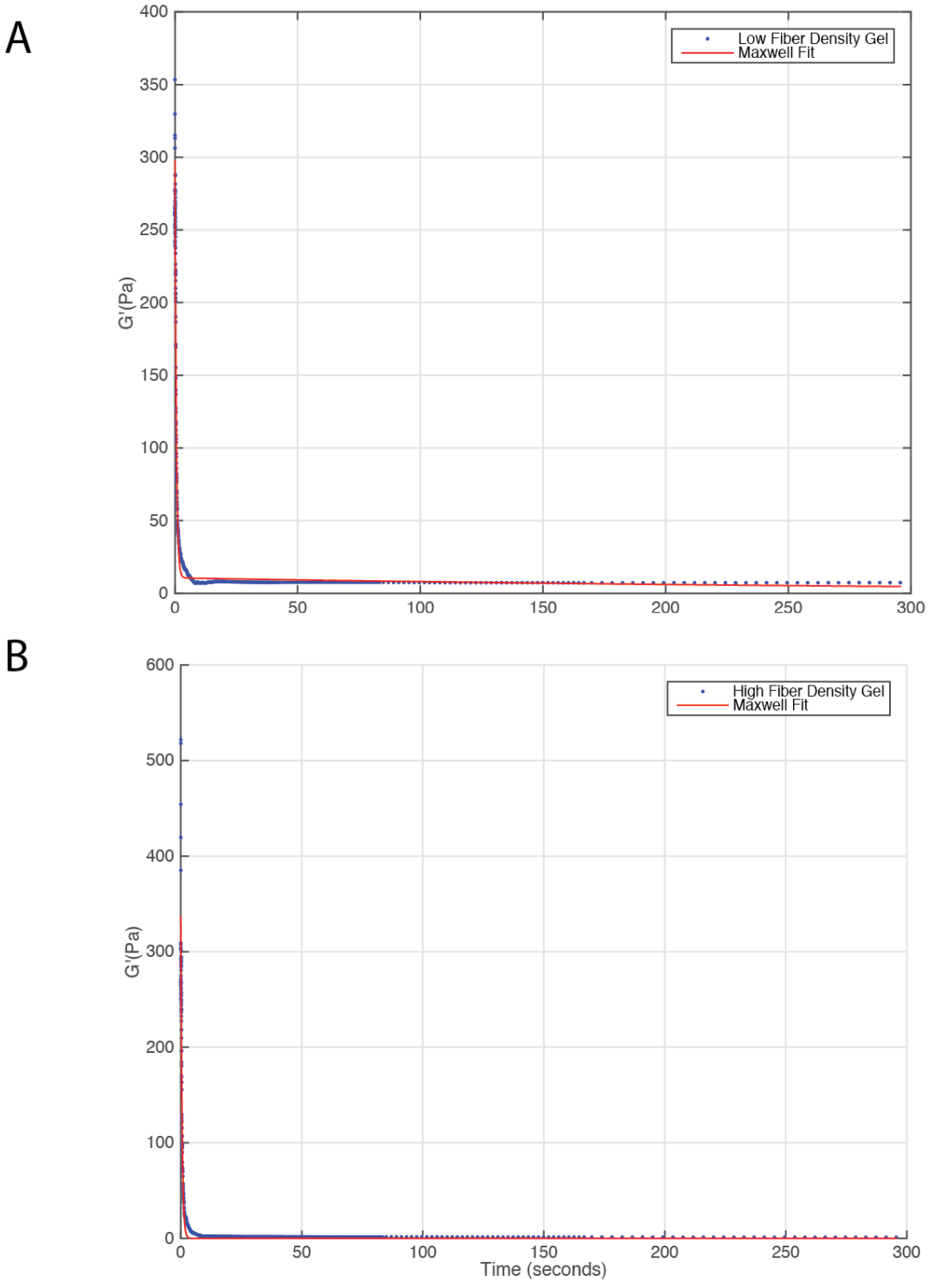

Supplementary Figure 4-2: Example of Maxwell Fits.
Low (A) and high (B) fiber density gels for shear rheometry data from Figure 4-4.

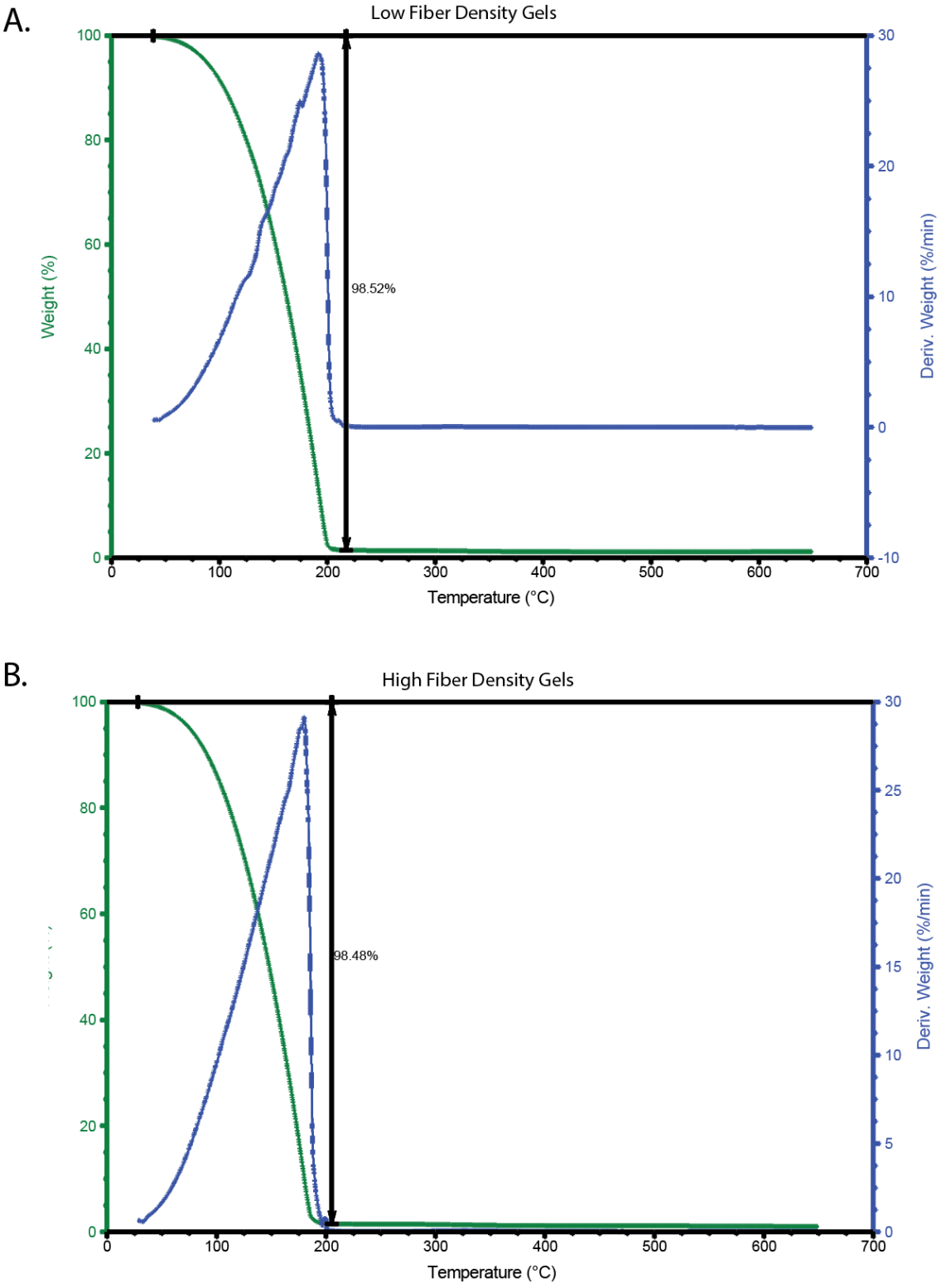

Supplementary Figure 4-3: TGA analysis.

Low (A) and high (B) fiber density collagen gels. The representative trial shows that samples had a moisture level round 98.5% by weight.

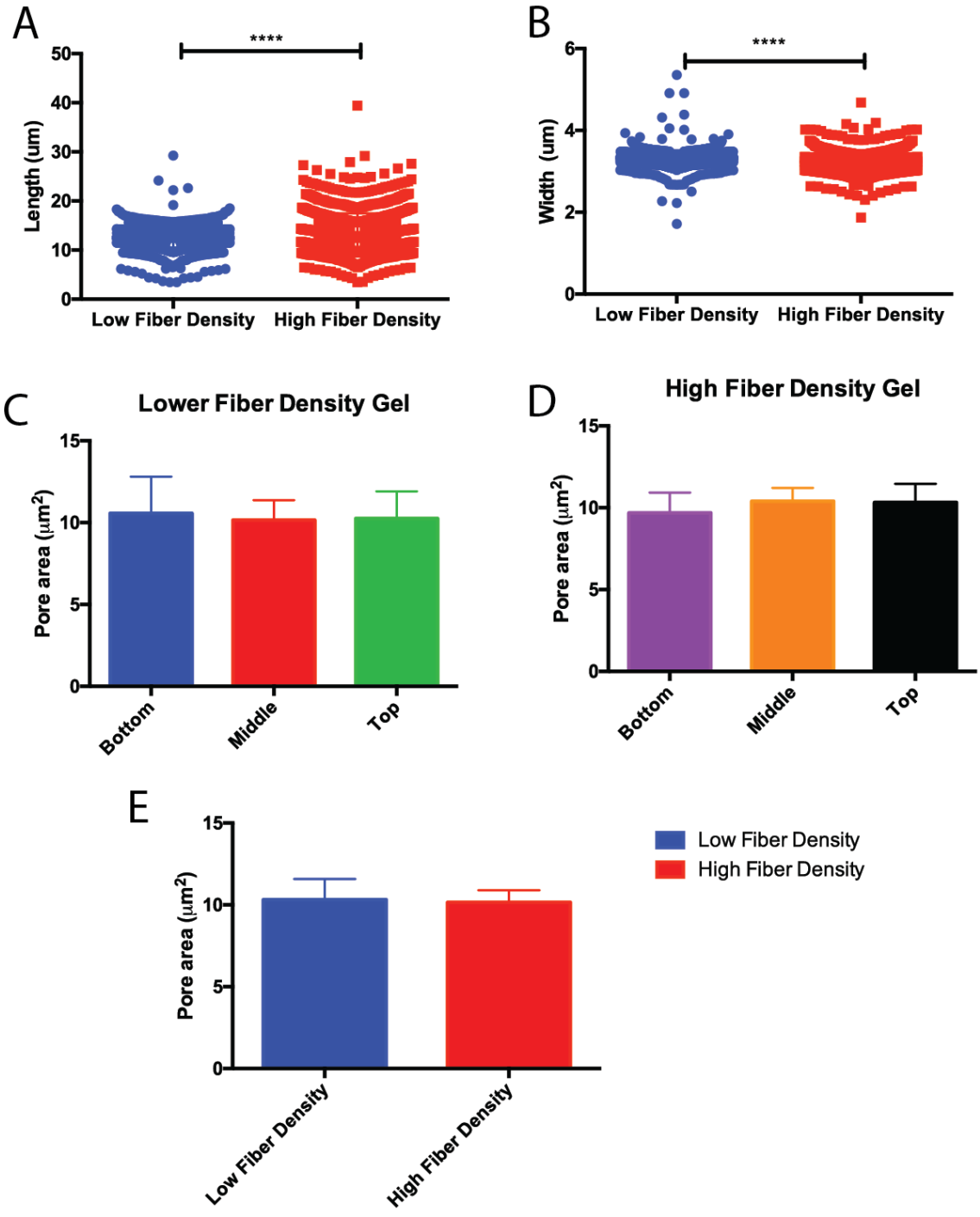

Supplementary Figure 4-4: Fiber length and width analysis of confocal images. Fiber length (A) and width (B) were quantified using MATLAB analysis of reflective microscopy images as those shown in Figure 4-3A. The pore area of those reflective microscopy images were calculated using the method shown in

Supplementary Figure 4-2 at the top, middle, and bottom of the low (C) and high (D) fiber density collagen hydrogel. The overall pore area was also determined (E). Significance levels were set at ****P<0.0001.

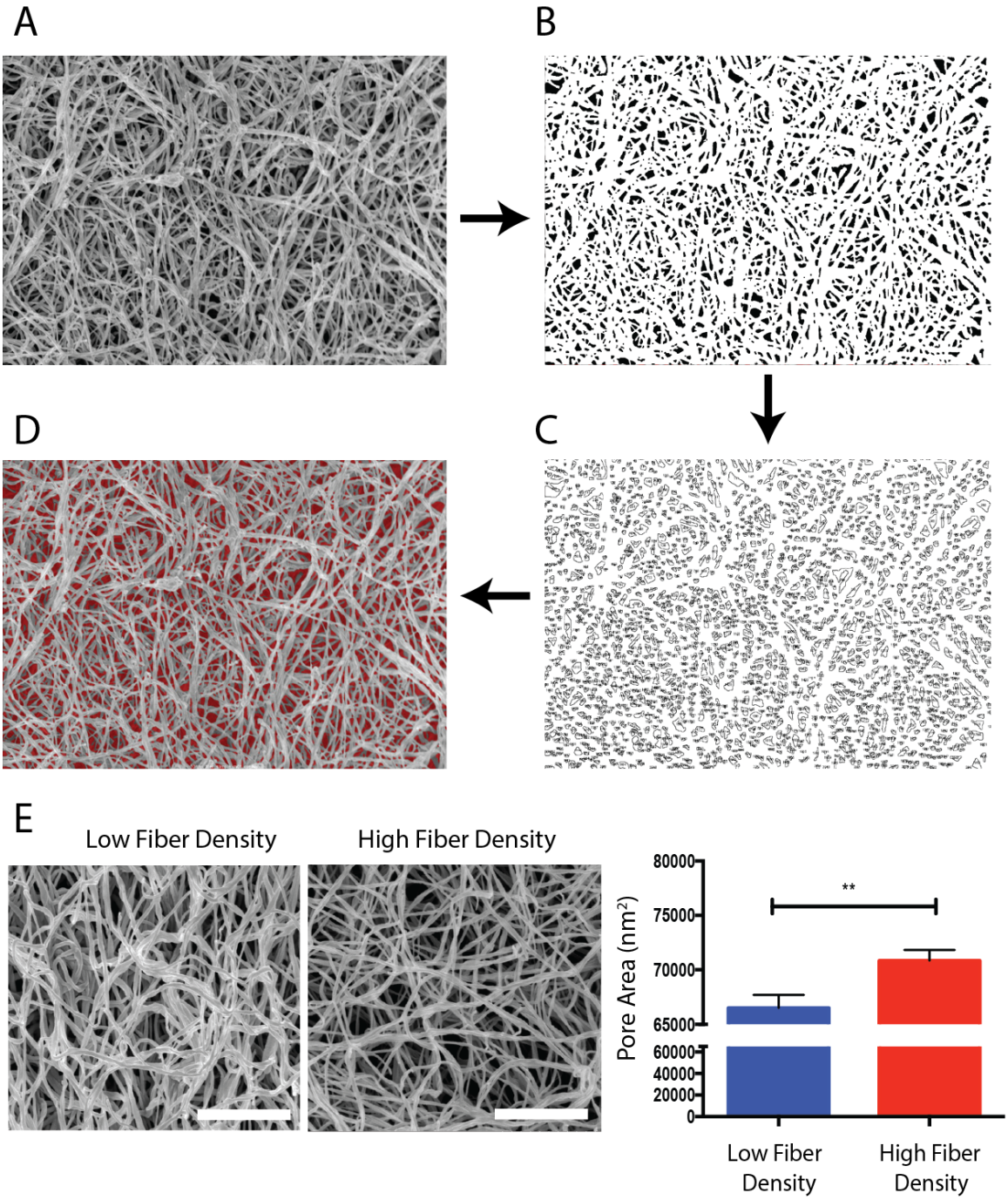

Supplementary Figure 4-5: Pore area analysis sequence from SEM images. (A) Original image is cropped. (B) Pores are segmented using Phansalkar auto local thresholding with a radius of 15 pixels and smoothed by performing morphological opening. (C) Areas of connected objects in the image are recorded. (D) Segmented

pores are overlayed onto original image. (E) Scanning electron microscopy (SEM) images of the low and high fiber density gels, showing an increase in pore size as fiber density increases. Significance levels were set at **P<0.01.

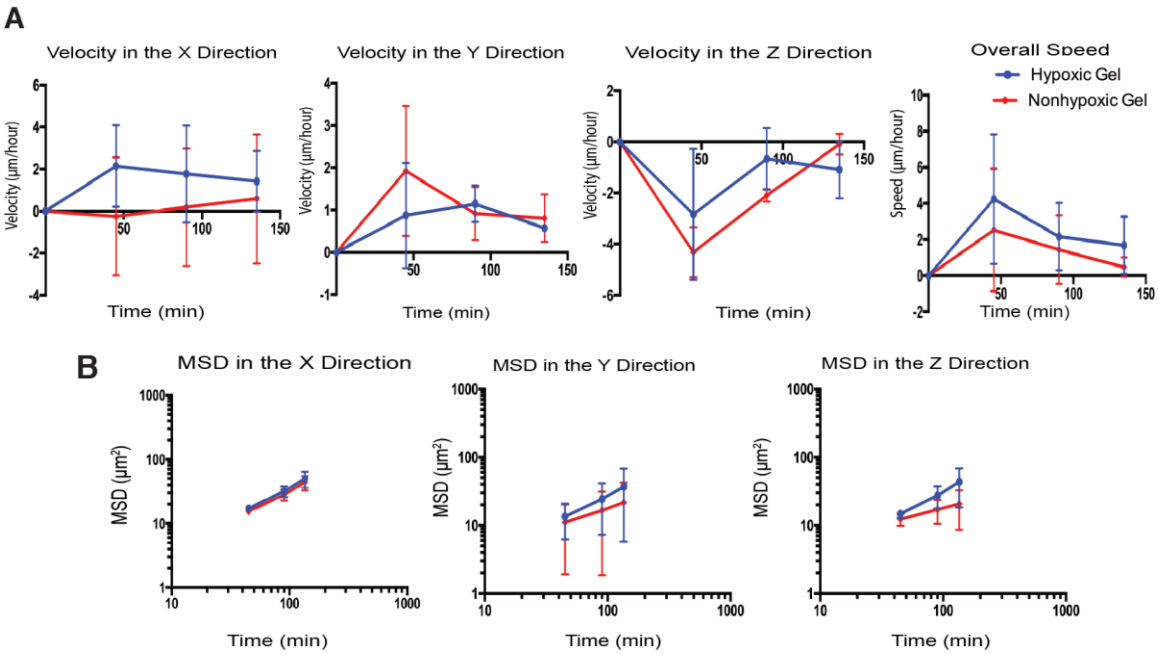

Supplementary Figure 4-6: Comparison of low fiber density gels.
(A) Velocity, overall speed, and (B) Mean square displacement (MSD) in the x, y, and z directions. Plots were created using position of KIA-GFP cells in the low fiber density hydrogels on day 3.

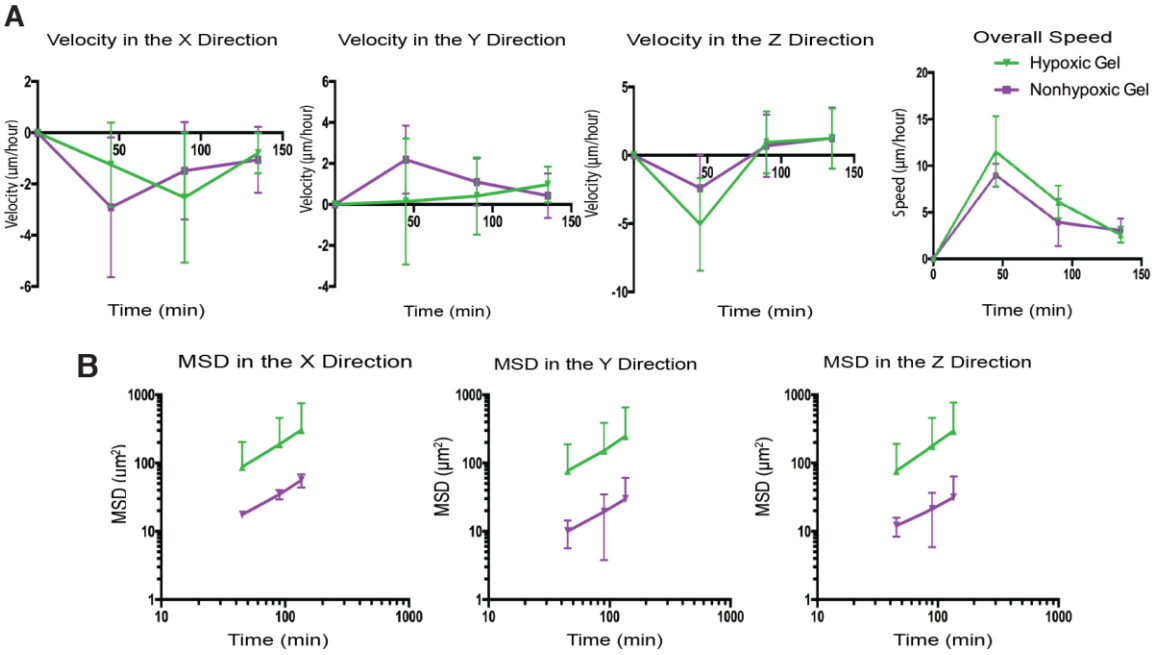

Supplementary Figure 4-7: Comparison of high fiber density gels.

(A) Velocity, overall speed, and (B) Mean square displacement (MSD) in the x, y, and z directions. Plots were created using position of KIA-GFP cells in the high fiber density hydrogels on day 3.

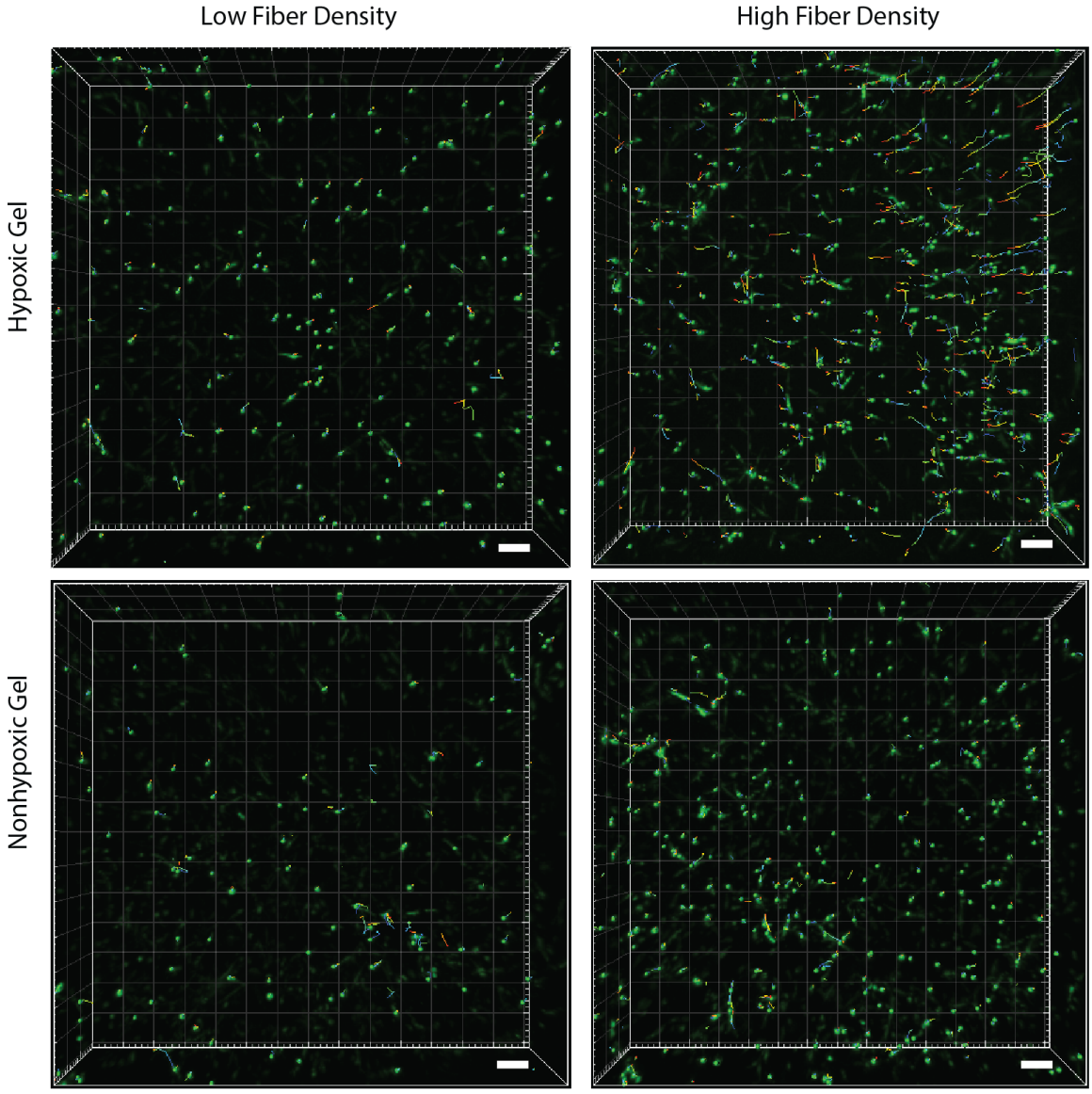

Supplementary Figure 4-8: Trajectories of sarcoma cells.
Trajectories generated by Imaris used to track cells moving in three-dimensional space. The color of the trajectory green to red indicates time with purple being the earliest and red being the latest time-point. Scale bar is 100 μm.

Supplementary Table: 4-1: Summary of results*

Hydrogel	Fiber	Cell	Matrix	MSD X	MSD Y	MSD Z

	Alignment	Elongation	Degradation			
Low Fiber Density Nonhypoxic Gel	1	3	1	1	2	2
Low Fiber Density Hypoxic Gel	4	1	3	2	3	3
High Fiber Density Nonhypoxic Gel	3	2	2	3	1	1
High Fiber Density Hypoxic Gel	2	4	4	4	4	4

* Graded from Lowest (1) to Highest (4)

5 *Quicker Stress Relaxation Time Increases Migration Speed of Sarcoma Cells in Hypoxic Gradients*

5.1 *Introduction*

Cell migration through the extracellular matrix is a key factor in the disease progression of cancer. There are a plethora of factors that have been linked to cancer cell migration such as oxygen[59, 70] and crosslinking of the extracellular matrix (ECM)[40]. Specifically in sarcoma an increase in procollagen-lysine,2-oxoglutarate 5-dioxygenase 2 (PLOD2) has been shown with more a more metastatic phenotype[40, 42]. The ability to experimentally recapitulate these factors in an in-vitro platform is especially difficult, as the biophysical and biochemical properties of native ECMs are hard to control. Collagen is one of the most abundant ECM matrix proteins[203], and increased levels of collagen have led to increases in sarcoma cell migration[40, 70]. In addition to extracellular matrix components, oxygen gradients are a key factor of the tumor microenvironment. Intratumoral hypoxia occurs when oxygen drops below 5%. As tumors rapidly outgrow their blood supply they create an oxygen gradient in the developing site. This oxygen gradient has been revealed to increase cell migration in hypoxia[40, 59, 70] compared to non-hypoxic hydrogels.

Hydrogels are commonly used to recapitulate a three-dimensional (3D) cellular microenvironment. These scaffolds are typically composed of synthetic or naturally occurring materials. These materials seek to mimic the chemical and physical properties of the tumor microenvironment as well as the ECM. In viscoelastic materials such as the ECM, stress relaxation is a key property of the matrix. It has previously been shown that different cancers have unique stress relaxation profiles[67]. Stress relaxation, or the rate at which materials deform under force, is an understudied viscoelastic property of ECM proteins. Few studies have investigated the effect of stress relaxation on cell behavior[68-71] and particularly in cancer. Stress relaxation has been revealed to affect numerous behaviors, including cell motility[72], mesenchymal stem cell differentiation [66], and the cell's ECM sensing capability [73]. Since changes in the ECM have been revealed to decrease survival rates in many cancers[204], we sought to explore the effect of stress relaxation on cancer cell migration and tumorigenesis.

When designing a novel hydrogel matrix, in order to assay biological functions, it is important to make sure the control and experimental conditions have similar properties such as stiffness, pore size[177, 178] and fiber density[142, 174] in order to properly mimic the cellar microenvironment. We have previously demonstrated the importance of collagen in sarcoma cell migration[70], however it is very difficult to alter a single mechanical property in collagen gels without drastically changing the collagen fiber structure, pore size, and binding site density. In this study, we have developed a novel method to control stress relaxation independently of collagen fiber density, collagen stiffness, and oxygen concentration, in order to explore the ability for stress relaxation with and without hypoxia to effect sarcoma cell migration. In the collagen hydrogel

platform, collagen fiber density was controlled by standardizing ice incubation times prior to polymerization. After polymerization, microbial transglutaminase (mTG) was added to modulate the stress relaxation time of the hydrogel without modulating the collagen architecture. This methodology allowed us to maintain the structure of the collagen, as confirmed by reflective, scanning electron, and transmission electron microcopy without altering the stiffness of the matrix. In addition, oxygen concentration could be controlled as previously developed[70]. The combinatory effect of these conditions allowed, for the first time, to explore the synergistic effect of stress relaxation in oxygen gradients comprised of 100% pure collagen structures. Using murine undifferentiated pleomorphic sarcoma cells (KIA) and primary patient undifferentiated pleomorphic sarcoma cells (hUPS), we found that quicker stress relaxation time in oxygen gradients led to increase speed of sarcoma cell motility via procollagen-lysine,2-oxoglutarate 5-dioxygenase 2 (PLOD2), with the quicker stress relaxation stimulating PLOD2 via transforming growth factor beta (TGF-β). Finally, upon implanting the quicker and slower stress relaxation hydrogels in a murine model, there was a significant increase in tumor growth once implanted; as well as an increase in PLOD2 expression and collagen secretion in the quicker stress relaxation hydrogel.

5.2 *Materials and Methods*

5.2.1 **Cell Culture and Primary Tumor Cell Extraction**

KIA was derived from murine model of sarcoma, LSL-$Kras^{G12D/+}$,$Ink4a/Arf^{fl/fl}$ as established previously[40]. KIA-GFP was expanded under standard culture conditions in high glucose DMEM with 10% FPBS and 1% penicillin/streptomycin. hUPS cells were extracted from a primary human tumor sample provided by Dr. Weber and Dr. Eisinger-

Mathason. hUPS cells were extracted by incubating the primary tumor with a 3 mg/mL collagenase solution in DMEM for 45 min at 37°C. The tumor was then spun down and the supernatant was aspirated and replaced with 0.05% trypsin EDTA solution and again incubated for 15 minutes at 37°C. The digestion is then stopped with complete cancer media. The tumors again were spun down, aspirated, and replaced with serum free media. The tumor is washed 2 more times and then triturated through a 40 μm cell trainer into a 50 mL conical tube. The cells are then spun down and plated. Cells were selected by continuous culture for up to 8 passages prior to use.

5.2.2 **Collagen Gel Preparation and Cell Encapsulation**

Collagen gel was prepared as previously reported[70]. In short, to make 1 mL of 3 mg/mL collagen solution, 35.96 μL of M199 10× medium (Thermo Fisher Scientific) was mixed with 11.51 μLof1M NaOH until it turned dark pink. Next, we used acid soluble rat tail collagen I at 9.61 mg/mL (Corning #354249). A total of 312 μL of collagen was added to the dark pink solution and mixed thoroughly. A total of 640.35 μL of M199 1× medium (Thermo Fisher Scientific) was then mixed with the solution to create our final collagen gel solution. The solution was then incubated on ice for 2 hours. For cancer cell encapsulation, we first prepared cell pellets of hUPS-GFP and KIA-GFP cells (7.5 × 105 cells) in a 1.5 mL eppendorf tube. We then mixed the pellet with 0.5 mL of collagen solution by gentle pipetting to give a homogeneous cell suspension. After mixing, the solution was pipetted into a 96 well plate (BD Bioscience) and incubated for 30 min at 37 °C. Non-hypoxic gels were made with 45 μL of collagen and hypoxic gels were made with 90 μL of collagen.

To alter the stress relaxation, gels were incubated with PBS or 24 mg/mL microbial transglutaminase (mTG) for 2 hours at room temperature. After 2 hours, the solutions were aspirated and the gels were cultured in normal culture media. 200 μL of media was added to the hypoxic gels and 100 μL was added to the non-hypoxic gels.

5.2.3 **Noninvasive and Invasive Oxygen Measurements**

Dissolved oxygen levels were monitored non-invasively and invasively as previously reported[59, 70]. A commercially available sensor patch (PreSens) and a Needle-Type Housing Fiber-Optic Oxygen Microsensor (PreSens) were used for the non-invasive and invasive experiments respectively. Hydrogels were prepared as stated above and oxygen measurements were performed on day 3..

5.2.4 **Matrix Degradation**

Degradation of the matrix was performed as previously published[70] by incorporating 10 μg/mL of DQ collagen (Invitrogen) into polymer solution prior to cell encapsulation. On day 3 DQ Collagen was analyzed by fluoresce microscopy (Axio Observer Z1 Zeiss) and measured using a fluorescence spectrophotometry at a wavelength of 495 nm excitation and 515 nm emissions (Molecular Devices).

5.2.5 **Cell Tracking and Drug Treatment**

For cell tracking, a previously developed method[59, 70, 205] was used to assess sarcoma cell migration. KIA-GFP cells were encapsulated in hydrogels with different oxygen levels and mTG treatment. On day 3, cells were tracked with live-cell 3D confocal microscopy (LSM 780; Carl Zeiss) equipped with an incubator (5% CO_2 and 37 °C). The time-lapse and z-stack images (>200 μm thickness) were collected every 30

minutes up to 24 hours at five randomly selected positions. Cells that did not start in frame were not included in the analysis in order to properly optimize the experiment. The images were analyzed with Imaris spot analysis software (Imaris 8.2; Bitplane). The 3D migration analysis was performed with a previously developed strategy[59, 70, 205]. A minimum of 100 individual cells were tracked to generate x, y, and z coordinates at each time point. These were then sorted to only include cells present at time 0. The time that each of the sorted cells were in frame was calculated and the most common time was used to pick cells for tracking analysis, maximizing the sample size of cells in the analysis. Velocity, speed and Mean Squared Displacements were calculated using code adapted from previously established methods for triplicate tracking trials (n=3)[59, 70, 205]. The statistical analysis was performed using MATLAB (Mathworks, Inc.) to calculate the mean, SD, and SE of the mean. Where appropriate, a t test was performed where appropriate to determine significance (GraphPad Prism 4.02; GraphPad Software, Inc.). Graphed data are presented as average ± SD. Significance levels were set at *$P<0.05$.

For minoxidil and TGF-β inhibitor treatment, cells were cultured in hydrogels under the conditions and methods described above for 3 days. On day 3, 0.5 mM minoxidil or 10 μM TGF-β inhibitor dissolved in KIA cell culture media was added to the wells containing the hydrogels and the cells were tracked for 24 hours. Untreated cultures served as controls. Cell tracking and data analysis were performed as described above.

5.2.6 Rheology and Stress Relaxation Analysis

For all rheological experiments an AR1500EX rheometer (TA Instruments) was used. A time sweep was performed on the mTG and control gels at 1% strain and 10 Hz to monitor the storage (G') and loss modulus (G'') at 37°C. A solvent trap with DI water or an immersion cup with PBS was used to prevent evaporation. Stress relaxation experiments were performed for strains from 0.5%-1% for 2 minutes. As previously reported a single element Maxwell model was used to fit the stress relaxation constants[70]. Frequency sweep was performed at 1% strain from 0.5 to 10 Hz to study the change in moduli in response to increasing frequency. Creep and recovery test was also performed. All samples were initially stressed at 10 Pa and relaxed for 2 minutes followed by a strain recovery test. In the strain recovery test the applied stress was removed and strain was monitored over time. A four element Maxwell-Voight model was used to fit the relaxation constant as previously performed[206]. A stress strain curve was generated by getting the corresponding stress value at a given strain.

5.2.7 Second Harmonic Generation and Reflective Microscopy

In order to study collagen fibers in collagen gels reflective microscopy was used. Images were collected using a LSM 780 (Zeiss) microscope. A 40x oil immersion objective was used to capture the images and were configured to use the 405 nm light to illuminate and be collected to visualize the collagen fibers. Second harmonic generation (SHG) microcopy was carried out with a LSM 510 (Zeiss) microscope equipped with a Chameleon Ultravision II Laser Module (Coherent). A wavelength of 810 nm was used to image H and E slides of tumors and light was collected at 488 nm wavelength. For

examining collagen in the murine tumors, H and E slides were imaged using SHG microscopy.

5.2.8 **Collagen Fiber Morphology, Orientation, and Cell Aspect Ratio Analysis**

Collagen fiber orientation was adapted from a previously developed method using MATLAB (Mathworks)[70]. Collagen fiber width and length were analyzed using a previously established method[70]. The software segments the image and calculates intensity gradients within subregions of images and uses them to track the overall directions of fibers. To study cell aspect ratio, code was developed to fit an ellipse around the cell and the aspect ratio is the ratio of the major to minor axis.

5.2.9 **Scanning Electron Microscopy**

Collagen hydrogels, with and without cells, were fixed as previously described and processed for conventional scanning electron microscopy[207].

Briefly, dime-size gels were fixed in 100mM cacodylate buffer, pH 7.4, containing 3% formaldehyde, 1.5% glutaraldehyde, and 2.5% sucrose for 1 hr, washed, and osmicated at 4˚C in Palade's fixative containing 1%OsO_4. Cells were then dehydrated through a graded series of ethanol; critical point dried using a Tousimis Model 795 critical point dryer (Rockville, MD); and coated with 4nm platinum using a Anatech Hummer 6.1 sputter coater (Hayward, CA). Samples were imaged in an FEI Quanta 200 ESEM (Hillsboro, OR) using the Everhart-Thornley secondary electron detector at 1.2keV under high vacuum.

5.2.10 **Transmission Electron Microscopy**

Collagen hydrogels, with and without cells, were fixed as previously described[207]. Briefly, for conventional electron microscopy (EM), gels were fixed in 100mM cacodylate buffer, pH 7.4, containing 3% formaldehyde, 1.5% glutaraldehyde, and 2.5% sucrose for 1 hr, washed; and osmicated at 4˚C in Palade's fixative containing 1%OsO_4. Cells were then washed; en bloc stained with Kellenberger's uranyl acetate over night; dehydrated through a graded series of ethanol; and subsequently embedded in epon. 80nm sections were cut on a LEICA UCT ultramicrotome;collected onto 300 mesh formvar/carbon coated grids; and post-stained in uranyl acetate and lead citrate. . Images were recorded using a Soft Imaging System Magaview III camera mounted on a Tecnai 12 TEM operating at 100keV; and figures were assembled in Adobe Illustrator.

5.2.11 **RT-PCR**

A quantitative real-time RT-PCR assay was used to assess gene expression. Total RNA was extracted from cells encapsulated in hydrogels with TRIzol (Invitrogen) in accordance with manufacturer instructions. Hydrogels were placed in 500 μL of TRIzol and homogenized with a microhomogenizer. The suspension was then centrifuged at 12,000 x g for 15 min and the supernatant was separated. 100 μL of chloroform was mixed with the solution by manual agitation for 20 s and the mixture was centrifuged at 12,000 x g for 10 min. The supernatant was isolated and mixed with 250 μL isopropyl alcohol and kept at -4 °C for 1 h. The precipitates were separated by centrifugation at 7,500 x g for 5 min and washed with 70% ethyl alcohol. Total RNA was quantified using an UV spectrometer and validated by lack of DNA contamination. One microgram of RNA was transcribed using reverse-transcriptase M-MLV and oligo(dT) primers (both

from Promega), according to the manufacturer's instructions. TaqMan Universal PCR MasterMix and Gene Expression Assay (Applied Biosystems) was used according to the manufacturer's instructor for PLOD2, MMP2, MMP9 and HPRT1.

5.2.12 **TCGA Analysis**

Gene Expression Profiling Interactive Analysis (GEPIA)[208] was used to generate survival curves as well as study trends in RNA-sequence data, based of querying the cancer genome atlas database. GEPIA also generated and provides all the statistics.

5.2.13 **Generation of GpNLuc KIA stable cell lines**

KIA cells (70% confluent) were transfected with pRetroX-Tight-MCS_PGK-GpNLuc (Addgene plasmid #70185) using Lipofecatime 2000 (Thermofisher scientific) in serum free medium as per the manufacturer's instructions. Mixed populations were then FACS sorted for high GFP signal using a Sony Biotechnology SH-800 'chip' cell sorter at one cell per well in a 96 well plate. Stably expressing clonal populations were then utilized for downstream experiments.

5.2.14 **In-vivo and IVIS Imaging**

KIA cells, expressing GFP or GpNLuc that were encapsulated in quick and slow stress relaxation hydrogels as reported above, were subcutaneously implanted in 8-10 week in nude mice. Caliper measurements were performed to track subcutaneous tumor growth. The volume of the tumor was calculated using the following equation:

$$V = \frac{1}{2} * L * W^2$$

where V is the volume of the tumor, L is the major axis, and W is the minor axis of the tumor [143]. In addition to caliper measurements mice were injected intraperitoneally

with 20 μg/mL of furimazine followed by luminescence imaging with IVIS Spectrum (PerkinElmer) within 5 minutes of injections. Average radiance (photons per second per centimeter squared per steradian) was monitored at each time point and tumor.

5.2.15 **Histology and Immuno-fluorescent Staining**

For murine tissue, following fixation the tissue was dehydrated with serial ethanol (70%-100%); embedded in paraffin; 5 μm sections were cut; and subsequently treated with hematoxylin and eosin (H and E) stain, mason trichrome, or PLOD2. Immunofluorescent stains were performed as previously reported on gels[205]. SMAD2 (Proteintech), vinculin (Sigma), phaloidin, and YAP (SantaCruz) were all used at a 1:200 dilution and counterstained with DAPI. An anti-rabbit Alexa Fluor 564 (Life Technologies) was used at 1:500 dilution and imaged with Zeiss LSM 780 or LSM 800 microscope. PLOD2 (Proteintech) was also used at 1:200 dilution for histology sections.

5.2.16 **Histological, SEM, TEM, and Immuno-fluorescent Quanitificaiton**

Histology stains were quantified as previously reported[209]. In short background was taken from an empty portion of the slide, the color deconvolution plug-in ImageJ (National Institutes of Health) was used to extract the DAB color of the image. Finally, the mean intensity was calculated from the DAB intensity over the entirety of the image.

SEM images cells moving through the hydrogel were analyzed using ImageJ. The pore area was measured by drawing a region of interest over the pore. ImageJ was also used to measure the bands in TEM images of the collagen fibers.

For SMAD2 quantification IMARIS (Bitplane) was used to find the colocalization of SMAD2 and DAPI from a z stack of the cells. Surface area of the colocalization channel was then calculated using the surface package in IMARIS.

5.2.17 **Statistical Analysis**

Statistical analysis was performed using MATLAB (Mathworks, Inc), or Prism 4 (GraphPad Software, Inc.) to calculate the mean, standard deviation, and standard error mean. T test and one way ANOVA were perfumed where appropriate to determine significance (GraphPad). All experiments were performed in triplicate.

5.3 *Results and Discussion*

5.3.1 **Design of Stress Relaxation Collagen Gel**

Collagen gels have been a standard platform for cancer cell research and migration for many years[70, 177, 201]. Recently, we have explored how to create complex hypoxic collagen gel scaffolds in order to explore the roll that fiber density plays on sarcoma cell migration[70]. In the previous version of the platform, stress relaxation time was the one difference between the low and high fiber density hypoxic gels; with the low fiber density having a slower stress relaxation time as compared with the high fiber density. In the present study, we explored the effect of stress relaxation, independently of collagen fiber density and architecture, on cell migration in oxygen gradients.

Briefly, to establish the hypoxic hydrogel, we balance the diffusion coefficient of the material, boundary conditions, and cell concentration. Collagen was chosen due to its low oxygen diffusion coefficient[70]; polystyrene was chosen as well due to its low oxygen diffusion coefficient; and the cell concentration was chosen to balance the oxygen diffused in from the media. To control the collagen fiber density, the collagen solution was kept at 4°C for two hours[70]. This allows for collagen fibers to aggregate without crosslinking. In order to initiate crosslinking, gels were formed at 37°C. This allows for the collagen fibers to entangle and the hydrogel to be formed. Once the hydrogel structure was established, microbial transglutaminase was used to crosslink further crosslink collagen fiber bundles. 24 mg/mL microbial-transglutaminase (mTG) was chosen to allow for crosslinking of collagen fibers as a means to change stress relaxation without changing the stiffness of the hydrogel scaffold (**Figure 5-1A-C**). Consequently,

the stress relaxation time coefficient decreased by a half order of magnitude (**Figure 5-1B-C**)**.** The stress relaxation was also verified using a creep and stress; and relaxation test (**Supplementary Figure 5-1A-B**); and a similar decrease in stress relaxation was observed. Furthermore, the different hydrogels response to frequency was evaluated to explore a difference in slope, which is correlated with differences in stress relaxation (**Supplementary Figure 5-1C-D**). Finally, to fully characterize the material properties, the stress versus strain curve was plotted to determine the differences in hydrogel properties that result from a change in stress relaxation (**Supplementary Figure 5-1E**).

In order to further characterize the hydrogel scaffold, reflection microscopy, scanning electron microscopy (SEM), and transmission electron microscopy (TEM) were performed on the mTG hydrogel and the control. From reflective microscopy, TEM, and SEM results, no visible difference between the two hydrogel structures can be detected (**Figure 5-1D**). Additionally, TEM revealed no significant difference in the light and dark segments of the collagen fibers (**Figure 5-1D-E**). We thus conclude, from these analyses, that there is no significant structural difference in the mTG hydrogel and the control.

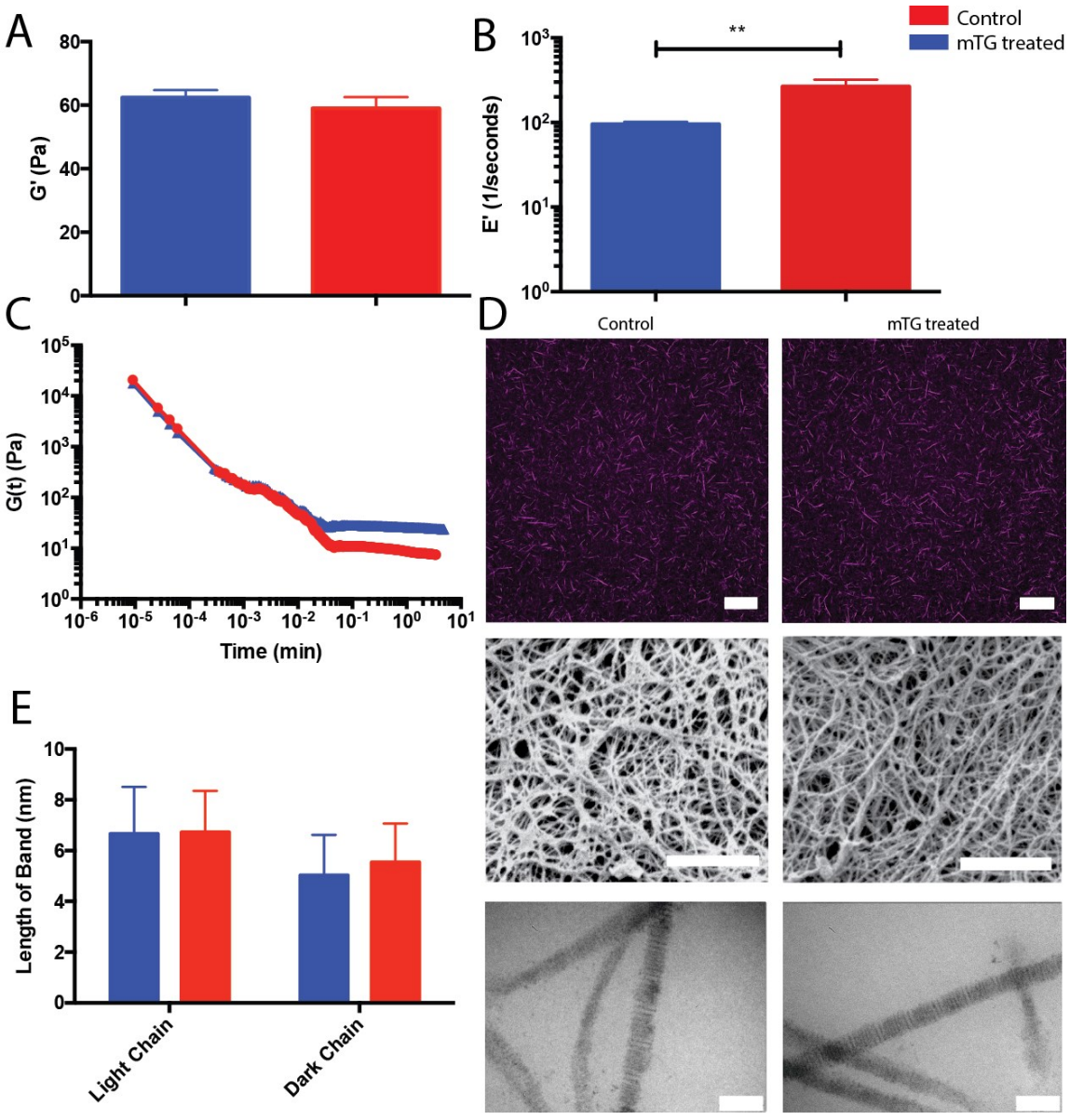

Figure 5-1: Material properties of collagen stress relaxation gels.
A.) Stiffness of the two hydrogels are the same, while the stress relaxation time (B,C) quickens with the addition of mTG. D.) Reflection, scanning electron microscopy (SEM), and transmission electron microscopy (TEM) displayed no difference in the structure of the hydrogels with the addition of mTG. E.) The length of the light and dark chains from the TEM images to demonstrate no difference in the light and dark chain length of the fibers.

5.3.2 **Morphology and Migration of Cells in the Stress Relaxation Hydrogels**

Having established the hydrogel platform, the influence of stress relaxation on sarcoma cell migration was explored in both hypoxic and non-hypoxic gradients. This was investigated using KIA cells, a mouse undifferentiated pleomorphic sarcoma line. KIA cells (**Figure 5-2A**) displayed an increase in the cell spreading in both hypoxic and atmospheric mTG gels. The hypoxic gradient was measured for both cell lines in the collagen gels on day 3 (**Figure 5-2B**). Further analysis of the cell morphology displayed an increase in the aspect ratio of cells in the quicker stress relaxation conditions, such as the mTG hypoxic conditions (**Figure 5-2C**). We have previously demonstrated that a large aspect ratio is consistent with a more migratory cells phenotype[70].

KIA cell were tracked on day 3 of culture using IMARIS and MATLAB. From this analysis, there is a minimal increase in cell migration for the KIA cells in atmospheric conditions (**Figure 5-2D**). In the hypoxic gradient, however, there is a slight increase in the cell migration in the x and y directions, but a significant increase in the z direction in the mTG gels (**Figure 5-2E**); and there were minimal changes in the instantaneous cell velocities in the different conditions (**Supplementary Figure 5-2A-B**). In addition, the fiber alignment was analyzed using previously established methods[70] (**Supplementary Figure 5-2C**). From this analysis, a slight increase in fiber density was detected in the control gels, specifically in the hypoxic conditions.

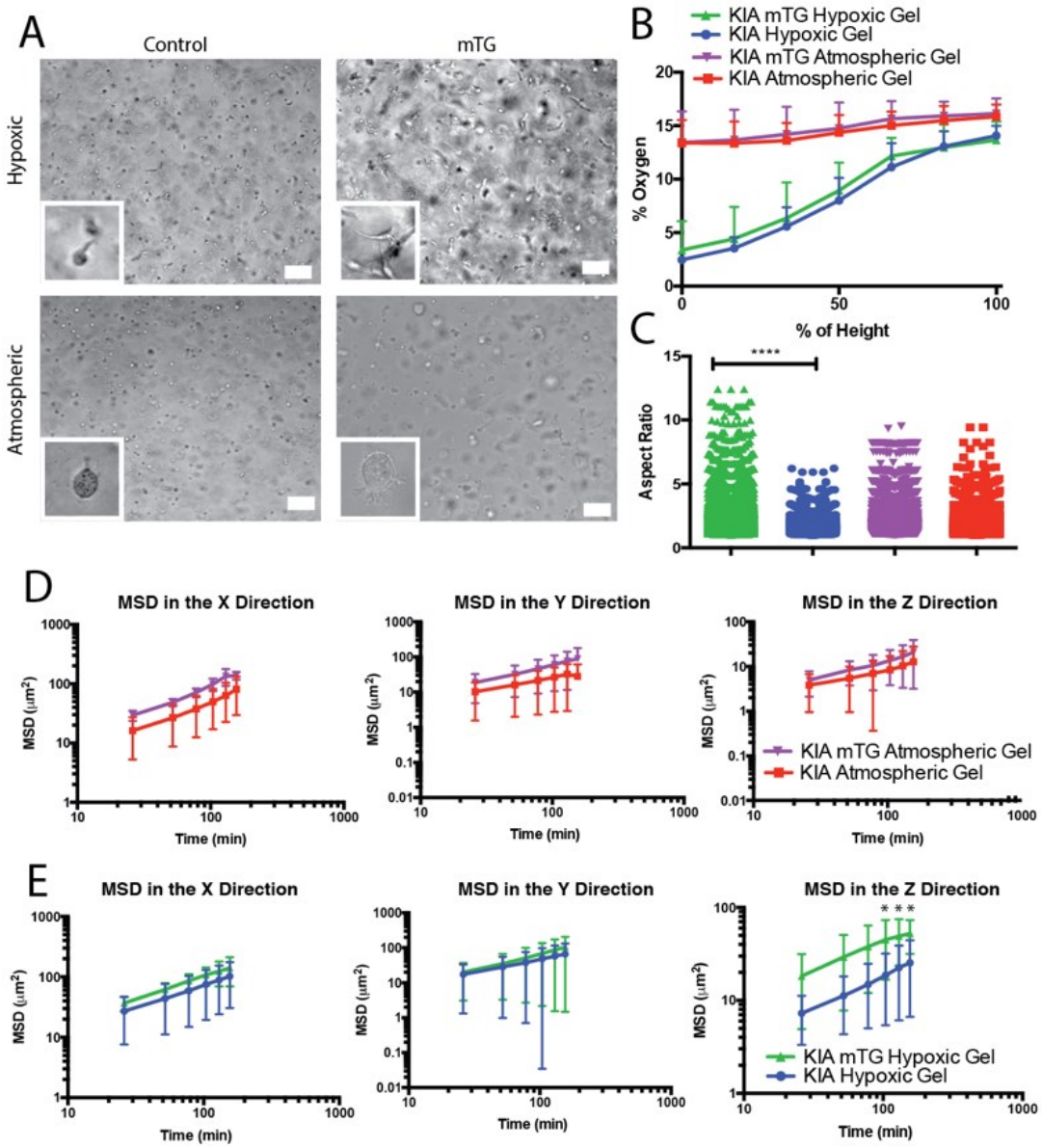

Figure 5-2: Sarcoma cell migration increases with the quicker stress relaxation time in hypoxia.
A.) Representative photos of the KIA cells in hypoxic and atmospheric hydrogels with two different stress relaxations. B.) Oxygen gradients on day three for the hypoxic and atmospheric hydrogels with KIA cells. C.) The aspect ratio of the KIA cells D.) Migration of KIA cells in the atmospheric hydrogels on day 3 displaying minimal difference in migration. E.) Migration of the KIA cells in hypoxic hydrogel on day 3.

5.3.3 **PLOD2 Increase in mTG Gels**

In order to better understand the cause for an increase in cell migration, cellular response in mTG gels was investigated. It has been demonstrated that TGF-β signaling initiates SMAD2/3 nuclear localization and has been linked to an increase in collagen cross-linkers, such as procollagen-lysine,2-oxoglutarate 5-dioxygenase 2 (PLOD2) [210-212]. Specifically, in breast cancer TGF-β and SMAD2/3 have been linked to cell mechano-sensing and in stiffer matrixes there is an increased in the expression of SMAD2/3 [213]. In pancreatic cancer TGF-β increase leads to more migratory cells[214] and induced epithelial to mesenchymal transition in cervical cancer as well an increase in patient mortality[215]. In order to explore TGF-β and SMAD2/3 signaling the different hydrogels were stained for SMAD2 to observe nuclear localization (**Figure 5-3A**). Using 3D images of cells the surface area SMAD2 at nucleus was calculated. There is a significant increase in SMAD2 localization in the mTG hydrogels. From this increase in SMAD2 we sought to explore the increased effect of PLOD2 signaling. From previously published works, procollagen-lysine,2-oxoglutarate 5-dioxygenase 2 (PLOD2) has been demonstrated to be a key factor in sarcoma cell migration, especially in hypoxia[40, 59]. Using PCR an increase in PLOD2 expression was observed in the mTG gel, both in hypoxia and atmospheric conditions as well as in the control hypoxic gel (**Figure 5-3B**). The increase in PLOD2 expression in the hypoxic condition is similar to what we have previously demonstrated[40, 59]. In addition the increase in the mTG atmospheric condition is similar to what was observed in other cells lines that have increased TGF-β signaling[210]. In the mTG hypoxic gels we observe a combinatory effect TGF-β and hypoxia yielding a threefold increase in PLOD2 expression (**Figure 5-3C**). In order to

confirm that the PLOD2 expression is linked to TGF-β signaling in the mTG treated gels, PCR was performed (**Figure 5-3C**). mRNA expression of the mTG hypoxic gel returned to the same level as the control hypoxic gel and the mTG atmospheric gel had similar PLOD2 expression as the control atmospheric gel. This demonstrates that the increase in PLOD2 is due to TGF-β.

Furthermore, to explore confounding factors, there was no difference in the number of vinculin spots, indicative of focal adhesions (**Supplementary Figure 5-3A**). This indicated that the cell interaction with the matrix is relatively the same amongst all four conditions. The amount of actin fibers present was also the same in all four conditions (**Supplementary Figure 5-3A**). Actin rearrangement and localization has been demonstrated as a factor in mechanotransduction pathways[216]. Finally, to study mechanical sensing via the yes-associated protein (YAP) pathway, immunofluorescent imaging was performed. YAP has been observed as a key molecule in cell mechano-sensing when localized to the nucleus[217]. However, in our study YAP localization was present only in the cytoplasm in all four conditions (**Supplementary Figure 5-3A**) displaying that it is not active; this is most likely due to the fact that the hydrogels are roughly 100 Pa (**Figure 5-1A**).

To explore at the consequences from the increase in PLOD2 expression, SEM images of mTG and control hypoxic gels to explore how the cells interact or pull on the matrix. From these images, we demonstrate that the cells are creating larger pores in the mTG treated gels (**Figure 5-3D**). This is most likely due to the cells pulling on the fibers. To confirm that the pathway was not protease mediated, PCR was performed to explore the MMP2 and MMP9 activity (**Supplementary Figure 5-4A**). From this data, we display

no significant difference in MMP2 mRNA expression. In order to confirm whether there was a difference in protease activity amongst the different conditions at the protein level a DQ collagen assay was performed. There was no difference in the normalized RFU values, which correlates to protease secretion, amongst all four conditions (**Supplementary Figure 5-4B**). Using fluorescent microscopy, the study displayed minimal differences in the localization of the proteases, with the majority of protease localization amongst the circular cells in the gels (**Supplementary Figure 5-4C**).

To further explore the cell behavior change due to an increase of PLOD2 a variety of tracking studies were performed with a PLOD2 knockdown line as well as normal KIA cells treated with minoxidil[40, 59] or TGF-β inhibitor. From these experiments, we observed no difference in the migration of the KIA cells in hypoxic gradients in the z direction when PLOD2 was knockdown or inhibited specifically with minoxidil (**Figure 5-3E**). It was also observed that these studies dropped the migration speeds below the hypoxic control gel. In addition, when TGF-β inhibitor was added the mTG hydrogel and control hydrogel ended up having the same MSD trend as the untreated control hypoxic gel (**Figure 5-3E**) This demonstrates that the increase in migration in the mTG gels is from an increase in PLOD2 caused by TGF-β stimulation. From these results, there is a clear correlation with PLOD2 expression and stress relaxation, and the combinatory increase in hypoxic gradients.

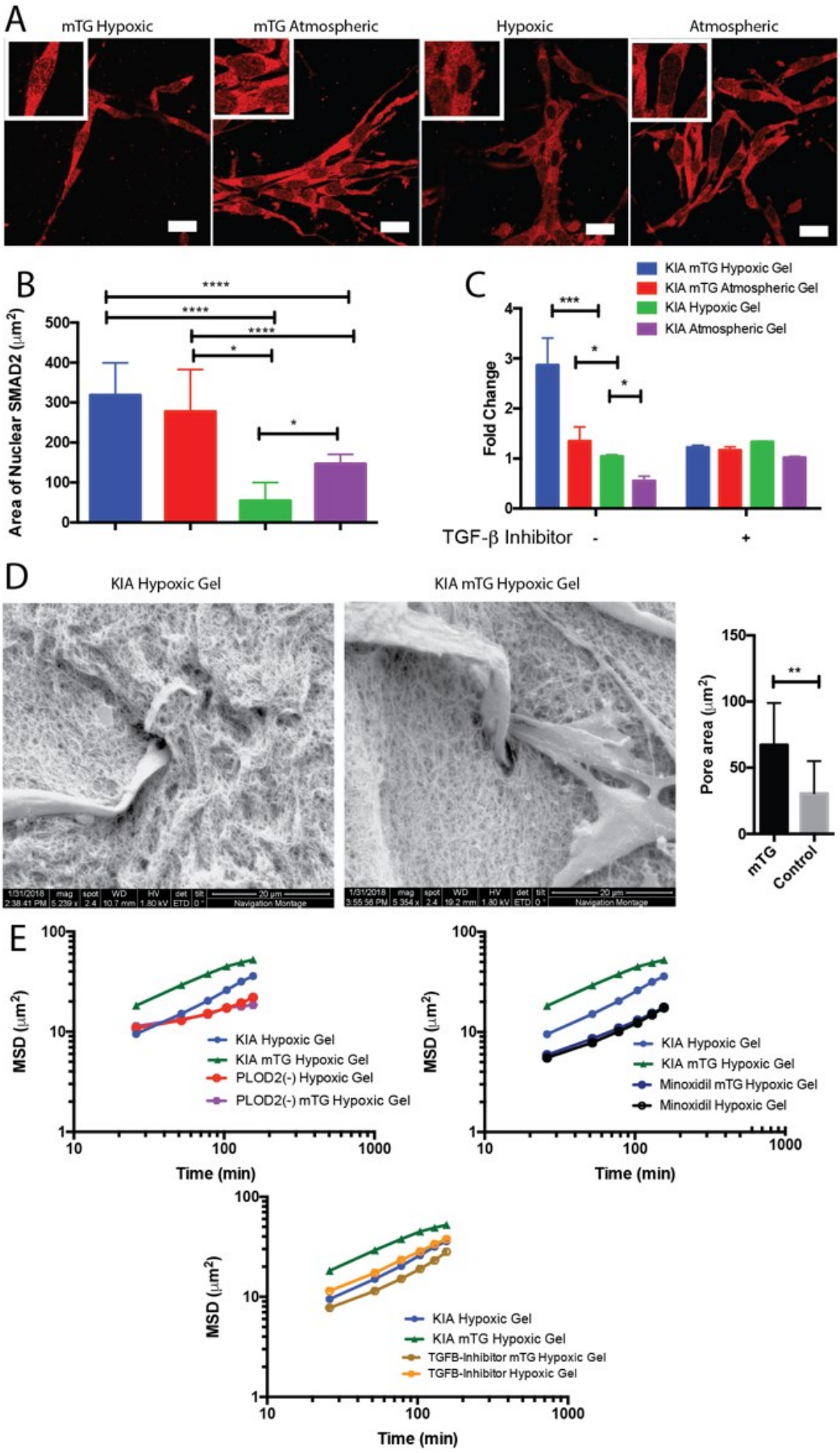
A
mTG Hypoxic
mTG Atmospheric
Hypoxic
Atmospheric
B
Area of Nuclear SMAD2 (μm²)
C
KIA mTG Hypoxic Gel
KIA mTG Atmospheric Gel
KIA Hypoxic Gel
KIA Atmospheric Gel
Fold Change
TGF-β Inhibitor
D
KIA Hypoxic Gel
KIA mTG Hypoxic Gel
Pore area (μm²)
mTG
Control
E
MSD (μm²)
Time (min)
KIA Hypoxic Gel
KIA mTG Hypoxic Gel
PLOD2(-) Hypoxic Gel
PLOD2(-) mTG Hypoxic Gel
Minoxidil mTG Hypoxic Gel
Minoxidil Hypoxic Gel
TGFB-Inhibitor mTG Hypoxic Gel
TGFB-Inhibitor Hypoxic Gel

Figure 5-3: Biochemical and Biomechanical ques from stress relaxation hydrogels (A).SMAD2 nuclear localization in KIA cells cultured in mTG and control hydrogel sin hypoxic and atmospheric conditions. (B). Quantification of SMAD2 localization to nucleus. (C). PLOD2 expression of KIA cells treated with and without TGF-β inhibitor. (D). SEM images of the KIA cells cultured mTG and control hypoxic gels, characterizing the pore size that cells migrate through. (E).Means squared displacement in the z direction of KIA cells in hypoxic mTG and control gels treated having PLOD2(-).

5.3.4 Stress Relaxation Hydrogel Leads to Increase in Tumorigenesis

In order to recapitulate the importance of PLOD2 in an animal model, mTG and control hydrogels were implanted subcutaneously (**Figure 5-4A**). KIA cells transfected with a bioluminescent resonance energy transfer (BRET) reporter was used for all in-vivo experimentation[218]. Tumors were allowed to grow for up to 20 days before euthanasia, and monitored using IVIS imaging (**Figure 5-4B**), displaying enhanced fluorescent signal over time in mTG gels compared to the control gels. This was also correlated with an increase in tumor volume (**Figure 5-4C**).

With the increase in tumor size we decided to study the collagen fiber architecture in the tumor using second harmonic generation (SHG) microcopy (**Figure 5-4D**). The images indicate a dramatic increase in collagen secretion in the tumors (**Figure 5-4E**). In addition, images were analyzed using ct-FIRE code suite[185], which allows for the analysis of multiple parameters of collagen fibers, such as width and length. Using images taken of the mTG and control tumors we detected an increase in collagen fiber width and length in the mTG tumors (**Figure 5-4E**). This increase in collagen density is similar to what has been previously demonstrated (Eisinger et al) when PLOD2 is modulated[40]. To confirm the increase in collagen expression mason trichrome was performed and there is an increase in collagen fibers in tumors grown from mTG hydrogels (**Figure 5-4F)**. Finally, day 20 tumors were stained for PLOD2 (**Figure 5-4G**).

Using a previously established method[209] PLOD2 intensity was calculated. There was a significant increase in PLOD2 expression in mTG tumors. This in-vivo work demonstrates how the quicker stress relaxation and increase in PLOD2 expression increases tumorigenesis.

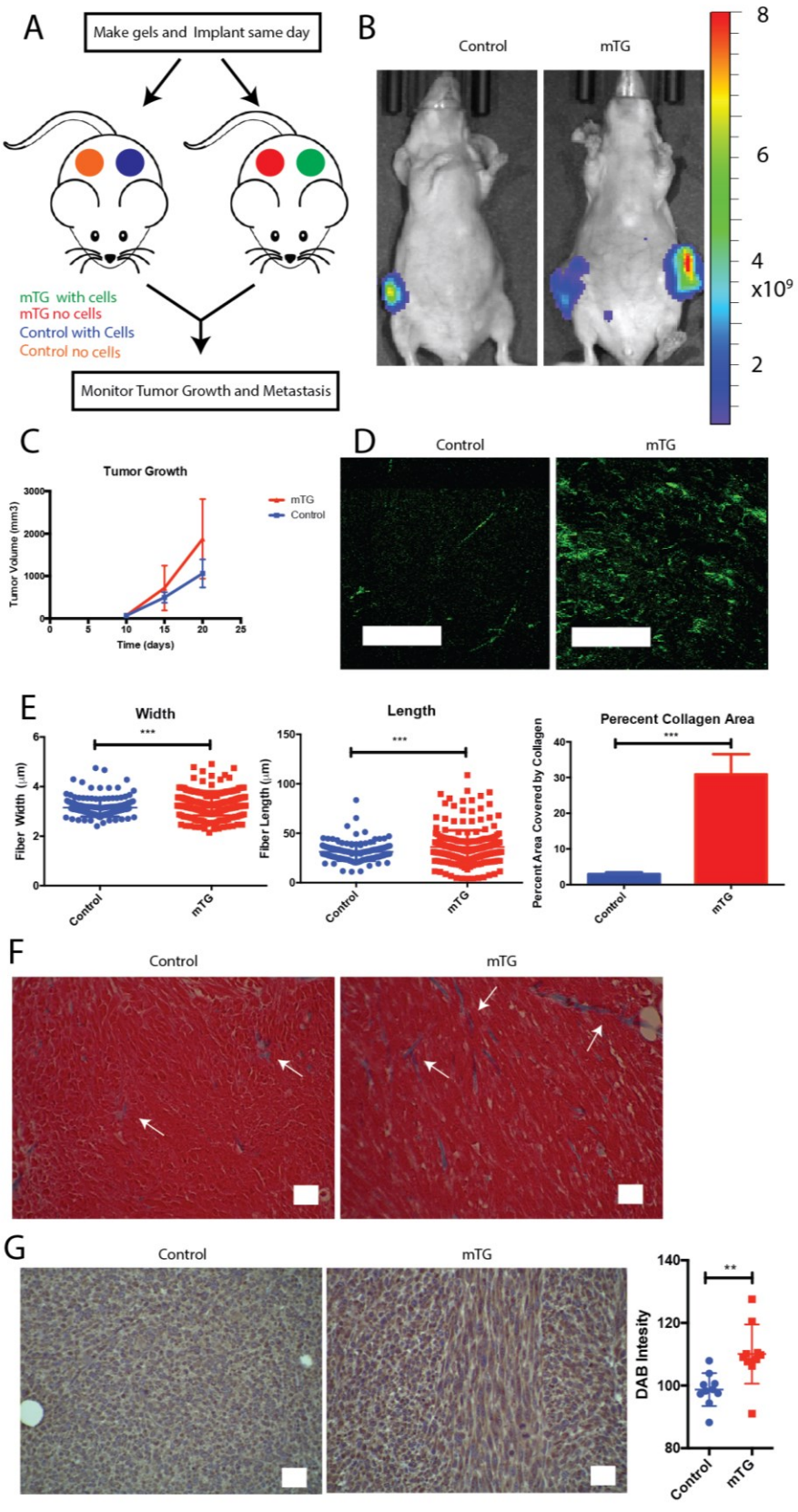
A
Make gels and Implant same day
mTG with cells
mTG no cells
Control with Cells
Control no cells
Monitor Tumor Growth and Metastasis
B
Control
mTG
8
6
4
x10^9
2
C
Tumor Growth
Tumor Volume (mm3)
Time (days)
mTG
Control
D
Control
mTG
E
Width
Fiber Width (μm)
Length
Fiber Length (μm)
Perecent Collagen Area
Percent Area Covered by Collagen
Control
mTG
F
Control
mTG
G
Control
mTG
DAB Intesity
Control
mTG

Figure 5-4: Tumor growth and collagen express in quicker stress relaxation tumors (A). Schematic of in-vivo experiments, by subcutaneously implanting hydrogels. (B) IVIS imaging was used to image tumor growth and cell density via a BRET reporter and fluorescent intensity (unit is in radiant efficacy). (C) Tumor volume was measured to track the growth of mTG and control tumors. (D) Second harmonic generation microscopy was used to study collagen fiber density in day 20 tumors. (E). ct-FIRE analysis was used to analyze collagen fiber width, length, and percent collagen area. (F). Mason trichrome stain for day 20 tumors grown from gels implanted subcutaneously. The arrows are pointing to collagen fibers in the sections. (G). PLOD2 stain of day 20 tumors. DAB intensity was quantified displaying more PLDO2 expression in the mTG tumors.

5.3.5 **TCGA Analysis and Patient Relevance of High PLDO2 Expression**

To study the clinical significance of PLOD2 expression in sarcoma, the cancer genome atlas (TCGA) database was queried to study survival rates as well as correlations from patient RNA-seq data. 261 patients were queried and the results were pooled using GEPIA to generate RNA-seq correlations, disease free survival, and overall survival[208]. Firstly, we explored the correlation between upregulation of SMAD2, TGF-β, and hypoxia inducible factor 1-alpa (HIF1-α) with PLOD2, and a significant Pearson correlation between the each of the two genes in sarcoma patients (**Figure 5-5A**). HIF1-α is one of the key factors that is up-regulated in hypoxia[219]. This is expected given our previous results displaying the effect of hypoxia on PLOD2 expression[40, 59]. Additionally, we also observed a correlation between PLOD2 and SMAD2 as well as PLOD2 and TGF-β. This was expected based off of the data in Figure 3. Secondly the disease-free survival data was queried and graphed (**Figure 5-5B**). When SMAD2 TGF-β, or HIF1-α expression was used to segment survival data there was no significant change in mortality and disease-free survival. However, when PLOD2 expression was used partition survival data there is a significant decrease in survival with and upregulation of PLOD2. Finally, when overall survival was explored there was a significant increase in mortality rates of patients from 40% for low expressing PLOD2 to 20% for high expressing PLOD2 (**Figure 5-5B**).

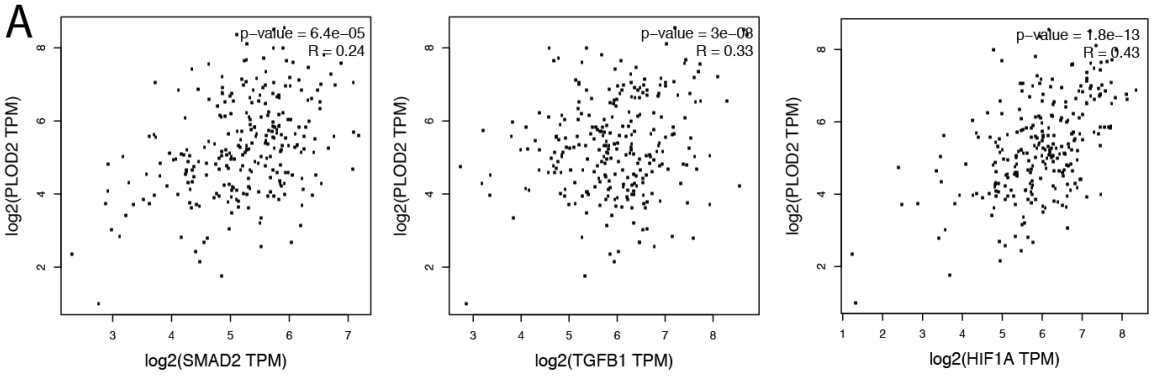
A
p−value = 6.4e−05
R = 0.24
log2(PLOD2 TPM)
log2(SMAD2 TPM)
p−value = 3e−08
R = 0.33
log2(PLOD2 TPM)
log2(TGFB1 TPM)
p−value = 1.8e−13
R = 0.43
log2(PLOD2 TPM)
log2(HIF1A TPM)

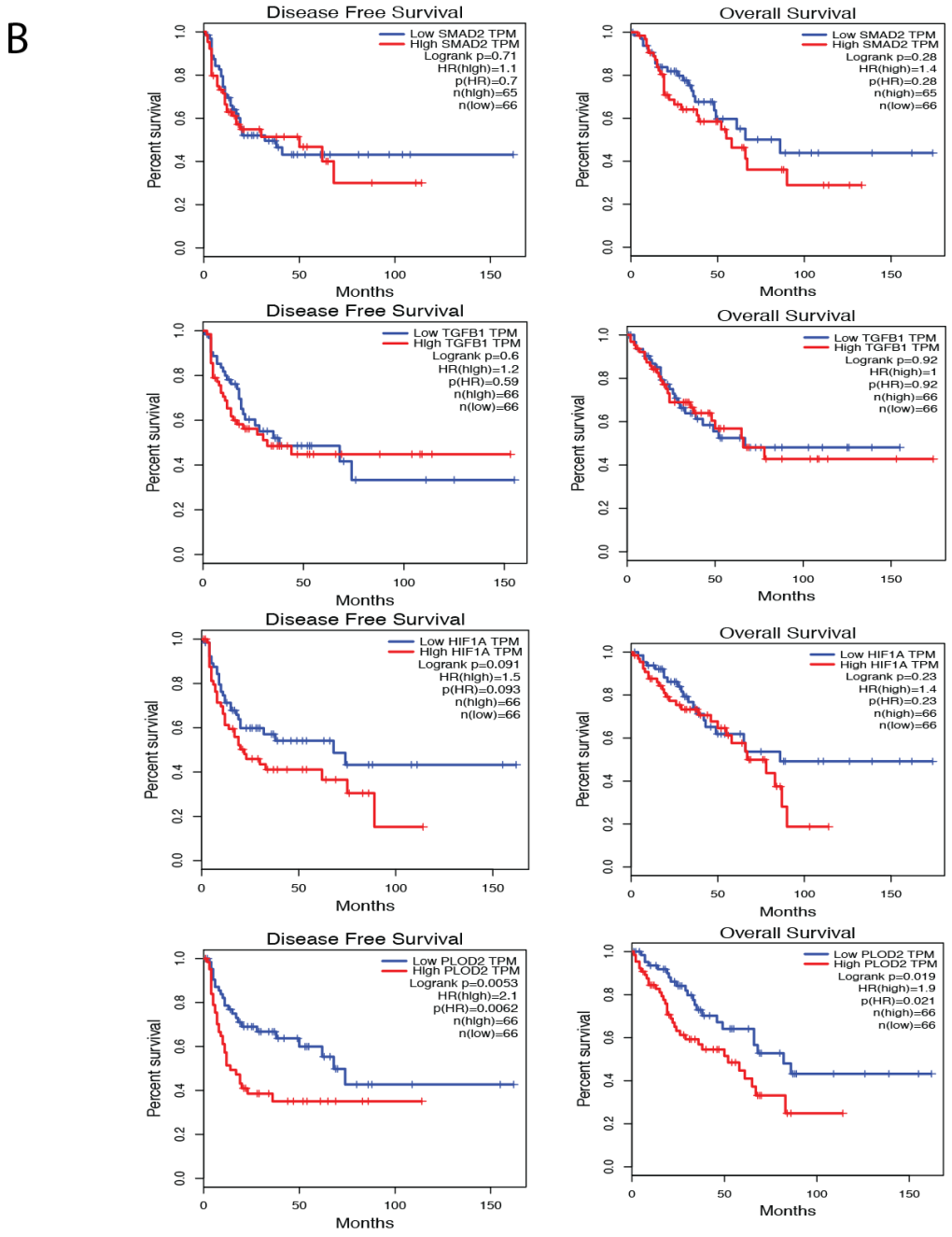
B
Disease Free Survival
Low SMAD2 TPM
High SMAD2 TPM
Logrank p=0.71
HR(high)=1.1
p(HR)=0.7
n(high)=65
n(low)=66
Overall Survival
Low SMAD2 TPM
High SMAD2 TPM
Logrank p=0.28
HR(high)=1.4
p(HR)=0.28
n(high)=65
n(low)=66
Disease Free Survival
Low TGFB1 TPM
High TGFB1 TPM
Logrank p=0.6
HR(high)=1.2
p(HR)=0.59
n(high)=66
n(low)=66
Overall Survival
Low TGFB1 TPM
High TGFB1 TPM
Logrank p=0.92
HR(high)=1
p(HR)=0.92
n(high)=66
n(low)=66
Disease Free Survival
Low HIF1A TPM
High HIF1A TPM
Logrank p=0.091
HR(high)=1.5
p(HR)=0.093
n(high)=66
n(low)=66
Overall Survival
Low HIF1A TPM
High HIF1A TPM
Logrank p=0.23
HR(high)=1.4
p(HR)=0.23
n(high)=66
n(low)=66
Disease Free Survival
Low PLOD2 TPM
High PLOD2 TPM
Logrank p=0.0053
HR(high)=2.1
p(HR)=0.0062
n(high)=66
n(low)=66
Overall Survival
Low PLOD2 TPM
High PLOD2 TPM
Logrank p=0.019
HR(high)=1.9
p(HR)=0.021
n(high)=66
n(low)=66
Percent survival
Months

Figure 5-5: TCGA Data:
(A). RNA-seq correlation of TCGA data of expression of SMAD2, TGF-β, HIF1-α with PLOD2 (B) Disease free survival and overall survival of patients from TCGA database displaying no difference in survival in relation to the expression of SMAD2, TGF-β, or HIF1-α and increase in survival with lower expression of PLOD2.

To further confirm the TCGA data we explored the ability for the mTG hydrogel platform to explore the response of primary patient undifferentiated pleomorphic sarcoma cells (hUPS). In the different hydrogels, we observed distinct phenotypes in the different gels (**Supplementary Figure 5A**). The oxygen profiles in the gels on day 3 were similar to the KIA cells (**Supplementary Figure 5B**). We also observed an increase in aspect ratio in the more migratory cells (**Supplementary Figure 5C**). Finally, when the migration was studied, there is no difference in the atmospheric conditions (**Supplementary Figure 5D**), but there was a significant increase in migration in the mTG hypoxic gel condition compared to the control hypoxic gel in the z direction (**Supplementary Figure 5E**). There was no difference in the velocity and fiber alignment of hUPS cells in the hydrogels (**Supplementary Figure 6A-C**). From this data we can demonstrate the predictive power of our platform to explore a more migratory phenotypes in primary human samples.

5.3.6 **Proposed Biological Response to Quicker Stress Relaxation Hydrogels**

From our above study we propose a mechanism for cellular response to quicker stress relaxation (**Figure 5-6**), in which hypoxia induces PLOD2 expression via HIF1-α upregulation. This increase in crosslinking yields a quicker stress relaxation of matrix which in turn stimulates TGF-β and therefore SMAD2 nuclear localization which causes an additional increase in PLOD2 expression.

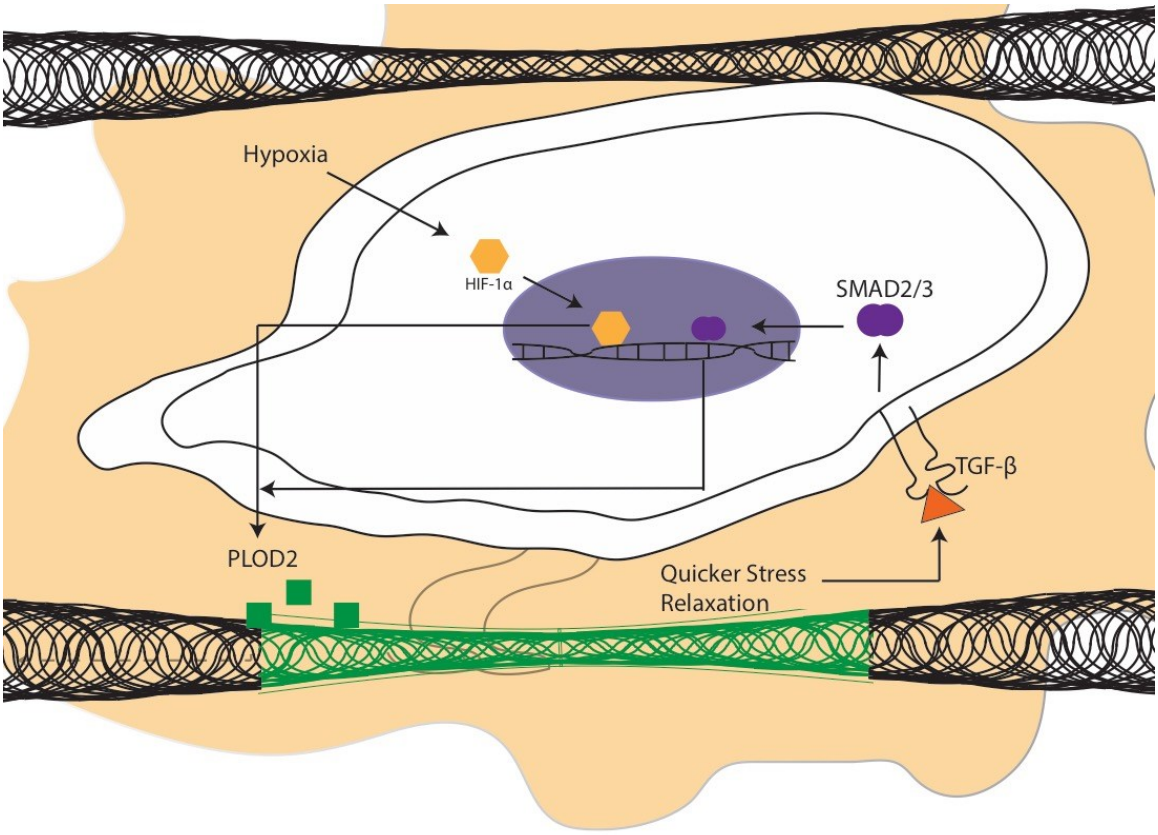

Figure 5-6: Proposed biological response to quicker stress relaxation: HIF1-α upregulation due to hypoxia increases PLOD2 expression causing a quicker stress relaxation which in turn additionally upregulates PLOD2 via TGF-β and SMAD2.

5.4 *Conclusion*

The current study demonstrates the importance of stress relaxation as a new potential mechanical property that should be further explored in cancer research. The novel collagen hypoxic hydrogel platform was used to explore this mechanical property. The platform allows us to control oxygen and stress relaxation without altering the micro and nano-scale collagen fiber architecture, allowing us to create a truly in vivo mimicking platform to study finite properties of the tumor micro-environment. From our studies, we observed an increase in sarcoma cell migration specifically in hypoxia. The cells in the

hypoxic hydrogels, with the quickest stress relaxation, had the greatest mean squared displacement, as well as a more elongated phenotype and aspect ratio.

In order to explore the molecular mechanisms behind the faster cell migration, we were able to deduce that the quicker stress relaxation increased PLOD2 expression in cells via TGF-β and SMAD2. This increase in PLOD2 had an additive effect when coupled with hypoxia. When the quicker stress relaxation hydrogels were implanted into a mouse, there was an increase in tumor cell growth, collagen secretion, and PLOD2 expression. The collagen fibers that were secreted were also wider and longer then the control gels. The clinical relevance of these observation was determined by querying publically available TCGA global expression data. TCGA data was queried using GEPIA there was a direct correlation with PLOD2 expression and TGF-β, SMAD2, or HIF1-α in patient samples; as well as a dramatic decrease in patient survival in patients who had increased expression levels of PLOD2. Finally, using this new hypoxic collagen gel platform the response of primary patient hUPS cells was displayed to be similar to what was predicated using the KIA line, demonstrating the ability for this platform to screen future therapeutics to minimize cancer progression. This is one of the first studies to study the effect of stress relaxation in regard to tumor growth and metastasis in a truly in vivo mimicking system. This platform can further be adapted to explore stress relaxation in oxygen gradients as they effect other cancers.

5.5 *Supplementary Figures*

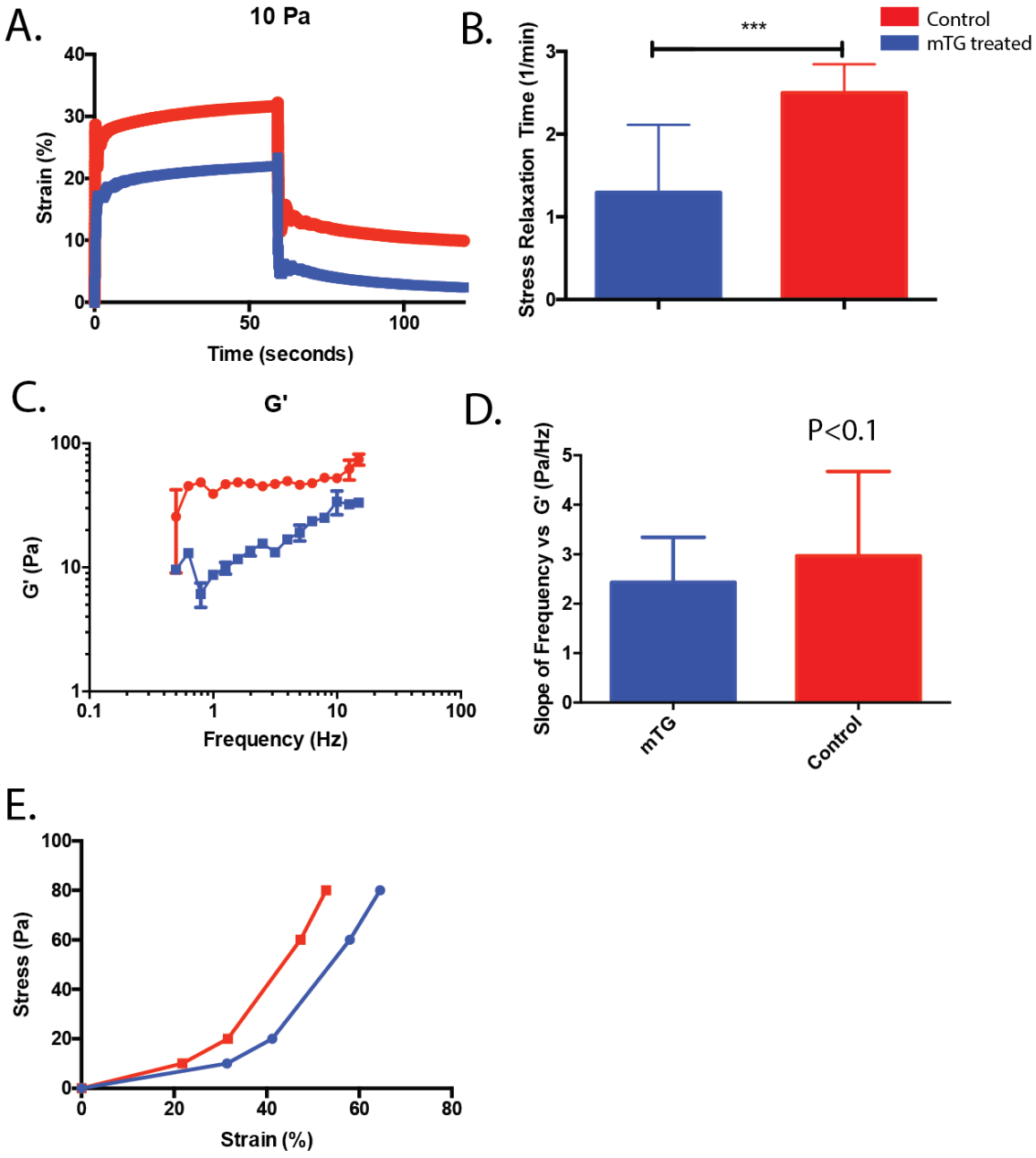

Supplementary Figure 5-1: Additional Mechanical Characterization of Hydrogel A.) Creep and recovery test was performed to *demonstrate* the relaxation time of the material after a constant stress was applied. B.) The relaxation time was calculated from the creep and recovery tests. C.) A frequency sweep was performed on the hydrogels and the slope (D) of the line was calculated showing a difference in slope between the two materials. D.) A stress vs. strain curve was generated to identify the linear frequency range.

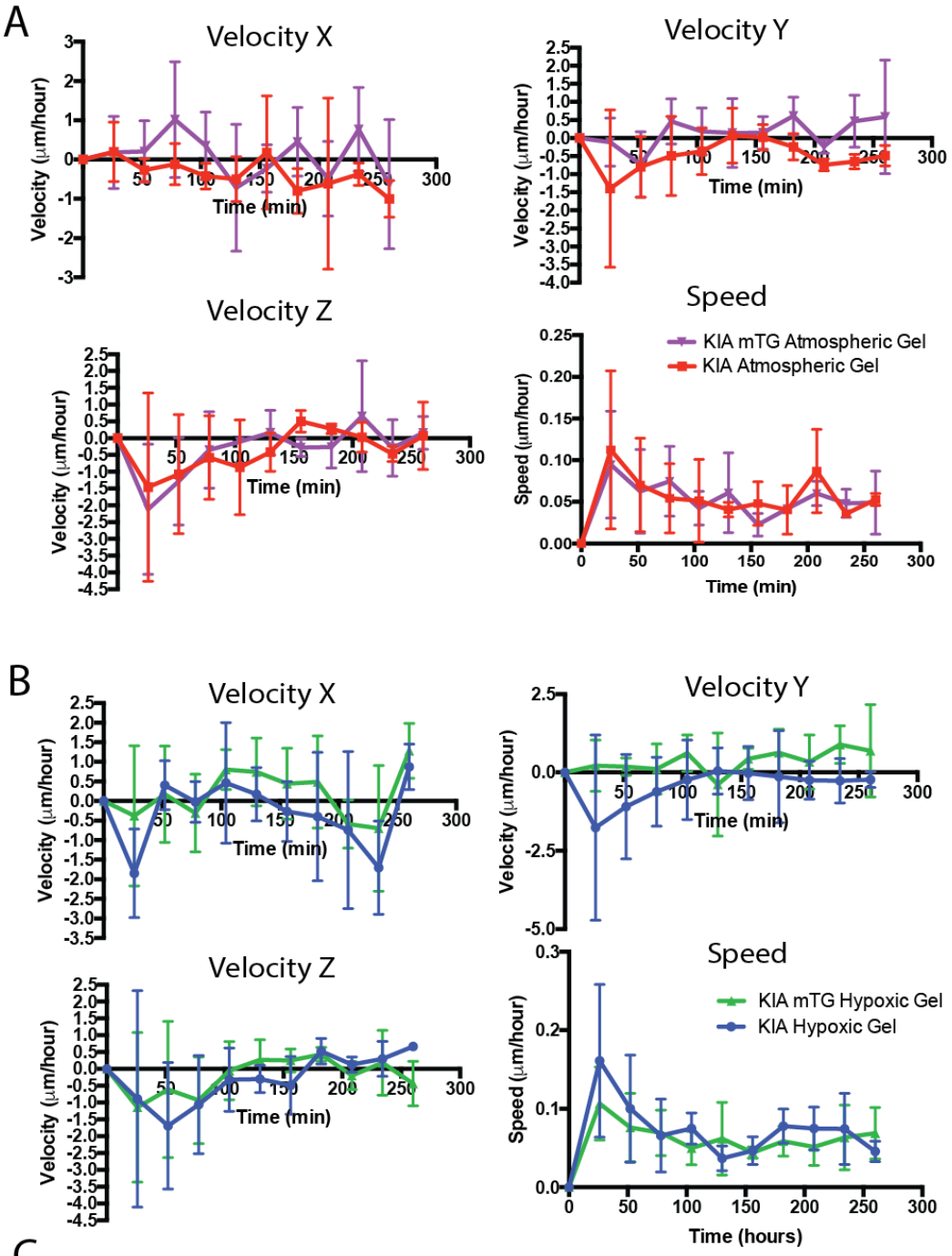
A
Velocity X
Velocity (μm/hour)
Time (min)
Velocity Y
Velocity (μm/hour)
Time (min)
Velocity Z
Velocity (μm/hour)
Time (min)
Speed
KIA mTG Atmospheric Gel
KIA Atmospheric Gel
Speed (μm/hour)
Time (min)
B
Velocity X
Velocity (μm/hour)
Time (min)
Velocity Y
Velocity (μm/hour)
Time (min)
Velocity Z
Velocity (μm/hour)
Time (min)
Speed
KIA mTG Hypoxic Gel
KIA Hypoxic Gel
Speed (μm/hour)
Time (hours)
C
Percent Aligned Fibers
KIA mTG Hypoxic Gel
KIA Hypoxic Gel
KIA mTG Atmospheric Gel
KIA Atmospheric Gel

Supplementary Figure 5-2: Instantaneous Velocity Profiles:
The velocity of KIA cells in the x,y,z direction as well as the speed was calculated for atmospheric (A) and hypoxic (B) gels C.) The percent alignment of collagen fibers within the different hydrogels.

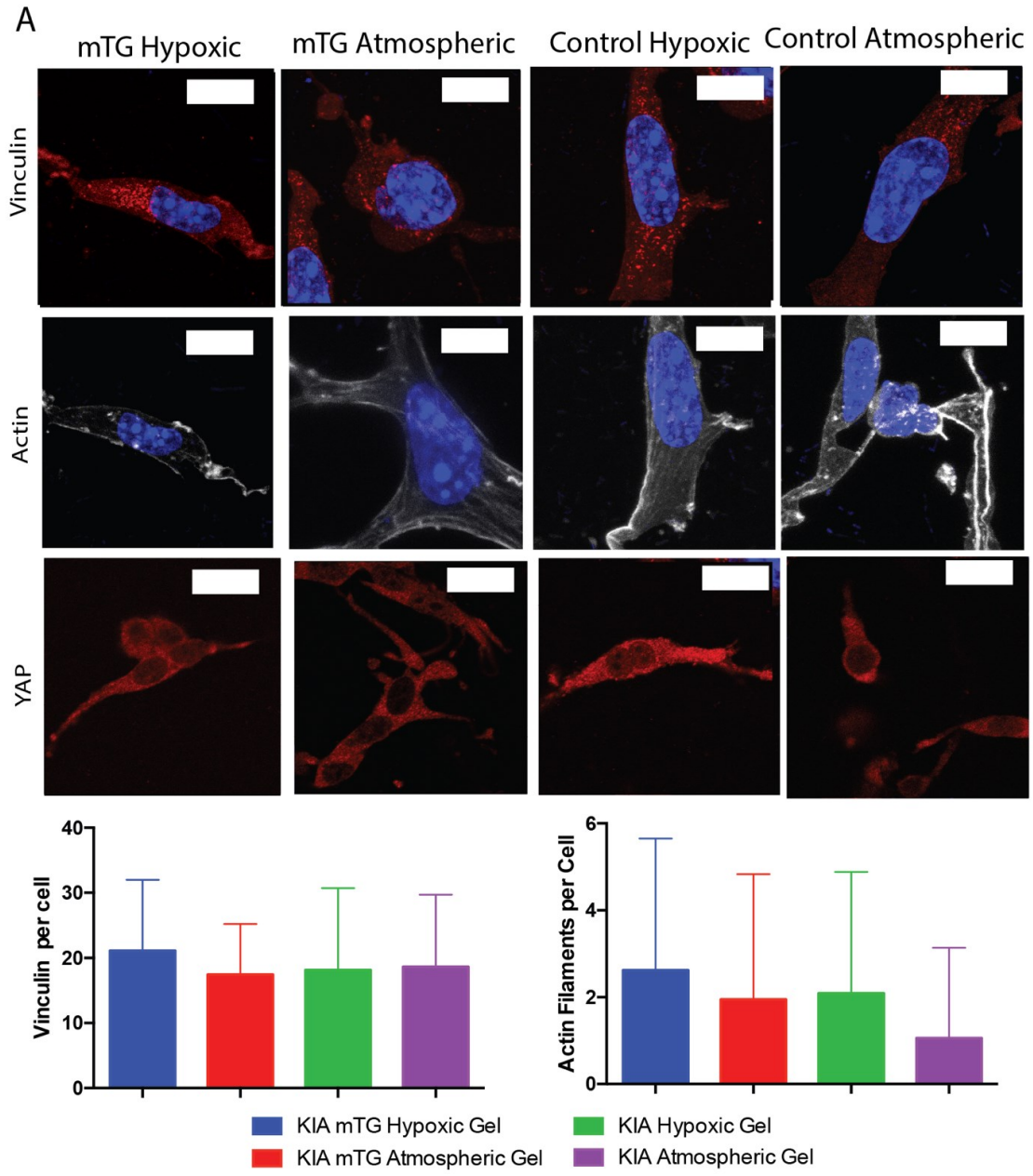

Supplementary Figure 5-3: Confounding factors for cell interaction with the matrix. Vinculin stain showed no difference in the four different hydrogels. Cytoskeletal actin also *was* similar in all four conditions. There was no nuclear localization of YAP in any of the four conditions. The amount of vinculin and actin filaments per cell was calculated.

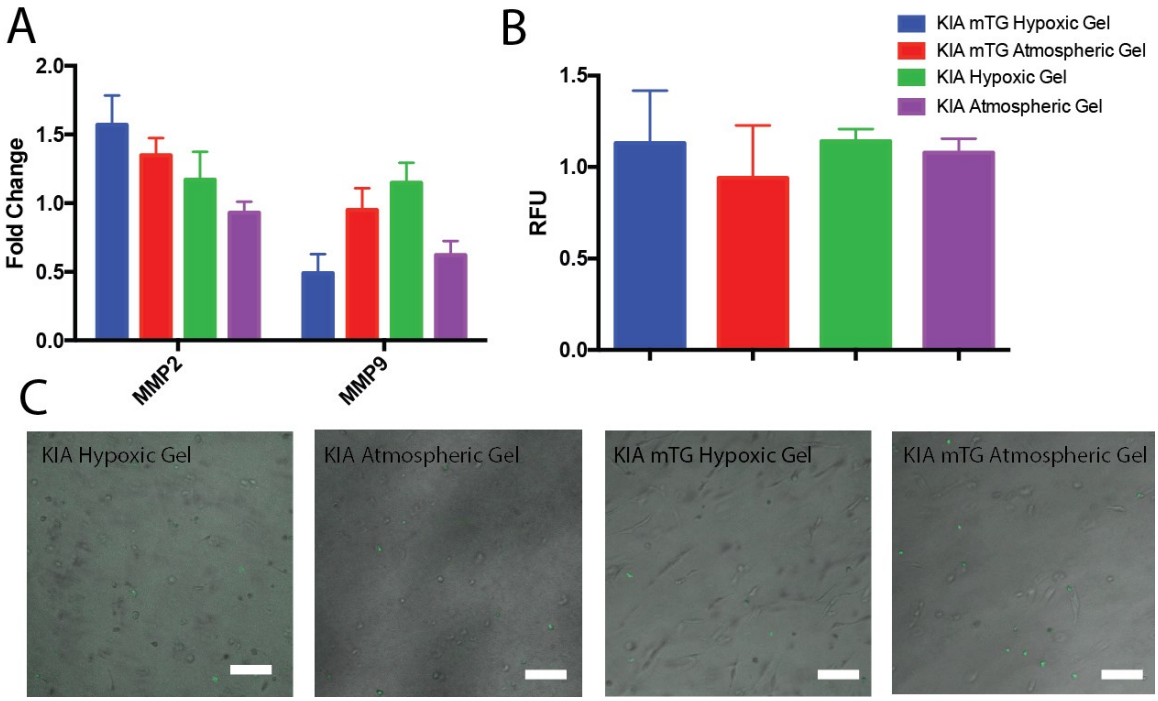

Supplementary Figure 5-4: MMP expression of KIA cells in the different hydrogels. (A). PCR was used to quantify expression of MMP2 and MMP9. (B). Protease activity was measured using DQ assay of cells on day 2 (C). Cell morphology and localization of proteases was imaged using fluorescent microscopy.

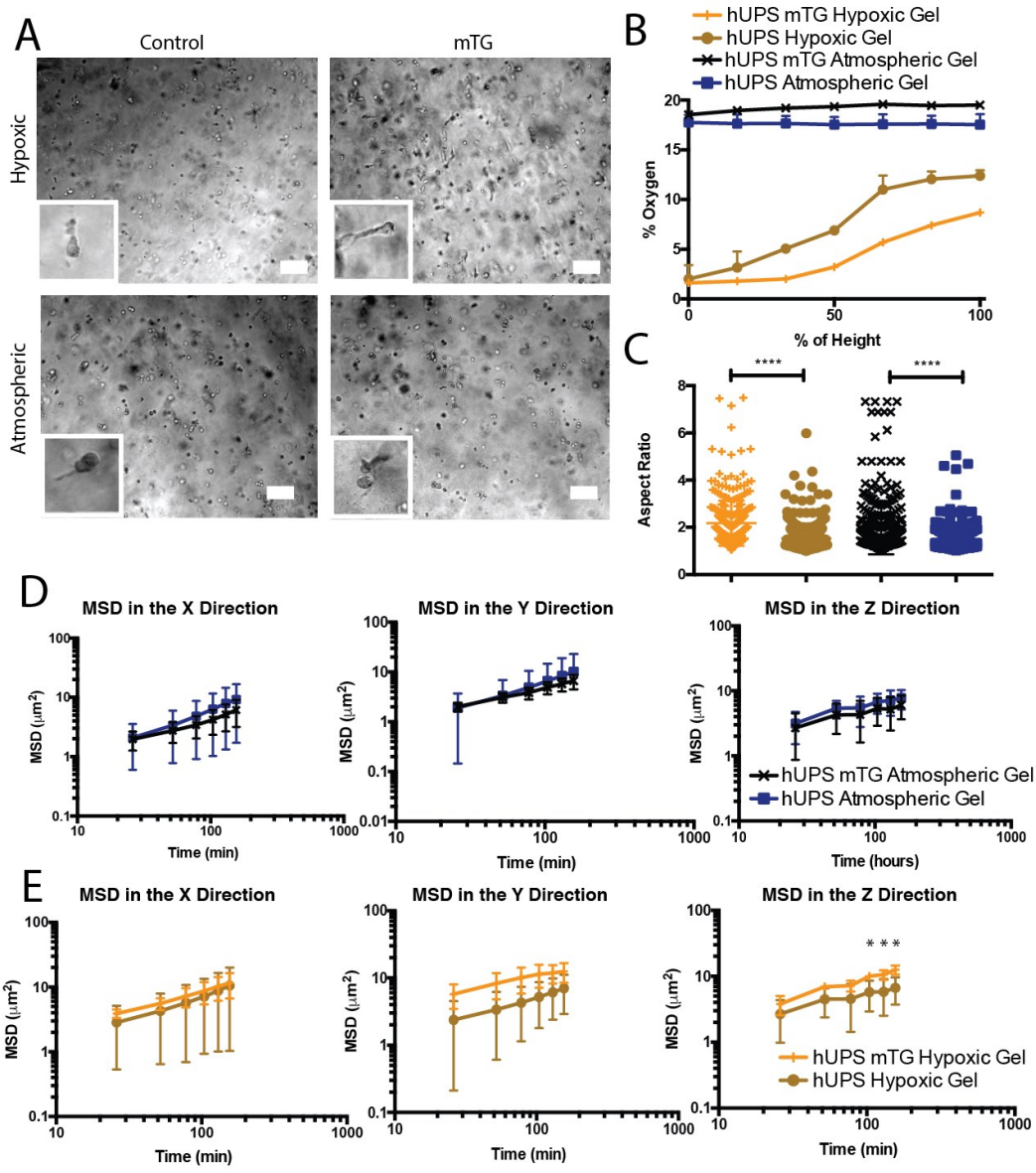

Supplementary Figure 5-5: hUPS cell migration increases with the quicker stress relaxation time in hypoxia.
A.) Representative photos of the hUPS cells in hypoxic and atmospheric hydrogels with two different stress relaxations. B.) Oxygen gradients on day three for the hypoxic and atmospheric hydrogels with hUPS cells. C.) The aspect ratio of the hUPS cells D.) Migration of hUPS cells in the atmospheric hydrogels on day 3 showing minimal difference in migration. E.) Migration of the hUPS cells in hypoxic hydrogel on day 3.

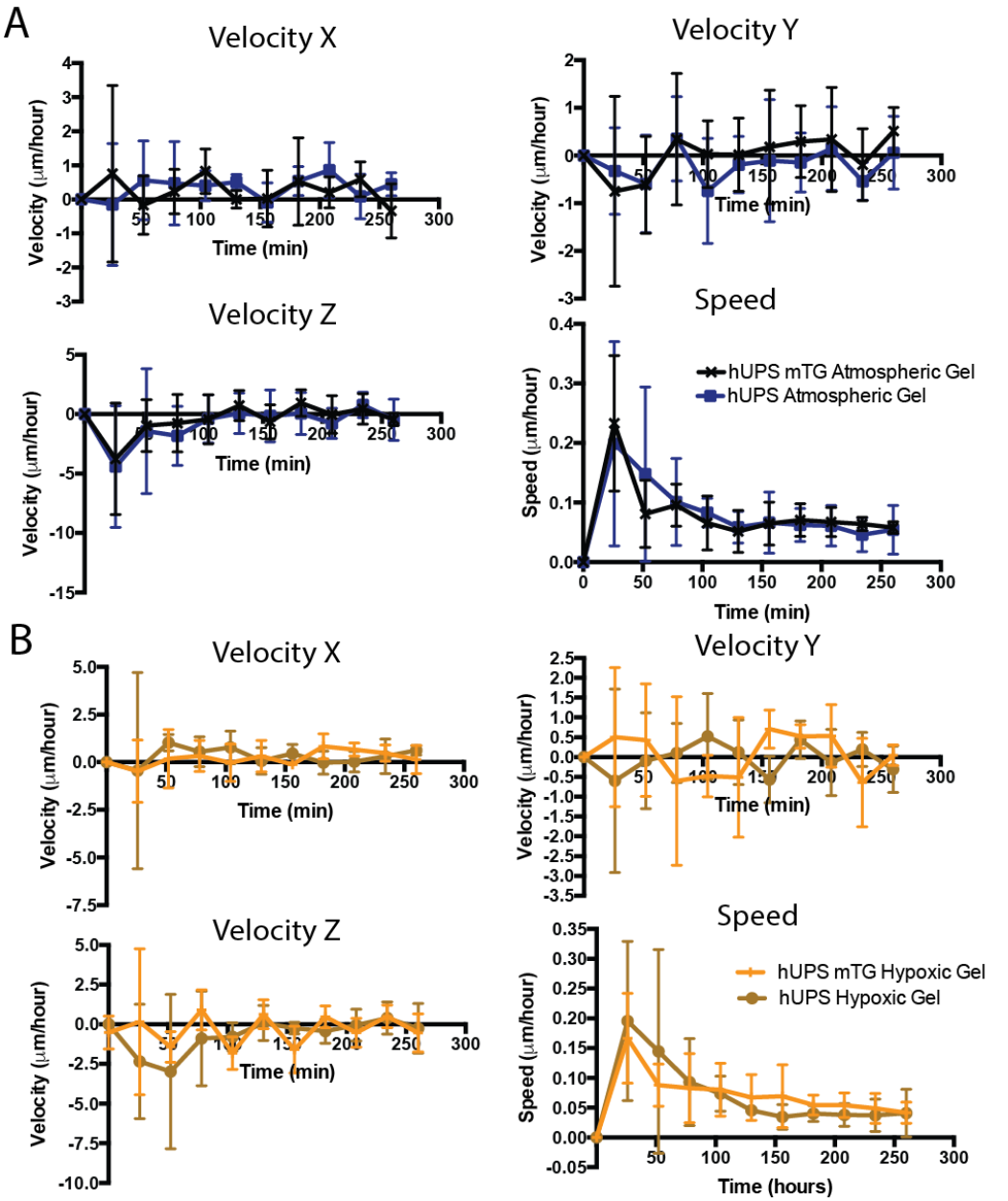
A
Velocity X
Velocity (μm/hour)
Time (min)
Velocity Y
Velocity (μm/hour)
Time (min)
Velocity Z
Velocity (μm/hour)
Time (min)
Speed
Speed (μm/hour)
Time (min)
hUPS mTG Atmospheric Gel
hUPS Atmospheric Gel
B
Velocity X
Velocity (μm/hour)
Time (min)
Velocity Y
Velocity (μm/hour)
Time (min)
Velocity Z
Velocity (μm/hour)
Time (min)
Speed
Speed (μm/hour)
Time (hours)
hUPS mTG Hypoxic Gel
hUPS Hypoxic Gel

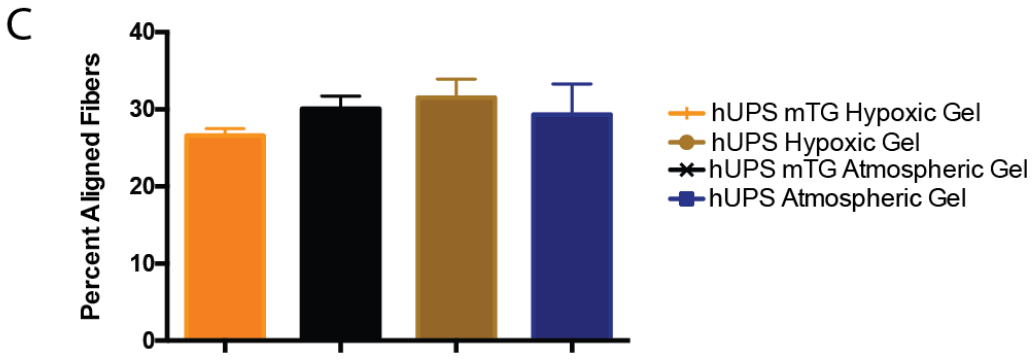
C
Percent Aligned Fibers
hUPS mTG Hypoxic Gel
hUPS Hypoxic Gel
hUPS mTG Atmospheric Gel
hUPS Atmospheric Gel

Supplementary Figure 5-6: The velocity of hUPS cells in the x,y,z direction as well as the speed was calculated for atmospheric
(A) and hypoxic (B) gels C.) The percent alignment of collagen fibers within the different hydrogels.

6 *Thesis conclusions and future work*

6.1 *Conclusions*

Oxygen gradients and mechanical cues are key pieces of the tumor microenvironment. Our goal was to create better in-vitro hydrogel models to control and mimic the tumor ECM and oxygen gradients. In **Chapter 3** we report the impact of hypoxic O_2 gradients on sarcoma cell invasion and migration. O_2 gradient measurements showed that large sarcomas mouse tumors (>300mm^3) contain a severely hypoxic core (≤0.1% pO_2) whereas smaller tumors possessed hypoxic gradients throughout the tumor mass (0.1%-6% pO_2). To analyze tumor invasion, we utilized O_2-controllable hydrogels to recreate the physio-pathological O_2 levels *in vitro*. Small tumor grafts encapsulated in the hydrogels revealed increased invasion that was both faster and extended over a longer-distance in the hypoxic hydrogels compared to nonhypoxic hydrogels. To accurately model the effect of the O_2 gradient, we examined individual sarcoma cells embedded in the O_2-controllable hydrogel. We observed that hypoxic gradients guide sarcoma cell motility and matrix remodeling through HIF–1α activation. We further found that in the hypoxic gradient, individual cells migrate more quickly, across longer distances, and in the direction of increasing O_2 tension. Treatment with minoxidil, inhibitor of hypoxia-induced sarcoma metastasis, abrogated cell migration and matrix remodeling in the hypoxic gradient. Overall, we show that O_2 acts as a 3D physico-tactic

agent during sarcoma tumor invasion and propose the O_2-controllable hydrogels as a predictive system to study early stages of the metastatic process and therapeutic targets.

Secondly, in **Chapter 4** we utilized an oxygen gradient collagen gel platform to determine the impact of collagen fiber density and hypoxic gradient on sarcoma cell migration. The oxygen gradient was created by regulating the oxygen diffusion coefficient along with the cellular oxygen consumption rate. Collagen fiber density in the hydrogels is modified by changing the pre-incubation period of the collagen gel solution at 4°C, controlling fiber density independently of collagen concentration and oxygen tension. High fiber density gels have a similar micro-scale pore size with a larger nano-scale pore size and quicker stress relaxation time, compared to the low fiber density gel. Both gels have the same Young's modulus. We analyzed responses of sarcoma cells encapsulated in the different hydrogels for three days. In the nonhypoxic low fiber density constructs, sarcoma cells exhibit larger aspect ratio and the ECM has less fiber alignment compared to the nonhypoxic high fiber density constructs. Interestingly, we found minimal effect of fiber density on cell migration and the ability of the cells to degrade the matrix in nonhypoxic constructs. When compared with hypoxic constructs, we observed the opposite trend, where cells in low fiber density constructs exhibit a lower aspect ratio and the matrix has more aligned fibers compared to hypoxic high fiber density constructs. Sarcoma cells encapsulated in high fiber density hypoxic gels migrated faster and degraded the matrix more rapidly compared to the low fiber density hypoxic constructs. Overall, we show that hypoxic cell migration and matrix degradation are enhanced in high fiber density gels, while hypoxic matrix alignment is prominent in low fiber density gels. Our results indicate the differences in cellular responses under

hypoxic gradients are due the material architecture of the hypoxic hydrogel such as higher fiber density and stress relaxation.

Finally, in **Chapter 5** we created a new hypoxic collagen gel platform that allows for oxygen gradients and stress relaxation to be controlled independently from each other. This new platform allows us to explore the effect of quicker stress relaxation in sarcoma cell migration and tumorigenesis via three dimensional (3D) cell motility, molecular biology, and *in-vivo* tumor growth. We conclude that stress relaxation in hypoxic gradients leads to an increase in cell migration along the gradient, an increase in PLOD2 expression, as well as an increase in tumor growth. In addition stress relaxation is upregulating PLOD via TGF-β. Also, when TCGA global expression studies were queried we find a significant decrease in patient survival with an increase in PLOD2 expression. Finally, we were able to demonstrate the platforms ability to screen primary patient tissue which demonstrated a similar response as our mouse sarcoma cells.

6.2 *Suggestions for future works*

In recent years great advances in synthesis of hydrogel biomaterials and other 3D miniature devices have been explored for tissue regenerative applications, but have not yet been fully taken advantage of in the field of cancer research. For example, with recent advances in organ on a chip technologies, the next logical step is to make a tumor on a chip or to create more physiologically relevant diseases on a chip. For example, Huh and colleagues have developed a lung on a chip model, which can mimic the physiological environment of the lung[220]. The next step with this technology is to integrate cancer phenotypes in specific locations in the lung on a chip model, to mimic tumor metastasis. There have been many different applications of creating different angiogenic devices on a

chip which are slowly transitioning into looking at intravasation or extravasation of tumor cells in/out of existing vasculature[221]. However the majority of these devices use a basis of collagen gels as the 3D hydrogel portion of the device. The next generation of these approaches, should incorporate more advanced materials to augment these natural ECM's enabling more accurate mimicking of physiological relevant chemical and cytokine gradients.

These technologies will also have to further incorporate multiple cell types. As we have explored above, the tumor microenvironment is a complex combinations of ECM and multicellular cues. CAFs have been explored in their importance in tumor migration and ECM modification. Preliminary studies have been performed incorporating stromal cells into systems to study the change in cancer migration. In addition to CAFs role in augmenting the surrounding tumor ECM, they also change the barrier and structure of EC and vasculature. In order to culture multiple cell types that require different culture conditions and ECM components, a more complex patterning of hydrogels networks and matrixes needs to be developed for cancer research. Our lab have shown that one can control cancer and EC patterning solely via extracellular matrix proteins[222]. Technologies developed by Burdick and colleagues have shown the ability to take advantage of different properties of "self healing" and shear thinning gels to print controlled patterns that could be adapted for this multiple cell type and ECM co-culture platforms[223].

However, the end goal with the majority of these complex systems is to discover new mechanisms in cancer development, growth and metastasis. However, due to the complexity of these devices, there is limited use of them outside researchers in the

bioengineering fields. Classical biological researchers do not have the equipment to successfully perform these assays (i.e. 3D printers, syringe pumps, chemical equipment for biopolymer synthesis). Effort should be made to simplify the mode of operation to allow a friendly use. Moreover, these devices can be used for potential therapeutic evaluation and possible replacement of *in-vivo* studies. Such trials though complex, are still less expensive and more controllable than current *in-vivo* models. The ability to simplify the current technologies to be single or two component mixtures, would greatly enhance their translatability and wide spread use. If this could be accomplished, the transition from drug discovery to personalized medicine could be achieved.

Personalized medicine is a new and very exciting field in cancer research; however there are a few technologies that make the translatable jump from the bench top the clinic. Recently, Jonas et al demonstrated use of a very complex system in the clinic, which allows for the testing of up to sixteen different therapeutics in small micro-doses[224]. In this device they created Delrin acetal resin blocks that could hold sixteen different therapies individually by controlling the drug release kinetics in the tumor microenvironment. The device is then implanted in mice in human tumors via a biopsy needle, and then is extracted via a corning needle and evaluated under histological analysis. More technologies like this need to be adapted to either be usable in a clinical setting, or more importantly, over a wide variety of cancer cell types. Other challenges include the inherit heterogeneity nature of the tumor with wide variety of genomic changes and the ability to keep tumor samples alive outside the body. Finally, in addition to the biological challenges, wide application use and ease of use of these advanced tissue culture technologies have to be mass-produced. Mass production will allow for

researches across disciplines to access the latest technologies. Mass production will further require a better definition of fabrication and synthesis parameters for specific or general use. This may fulfill the need for truly controllable and reproducible systems that can be used for cancer diagnosis and treatment.

Bibliography

1. Health, N.I.o. *SEER Stat Fact Sheets: Cancer of Any Site*. 2016 [cited 2016 20 June]; Available from: http://seer.cancer.gov/statfacts/html/all.html.
2. Mullard, A., *New drugs cost US [dollar] 2.6 billion to develop.* Nature Reviews Drug Discovery, 2014. **13**(12): p. 877-877.
3. Hay, M., et al., *Clinical development success rates for investigational drugs.* Nat Biotech, 2014. **32**(1): p. 40-51.
4. Kantarjian, H.M., et al., *Cancer drugs in the United States: Justum Pretium—the just price.* Journal of Clinical Oncology, 2013. **31**(28): p. 3600-3604.
5. Ahmed, E.M., *Hydrogel: Preparation, characterization, and applications: A review.* Journal of advanced research, 2015. **6**(2): p. 105-121.
6. Zhu, J. and R.E. Marchant, *Design properties of hydrogel tissue-engineering scaffolds.* Expert review of medical devices, 2011. **8**(5): p. 607-626.
7. Hanjaya-Putra, D., et al., *Controlled activation of morphogenesis to generate a functional human microvasculature in a synthetic matrix.* Blood, 2011. **118**(3): p. 804-815.
8. Naba, A., et al., *The matrisome: in silico definition and in vivo characterization by proteomics of normal and tumor extracellular matrices.* Molecular & Cellular Proteomics, 2011: p. mcp. M111. 014647.
9. Van der Rest, M. and R. Garrone, *Collagen family of proteins.* The FASEB journal, 1991. **5**(13): p. 2814-2823.
10. Frantz, C., K.M. Stewart, and V.M. Weaver, *The extracellular matrix at a glance.* J Cell Sci, 2010. **123**(24): p. 4195-4200.
11. Rozario, T. and D.W. DeSimone, *The extracellular matrix in development and morphogenesis: a dynamic view.* Developmental biology, 2010. **341**(1): p. 126-140.
12. Robins, S., *Biochemistry and functional significance of collagen cross-linking.* Biochemical Society Transactions, 2007. **35**(5): p. 849-852.
13. Pankov, R. and K.M. Yamada, *Fibronectin at a glance.* Journal of cell science, 2002. **115**(20): p. 3861-3863.
14. Ioachim, E., et al., *Immunohistochemical expression of extracellular matrix components tenascin, fibronectin, collagen type IV and laminin in breast cancer: their prognostic value and role in tumour invasion and progression.* European journal of cancer, 2002. **38**(18): p. 2362-2370.
15. Nielsen, M., L. Christensen, and R. Albrechtsen, *The basement membrane component laminin in breast carcinomas and axillary lymph node metastases.* Acta Pathologica Microbiologica Scandinavica Series A: Pathology, 1983. **91**(1‐6): p. 257-264.
16. Albrechtsen, R., et al., *Basement membrane changes in breast cancer detected by immunohistochemical staining for laminin.* Cancer research, 1981. **41**(12 Part 1): p. 5076-5081.

17. Brown, E., et al., *Dynamic imaging of collagen and its modulation in tumors in vivo using second-harmonic generation.* Nature medicine, 2003. **9**(6): p. 796-800.
18. Gibb, L. and D. Matthews, *Two Photon Microscopy and Second Harmonic Generation*.
19. Kalluri, R. and M. Zeisberg, *Fibroblasts in cancer.* Nature Reviews Cancer, 2006. **6**(5): p. 392-401.
20. Tomasek, J.J., et al., *Myofibroblasts and mechano-regulation of connective tissue remodelling.* Nature reviews Molecular cell biology, 2002. **3**(5): p. 349-363.
21. Rodemann, H.P. and G.A. Müller, *Characterization of human renal fibroblasts in health and disease: II. In vitro growth, differentiation, and collagen synthesis of fibroblasts from kidneys with interstitial fibrosis.* American Journal of Kidney Diseases, 1991. **17**(6): p. 684-686.
22. Chang, H.Y., et al., *Diversity, topographic differentiation, and positional memory in human fibroblasts.* Proceedings of the National Academy of Sciences, 2002. **99**(20): p. 12877-12882.
23. Sieweke, M.H., et al., *Mediation of Wound-Related Rous Sarcoma Virus Tumorigenesis by TGF-(Beta).* Science, 1990. **248**(4963): p. 1656.
24. Page-McCaw, A., A.J. Ewald, and Z. Werb, *Matrix metalloproteinases and the regulation of tissue remodelling.* Nature reviews Molecular cell biology, 2007. **8**(3): p. 221-233.
25. Cawston, T.E. and D.A. Young, *Proteinases involved in matrix turnover during cartilage and bone breakdown.* Cell and tissue research, 2010. **339**(1): p. 221-235.
26. Nagase, H., R. Visse, and G. Murphy, *Structure and function of matrix metalloproteinases and TIMPs.* Cardiovascular research, 2006. **69**(3): p. 562-573.
27. SEIKI, M., *Membrane‐type matrix metalloproteinases.* Apmis, 1999. **107**(1‐6): p. 137-143.
28. Pei, D., T. Kang, and H. Qi, *Cysteine array matrix metalloproteinase (CA-MMP)/MMP-23 is a type II transmembrane matrix metalloproteinase regulated by a single cleavage for both secretion and activation.* Journal of Biological Chemistry, 2000. **275**(43): p. 33988-33997.
29. Nagase, H. and J.F. Woessner, *Matrix metalloproteinases.* Journal of Biological chemistry, 1999. **274**(31): p. 21491-21494.
30. Nabeshima, K., et al., *Matrix metalloproteinases in tumor invasion: role for cell migration.* Pathology international, 2002. **52**(4): p. 255-264.
31. Apte, S.S., *A disintegrin-like and metalloprotease (reprolysin-type) with thrombospondin type 1 motif (ADAMTS) superfamily: functions and mechanisms.* Journal of Biological Chemistry, 2009. **284**(46): p. 31493-31497.
32. Lu, P., et al., *Extracellular matrix degradation and remodeling in development and disease.* Cold Spring Harbor perspectives in biology, 2011. **3**(12): p. a005058.
33. Paszek, M.J., et al., *Tensional homeostasis and the malignant phenotype.* Cancer cell, 2005. **8**(3): p. 241-254.
34. Erler, J.T., et al., *Lysyl oxidase is essential for hypoxia-induced metastasis.* Nature, 2006. **440**(7088): p. 1222-1226.

35. Baker, A., et al., *Lysyl oxidase enzymatic function increases stiffness to drive colorectal cancer progression through FAK.* Oncogene, 2013. **32**(14): p. 1863-1868.
36. Bonnans, C., J. Chou, and Z. Werb, *Remodelling the extracellular matrix in development and disease.* Nature reviews Molecular cell biology, 2014. **15**(12): p. 786-801.
37. Rautavuoma, K., et al., *Characterization of Three Fragments That Constitute the Monomers of the Human Lysyl Hydroxylase Isoenzymes 1–3 THE 30-kDa N-TERMINAL FRAGMENT IS NOT REQUIRED FOR LYSYL HYDROXYLASE ACTIVITY.* Journal of Biological Chemistry, 2002. **277**(25): p. 23084-23091.
38. Pirskanen, A., et al., *Site-directed Mutagenesis of Human Lysyl Hydroxylase Expressed in Insect Cells IDENTIFICATION OF HISTIDINE RESIDUES AND AN ASPARTIC ACID RESIDUE CRITICAL FOR CATALYTIC ACTIVITY.* Journal of Biological Chemistry, 1996. **271**(16): p. 9398-9402.
39. Hyry, M., J. Lantto, and J. Myllyharju, *Missense mutations that cause Bruck syndrome affect enzymatic activity, folding, and oligomerization of lysyl hydroxylase 2.* Journal of Biological Chemistry, 2009. **284**(45): p. 30917-30924.
40. Eisinger-Mathason, T.K., et al., *Hypoxia-dependent modification of collagen networks promotes sarcoma metastasis.* Cancer discovery, 2013. **3**(10): p. 1190-1205.
41. Gilkes, D.M., et al., *Procollagen lysyl hydroxylase 2 is essential for hypoxia-induced breast cancer metastasis.* Molecular cancer research, 2013. **11**(5): p. 456-466.
42. Lewis, D.M., et al., *Intratumoral oxygen gradients mediate sarcoma cell invasion.* Proceedings of the National Academy of Sciences, 2016.
43. Damaghi, M., J.W. Wojtkowiak, and R.J. Gillies, *pH sensing and regulation in cancer.* Frontiers in physiology, 2013. **4**: p. 370.
44. Datta, M., et al., *Anti-vascular endothelial growth factor treatment normalizes tuberculosis granuloma vasculature and improves small molecule delivery.* Proceedings of the National Academy of Sciences, 2015. **112**(6): p. 1827-1832.
45. Bertout, J.A., S.A. Patel, and M.C. Simon, *The impact of O2 availability on human cancer.* Nature Reviews Cancer, 2008. **8**(12): p. 967-975.
46. Policastro, L.L., et al., *The tumor microenvironment: characterization, redox considerations, and novel approaches for reactive oxygen species-targeted gene therapy.* Antioxidants & redox signaling, 2013. **19**(8): p. 854-895.
47. Blumenson, L.E. and I. Bross, *A possible mechanism for enhancement of increased production of tumor angiogenic factor.* Growth, 1976. **40**(3): p. 205-209.
48. Van den Brenk, H., et al., *Production of metastases by a primary tumour irradiated under aerobic and anaerobic conditions in vivo.* British journal of cancer, 1972. **26**(5): p. 402.
49. Young, S., R. Marshall, and R. Hill, *Hypoxia induces DNA overreplication and enhances metastatic potential of murine tumor cells.* Proceedings of the National Academy of Sciences, 1988. **85**(24): p. 9533-9537.

50. Young, S. and R. Hill, *Effects of reoxygenation on cells from hypoxic regions of solid tumors: analysis of transplanted murine tumors for evidence of DNA overreplication.* Cancer research, 1990. **50**(16): p. 5031-5038.
51. Heacock, C. and R. Sutherland, *Enhanced synthesis of stress proteins caused by hypoxia and relation to altered cell growth and metabolism.* British journal of cancer, 1990. **62**(2): p. 217.
52. Wang, G.L., et al., *Hypoxia-inducible factor 1 is a basic-helix-loop-helix-PAS heterodimer regulated by cellular O2 tension.* Proceedings of the national academy of sciences, 1995. **92**(12): p. 5510-5514.
53. Jiang, B.-H., et al., *Hypoxia-inducible factor 1 levels vary exponentially over a physiologically relevant range of O2 tension.* American Journal of Physiology-Cell Physiology, 1996. **271**(4): p. C1172-C1180.
54. Jain, S., et al., *Expression of ARNT, ARNT2, HIF1α, HIF2α and Ah receptor mRNAs in the developing mouse.* Mechanisms of development, 1998. **73**(1): p. 117-123.
55. Tian, H., S.L. McKnight, and D.W. Russell, *Endothelial PAS domain protein 1 (EPAS1), a transcription factor selectively expressed in endothelial cells.* Genes & development, 1997. **11**(1): p. 72-82.
56. Wiesener, M.S., et al., *Widespread hypoxia-inducible expression of HIF-2α in distinct cell populations of different organs.* The FASEB Journal, 2003. **17**(2): p. 271-273.
57. Gilkes, D.M. and G.L. Semenza, *Role of hypoxia-inducible factors in breast cancer metastasis.* Future Oncology, 2013. **9**(11): p. 1623-1636.
58. Brown, J.M. and W.R. Wilson, *Exploiting tumour hypoxia in cancer treatment.* Nat Rev Cancer, 2004. **4**(6): p. 437-447.
59. Lewis, D.M., et al., *Intratumoral oxygen gradients mediate sarcoma cell invasion.* Proceedings of the National Academy of Sciences, 2016: p. 201605317.
60. Eales, K., K. Hollinshead, and D. Tennant, *Hypoxia and metabolic adaptation of cancer cells.* Oncogenesis, 2016. **5**(1): p. e190.
61. Cairns, R.A., I.S. Harris, and T.W. Mak, *Regulation of cancer cell metabolism.* Nature Reviews Cancer, 2011. **11**(2): p. 85-95.
62. Boyd, N.F., et al., *Mammographic densities and breast cancer risk.* Cancer Epidemiology Biomarkers & Prevention, 1998. **7**(12): p. 1133-1144.
63. Pathak, A. and S. Kumar, *Independent regulation of tumor cell migration by matrix stiffness and confinement.* Proceedings of the National Academy of Sciences, 2012. **109**(26): p. 10334-10339.
64. Haeger, A., et al., *Cell jamming: collective invasion of mesenchymal tumor cells imposed by tissue confinement.* Biochimica et Biophysica Acta (BBA)-General Subjects, 2014. **1840**(8): p. 2386-2395.
65. Wei, S.C., et al., *Matrix stiffness drives epithelial-mesenchymal transition and tumour metastasis through a TWIST1-G3BP2 mechanotransduction pathway.* Nat Cell Biol, 2015. **17**(5): p. 678-688.
66. Chaudhuri, O., et al., *Hydrogels with tunable stress relaxation regulate stem cell fate and activity.* Nature materials, 2016. **15**(3): p. 326-334.
67. Netti, P.A., et al., *Role of extracellular matrix assembly in interstitial transport in solid tumors.* Cancer research, 2000. **60**(9): p. 2497-2503.

68. Lou, J., et al., *Stress relaxing hyaluronic acid-collagen hydrogels promote cell spreading, fiber remodeling, and focal adhesion formation in 3D cell culture.* Biomaterials, 2017. **154**: p. 213-222.
69. Chaudhuri, O., et al., *Hydrogels with tunable stress relaxation regulate stem cell fate and activity.* Nature Materials, 2015(November).
70. Lewis, D., et al., *Collagen Fiber Architecture Regulate Hypoxic Sarcoma Cell Migration.* ACS Biomaterials Science & Engineering, 2017.
71. McKinnon, D.D., et al., *Biophysically defined and cytocompatible covalently adaptable networks as viscoelastic 3D cell culture systems.* Advanced Materials, 2014. **26**(6): p. 865-872.
72. Lo, C.-M., et al., *Cell Movement Is Guided by the Rigidity of the Substrate.* Biophysical Journal, 2000. **79**(1): p. 144-152.
73. Carey, S.P., et al., *Local extracellular matrix alignment directs cellular protrusion dynamics and migration through Rac1 and FAK.* Integrative Biology, 2016. **8**(8): p. 821-835.
74. DeVolder, R. and H.J. Kong, *Hydrogels for in vivo‐like three‐dimensional cellular studies.* Wiley Interdisciplinary Reviews: Systems Biology and Medicine, 2012. **4**(4): p. 351-365.
75. Gauvin, R., et al., *Hydrogels and microtechnologies for engineering the cellular microenvironment.* Wiley Interdisciplinary Reviews: Nanomedicine and Nanobiotechnology, 2012. **4**(3): p. 235-246.
76. Guvendiren, M. and J.A. Burdick, *Engineering synthetic hydrogel microenvironments to instruct stem cells.* Curr Opin Biotechnol, 2013. **24**(5): p. 841-6.
77. Rice, J.J., et al., *Engineering the regenerative microenvironment with biomaterials.* Adv Healthc Mater, 2013. **2**(1): p. 57-71.
78. Rosales, A.M. and K.S. Anseth, *The design of reversible hydrogels to capture extracellular matrix dynamics.* Nature Reviews Materials, 2016. **1**: p. 15012.
79. Seliktar, D., *Designing cell-compatible hydrogels for biomedical applications.* Science, 2012. **336**(6085): p. 1124-8.
80. Park, K.M., M.R. Blatchley, and S. Gerecht, *The design of dextran-based hypoxia-inducible hydrogels via in situ oxygen-consuming reaction.* Macromol Rapid Commun, 2014. **35**(22): p. 1968-75.
81. Park, K.M. and S. Gerecht, *Hypoxia-inducible hydrogels.* Nat Commun, 2014. **5**: p. 4075.
82. Park, K.M., et al., *Macro/nano-gel composite as an injectable and bioactive bulking material for the treatment of urinary incontinence.* Biomacromolecules, 2014. **15**(6): p. 1979-1984.
83. Shinde, U.P., B. Yeon, and B. Jeong, *Recent progress of in situ formed gels for biomedical applications.* Progress in polymer science, 2013. **38**(3): p. 672-701.
84. Leitinger, B. and E. Hohenester, *Mammalian collagen receptors.* Matrix biology, 2007. **26**(3): p. 146-155.
85. Place, E.S., N.D. Evans, and M.M. Stevens, *Complexity in biomaterials for tissue engineering.* Nature materials, 2009. **8**(6): p. 457-470.
86. Kadler, K.E., et al., *Collagens at a glance.* Journal of cell science, 2007. **120**(12): p. 1955-1958.

87. Girton, T., et al., *Mechanisms of stiffening and strengthening in media-equivalents fabricated using glycation.* Journal of biomechanical engineering, 2000. **122**(3): p. 216-223.
88. Orban, J.M., et al., *Crosslinking of collagen gels by transglutaminase.* Journal of biomedical materials research Part A, 2004. **68**(4): p. 756-762.
89. Zhang, X., et al., *The effects of different crossing-linking conditions of genipin on type I collagen scaffolds: an in vitro evaluation.* Cell and tissue banking, 2014. **15**(4): p. 531-541.
90. Liang, Y., et al., *A cell-instructive hydrogel to regulate malignancy of 3D tumor spheroids with matrix rigidity.* Biomaterials, 2011. **32**(35): p. 9308-9315.
91. Ahmed, T.A., E.V. Dare, and M. Hincke, *Fibrin: a versatile scaffold for tissue engineering applications.* Tissue Engineering Part B: Reviews, 2008. **14**(2): p. 199-215.
92. Fuss, C., J.C. Palmaz, and E.A. Sprague, *Fibrinogen: structure, function, and surface interactions.* Journal of Vascular and Interventional Radiology, 2001. **12**(6): p. 677-682.
93. Blombäck, B., *Fibrinogen and fibrin-proteins with complex roles in hemostasis and thrombosis.* Thrombosis research, 1996. **83**(1): p. 1-75.
94. Hogg, P.J. and C.M. Jackson, *Fibrin monomer protects thrombin from inactivation by heparin-antithrombin III: implications for heparin efficacy.* Proceedings of the National Academy of Sciences, 1989. **86**(10): p. 3619-3623.
95. Del Bufalo, F., et al., *3D modeling of human cancer: a PEG-fibrin hydrogel system to study the role of tumor microenvironment and recapitulate the in vivo effect of oncolytic adenovirus.* Biomaterials, 2016.
96. Hern, D.L. and J.A. Hubbell, *Incorporation of adhesion peptides into nonadhesive hydrogels useful for tissue resurfacing.* Journal of biomedical materials research, 1998. **39**(2): p. 266-276.
97. Yang, C., et al., *Mechanical memory and dosing influence stem cell fate.* Nature materials, 2014. **13**(6): p. 645.
98. Lutolf, M. and J. Hubbell, *Synthesis and physicochemical characterization of end-linked poly (ethylene glycol)-co-peptide hydrogels formed by Michael-type addition.* Biomacromolecules, 2003. **4**(3): p. 713-722.
99. Darling, N.J., et al., *Controlling the kinetics of thiol-maleimide Michael-type addition gelation kinetics for the generation of homogenous poly (ethylene glycol) hydrogels.* Biomaterials, 2016.
100. Rowley, J.A., G. Madlambayan, and D.J. Mooney, *Alginate hydrogels as synthetic extracellular matrix materials.* Biomaterials, 1999. **20**(1): p. 45-53.
101. Lee, K., E.A. Silva, and D.J. Mooney, *Growth factor delivery-based tissue engineering: general approaches and a review of recent developments.* Journal of the Royal Society Interface, 2011. **8**(55): p. 153-170.
102. Augst, A.D., H.J. Kong, and D.J. Mooney, *Alginate hydrogels as biomaterials.* Macromolecular bioscience, 2006. **6**(8): p. 623-633.
103. Dhoot, N.O., et al., *Peptide‐modified alginate surfaces as a growth permissive substrate for neurite outgrowth.* Journal of Biomedical Materials Research Part A, 2004. **71**(2): p. 191-200.

104. Hou, J., et al., *Enzymatically crosslinked alginate hydrogels with improved adhesion properties.* Polymer Chemistry, 2015. **6**(12): p. 2204-2213.
105. Sun, J.-Y., et al., *Highly stretchable and tough hydrogels.* Nature, 2012. **489**(7414): p. 133-136.
106. Klotz, B.J., et al., *Gelatin-Methacryloyl Hydrogels: Towards Biofabrication-Based Tissue Repair.* Trends in biotechnology, 2016. **34**(5): p. 394-407.
107. Van den Steen, P.E., et al., *Biochemistry and molecular biology of gelatinase B or matrix metalloproteinase-9 (MMP-9).* Critical reviews in biochemistry and molecular biology, 2002. **37**(6): p. 375-536.
108. Nichol, J.W., et al., *Cell-laden microengineered gelatin methacrylate hydrogels.* Biomaterials, 2010. **31**(21): p. 5536-5544.
109. Yue, K., et al., *Synthesis, properties, and biomedical applications of gelatin methacryloyl (GelMA) hydrogels.* Biomaterials, 2015. **73**: p. 254-271.
110. Bertassoni, L.E., et al., *Hydrogel bioprinted microchannel networks for vascularization of tissue engineering constructs.* Lab on a Chip, 2014. **14**(13): p. 2202-2211.
111. Colosi, C., et al., *Microfluidic Bioprinting of Heterogeneous 3D Tissue Constructs Using Low‐Viscosity Bioink.* Advanced Materials, 2015.
112. Shin, S.R., et al., *Cell‐laden Microengineered and Mechanically Tunable Hybrid Hydrogels of Gelatin and Graphene Oxide.* Advanced Materials, 2013. **25**(44): p. 6385-6391.
113. Allison, D.D. and K.J. Grande-Allen, *Review. Hyaluronan: a powerful tissue engineering tool.* Tissue engineering, 2006. **12**(8): p. 2131-2140.
114. Highley, C.B., G.D. Prestwich, and J.A. Burdick, *Recent advances in hyaluronic acid hydrogels for biomedical applications.* Current opinion in biotechnology, 2016. **40**: p. 35-40.
115. Turley, E.A., P.W. Noble, and L.Y. Bourguignon, *Signaling properties of hyaluronan receptors.* Journal of Biological Chemistry, 2002. **277**(7): p. 4589-4592.
116. Rodell, C.B., A.L. Kaminski, and J.A. Burdick, *Rational design of network properties in guest–host assembled and shear-thinning hyaluronic acid hydrogels.* Biomacromolecules, 2013. **14**(11): p. 4125-4134.
117. Khetan, S., et al., *Degradation-mediated cellular traction directs stem cell fate in covalently crosslinked three-dimensional hydrogels.* Nature materials, 2013. **12**(5): p. 458-465.
118. Kusuma, S., et al., *Self-organized vascular networks from human pluripotent stem cells in a synthetic matrix.* Proceedings of the National Academy of Sciences, 2013. **110**(31): p. 12601-12606.
119. Hanahan, D. and R.A. Weinberg, *Hallmarks of cancer: the next generation.* cell, 2011. **144**(5): p. 646-674.
120. Whiteside, T., *The tumor microenvironment and its role in promoting tumor growth.* Oncogene, 2008. **27**(45): p. 5904-5912.
121. Gu, L. and D.J. Mooney, *Biomaterials and emerging anticancer therapeutics: engineering the microenvironment.* Nature Reviews Cancer, 2016. **16**(1): p. 56-66.

122. Roudsari, L.C. and J.L. West, *Studying the influence of angiogenesis in in vitro cancer model systems.* Advanced drug delivery reviews, 2016. **97**: p. 250-259.
123. Zaman, M.H., *The role of engineering approaches in analysing cancer invasion and metastasis.* Nature Reviews Cancer, 2013. **13**(8): p. 596-603.
124. DeSantis, C.E., et al., *Cancer treatment and survivorship statistics, 2014.* CA: a cancer journal for clinicians, 2014. **64**(4): p. 252-271.
125. Taubenberger, A.V., *In vitro microenvironments to study breast cancer bone colonisation.* Advanced drug delivery reviews, 2014. **79**: p. 135-144.
126. Charoen, K.M., et al., *Embedded multicellular spheroids as a biomimetic 3D cancer model for evaluating drug and drug-device combinations.* Biomaterials, 2014. **35**(7): p. 2264-2271.
127. Fisher, S.A., et al., *Tuning the Microenvironment: Click‐Crosslinked Hyaluronic Acid‐Based Hydrogels Provide a Platform for Studying Breast Cancer Cell Invasion.* Advanced Functional Materials, 2015. **25**(46): p. 7163-7172.
128. Taylor, B.S., et al., *Advances in sarcoma genomics and new therapeutic targets.* Nature Reviews Cancer, 2011. **11**(8): p. 541-557.
129. Singh, S.P., et al., *A peptide functionalized poly (ethylene glycol)(PEG) hydrogel for investigating the influence of biochemical and biophysical matrix properties on tumor cell migration.* Biomaterials science, 2014. **2**(7): p. 1024-1034.
130. Agnihotri, S., et al., *Glioblastoma, a brief review of history, molecular genetics, animal models and novel therapeutic strategies.* Archivum immunologiae et therapiae experimentalis, 2013. **61**(1): p. 25-41.
131. Rape, A., B. Ananthanarayanan, and S. Kumar, *Engineering strategies to mimic the glioblastoma microenvironment.* Advanced drug delivery reviews, 2014. **79**: p. 172-183.
132. Wang, C., X. Tong, and F. Yang, *Bioengineered 3D brain tumor model to elucidate the effects of matrix stiffness on glioblastoma cell behavior using PEG-based hydrogels.* Molecular pharmaceutics, 2014. **11**(7): p. 2115-2125.
133. Siegel, R., D. Naishadham, and A. Jemal, *Cancer statistics, 2013.* CA: a cancer journal for clinicians, 2013. **63**(1): p. 11-30.
134. Loessner, D., B.M. Holzapfel, and J.A. Clements, *Engineered microenvironments provide new insights into ovarian and prostate cancer progression and drug responses.* Advanced drug delivery reviews, 2014. **79**: p. 193-213.
135. Fong, E.L., et al., *Hydrogel-based 3D model of patient-derived prostate xenograft tumors suitable for drug screening.* Molecular pharmaceutics, 2014. **11**(7): p. 2040-2050.
136. Siegel, R.L., K.D. Miller, and A. Jemal, *Cancer statistics, 2015.* CA: a cancer journal for clinicians, 2015. **65**(1): p. 5-29.
137. White, E.A., H.A. Kenny, and E. Lengyel, *Three-dimensional modeling of ovarian cancer.* Advanced drug delivery reviews, 2014. **79**: p. 184-192.
138. Kaemmerer, E., et al., *Gelatine methacrylamide-based hydrogels: an alternative three-dimensional cancer cell culture system.* Acta biomaterialia, 2014. **10**(6): p. 2551-2562.
139. Park, K.M., Gerecht, S., *Hypoxia-Inducible Hydrogels* Nature Communications, 2014. **5**: p. 4075.

140. Eisinger-Mathason, T.S., et al., *Hypoxia-dependent modification of collagen networks promotes sarcoma metastasis.* Cancer Discov, 2013. **3**(10): p. 1190-205.
141. Kusuma, S., B. Macklin, and S. Gerecht, *Derivation and network formation of vascular cells from human pluripotent stem cells.* Biomimetics and Stem Cells: Methods and Protocols, 2014: p. 1-9.
142. NGUYEN‐NGOC, K.V. and A. Ewald, *Mammary ductal elongation and myoepithelial migration are regulated by the composition of the extracellular matrix.* Journal of microscopy, 2013. **251**(3): p. 212-223.
143. Tomayko, M.M. and C.P. Reynolds, *Determination of subcutaneous tumor size in athymic (nude) mice.* Cancer chemotherapy and pharmacology, 1989. **24**(3): p. 148-154.
144. Wu, P.-H., A. Giri, and D. Wirtz, *Statistical analysis of cell migration in 3D using the anisotropic persistent random walk model.* Nature protocols, 2015. **10**(3): p. 517-527.
145. Wu, P.-H., et al., *Three-dimensional cell migration does not follow a random walk.* Proceedings of the National Academy of Sciences, 2014. **111**(11): p. 3949-3954.
146. Yoon, S.S., et al., *Angiogenic profile of soft tissue sarcomas based on analysis of circulating factors and microarray gene expression.* J Surg Res, 2006. **135**(2): p. 282-90.
147. Singer, S., et al., *Management of soft-tissue sarcomas: an overview and update.* Lancet Oncol, 2000. **1**: p. 75-85.
148. Jemal, A., et al., *Cancer statistics, 2010.* CA Cancer J Clin, 2010. **60**(5): p. 277-300.
149. Wasif, N., et al., *Influence of specialty and clinical experience on treatment sequencing in the multimodal management of soft tissue extremity sarcoma.* Ann Surg Oncol, 2012. **19**(2): p. 504-10.
150. Italiano, A., et al., *Trends in survival for patients with metastatic soft-tissue sarcoma.* Cancer, 2011. **117**(5): p. 1049-54.
151. Junttila, M.R. and F.J. de Sauvage, *Influence of tumour micro-environment heterogeneity on therapeutic response.* Nature, 2013. **501**(7467): p. 346-54.
152. Quail, D.F. and J.A. Joyce, *Microenvironmental regulation of tumor progression and metastasis.* Nat Med, 2013. **19**(11): p. 1423-37.
153. Fukumura, D. and R.K. Jain, *Tumor microenvironment abnormalities: causes, consequences, and strategies to normalize.* J Cell Biochem, 2007. **101**(4): p. 937-49.
154. Francis, P., et al., *Diagnostic and prognostic gene expression signatures in 177 soft tissue sarcomas: hypoxia-induced transcription profile signifies metastatic potential.* BMC Genomics, 2007. **8**: p. 73.
155. Brizel, D.M., et al., *Tumor oxygenation predicts for the likelihood of distant metastases in human soft tissue sarcoma.* Cancer Res, 1996. **56**(5): p. 941-3.
156. Bertout, J.A., S.A. Patel, and M.C. Simon, *The impact of O2 availability on human cancer.* Nat Rev Cancer, 2008. **8**(12): p. 967-75.
157. Keith, B., R.S. Johnson, and M.C. Simon, *HIF1alpha and HIF2alpha: sibling rivalry in hypoxic tumour growth and progression.* Nat Rev Cancer, 2012. **12**(1): p. 9-22.

158. Smeland, E., et al., *Prognostic impacts of hypoxic markers in soft tissue sarcoma.* Sarcoma, 2012. **2012**: p. 541650.
159. Shintani, K., et al., *Expression of hypoxia-inducible factor (HIF)-1alpha as a biomarker of outcome in soft-tissue sarcomas.* Virchows Arch, 2006. **449**(6): p. 673-81.
160. Abaci, H.E., et al., *Unforeseen decreases in dissolved oxygen levels affect tube formation kinetics in collagen gels.* Am. J. Physiol.: Cell Physiol., 2011. **301**(2): p. C431-40.
161. Kirsch, D.G., et al., *A spatially and temporally restricted mouse model of soft tissue sarcoma.* Nat Med, 2007. **13**(8): p. 992-7.
162. Eisinger-Mathason, T.S., et al., *Deregulation of the Hippo pathway in soft-tissue sarcoma promotes FOXM1 expression and tumorigenesis.* Proc Natl Acad Sci U S A, 2015. **112**(26): p. E3402-11.
163. Makareeva, E., et al., *Carcinomas contain a matrix metalloproteinase-resistant isoform of type I collagen exerting selective support to invasion.* Cancer Res, 2010. **70**(11): p. 4366-74.
164. Egeblad, M., M.G. Rasch, and V.M. Weaver, *Dynamic interplay between the collagen scaffold and tumor evolution.* Curr Opin Cell Biol, 2010. **22**(5): p. 697-706.
165. Zaman, M.H., et al., *Migration of tumor cells in 3D matrices is governed by matrix stiffness along with cell-matrix adhesion and proteolysis.* Proc Natl Acad Sci U S A, 2006. **103**(29): p. 10889-94.
166. Vandooren, J., et al., *Gelatin degradation assay reveals MMP-9 inhibitors and function of O-glycosylated domain.* World J Biol Chem, 2011. **2**(1): p. 14-24.
167. Lee, S.H., et al., *Poly(ethylene glycol) hydrogels conjugated with a collagenase-sensitive fluorogenic substrate to visualize collagenase activity during three-dimensional cell migration.* Biomaterials, 2007. **28**(20): p. 3163-70.
168. El-Naggar, A.M., et al., *Translational Activation of HIF1alpha by YB-1 Promotes Sarcoma Metastasis.* Cancer Cell, 2015. **27**(5): p. 682-97.
169. Gilkes, D.M., G.L. Semenza, and D. Wirtz, *Hypoxia and the extracellular matrix: drivers of tumour metastasis.* Nat Rev Cancer, 2014. **14**(6): p. 430-9.
170. Zuurmond, A.M., et al., *Minoxidil exerts different inhibitory effects on gene expression of lysyl hydroxylase 1, 2, and 3: implications for collagen cross-linking and treatment of fibrosis.* Matrix Biol, 2005. **24**(4): p. 261-70.
171. McKeown, S., *Defining normoxia, physoxia and hypoxia in tumours—implications for treatment response.* The British journal of radiology, 2014. **87**(1035): p. 20130676.
172. Semenza, G.L., *Cancer–stromal cell interactions mediated by hypoxia-inducible factors promote angiogenesis, lymphangiogenesis, and metastasis.* Oncogene, 2013. **32**(35): p. 4057-4063.
173. Yang, K.R., et al., *Niche inheritance: a cooperative pathway to enhance cancer cell fitness through ecosystem engineering.* Journal of cellular biochemistry, 2014. **115**(9): p. 1478-1485.
174. Fraley, S.I., et al., *Three-dimensional matrix fiber alignment modulates cell migration and MT1-MMP utility by spatially and temporally directing protrusions.* Scientific reports, 2015. **5**.

175. Ogawa, T., et al., *Spontaneous cutaneous soft tissue sarcoma with differentiation into fibroblasts in a Sprague-Dawley rat.* Journal of toxicologic pathology, 2016. **29**(2): p. 119-124.
176. Levental, K.R., et al., *Matrix crosslinking forces tumor progression by enhancing integrin signaling.* Cell, 2009. **139**(5): p. 891-906.
177. Yang, Y.-l., S. Motte, and L.J. Kaufman, *Pore size variable type I collagen gels and their interaction with glioma cells.* Biomaterials, 2010. **31**(21): p. 5678-5688.
178. Wolf, K., et al., *Physical limits of cell migration: control by ECM space and nuclear deformation and tuning by proteolysis and traction force.* The Journal of cell biology, 2013. **201**(7): p. 1069-1084.
179. Brandl, F., F. Sommer, and A. Goepferich, *Rational design of hydrogels for tissue engineering: impact of physical factors on cell behavior.* Biomaterials, 2007. **28**(2): p. 134-146.
180. Abaci, H.E., et al., *Unforeseen decreases in dissolved oxygen levels affect tube formation kinetics in collagen gels.* American journal of physiology. Cell physiology, 2011. **301**(2): p. C431-40.
181. Park, K.M. and S. Gerecht, *Hypoxia-inducible hydrogels.* Nat Commun, 2014. **5**.
182. Shen, Y.-i., et al., *Hyaluronic acid hydrogel stiffness and oxygen tension affect cancer cell fate and endothelial sprouting.* Biomaterials science, 2014. **2**: p. 655-665.
183. Abaci, H.E., et al., *Unforeseen decreases in dissolved oxygen levels affect tube formation kinetics in collagen gels.* American Journal of Physiology - Cell Physiology, 2011. **301**(2): p. C431-C440.
184. Fomovsky, G.M. and J.W. Holmes, *Evolution of scar structure, mechanics, and ventricular function after myocardial infarction in the rat.* American Journal of Physiology-Heart and Circulatory Physiology, 2010. **298**(1): p. H221-H228.
185. Bredfeldt, J.S., et al., *Computational segmentation of collagen fibers from second-harmonic generation images of breast cancer.* Journal of biomedical optics, 2014. **19**(1): p. 016007-016007.
186. Hotaling, N.A., et al., *DiameterJ: a validated open source nanofiber diameter measurement tool.* Biomaterials, 2015. **61**: p. 327-338.
187. Friedl, P. and K. Wolf, *Proteolytic interstitial cell migration: a five-step process.* Cancer and Metastasis Reviews, 2009. **28**(1-2): p. 129-135.
188. Fraley, S.I., et al., *Three-dimensional matrix fiber alignment modulates cell migration and MT1-MMP utility by spatially and temporally directing protrusions.* Scientific reports, 2015. **5**(October): p. 14580-14580.
189. Friedl, P., Y. Hegerfeldt, and M. Tusch, *Collective cell migration in morphogenesis and cancer.* Int J Dev Biol, 2004. **48**(5-6): p. 441-449.
190. Shen, Y.-I., et al., *Hyaluronic acid hydrogel stiffness and oxygen tension affect cancer cell fate and endothelial sprouting.* Biomaterials science, 2014. **2**(5): p. 655-665.
191. Abaci, H.E., et al., *Unforeseen decreases in dissolved oxygen levels affect tube formation kinetics in collagen gels.* American Journal of Physiology-Cell Physiology, 2011. **301**(2): p. C431-C440.

192. Di Lullo, G.A., et al., *Mapping the ligand-binding sites and disease-associated mutations on the most abundant protein in the human, type I collagen.* Journal of Biological Chemistry, 2002. **277**(6): p. 4223-4231.
193. Gao, Y., et al., *Activation barriers for oxygen diffusion in polystyrene and polycarbonate glasses: Effects of low molecular weight additives.* Macromolecules, 1994. **27**(24): p. 7041-7048.
194. Nguyen-Ngoc, K.-V., et al., *3D culture assays of murine mammary branching morphogenesis and epithelial invasion.* Tissue Morphogenesis: Methods and Protocols, 2015: p. 135-162.
195. Lodish, H., et al., *Collagen: the fibrous proteins of the matrix.* 2000.
196. Prockop, D.J. and K.I. Kivirikko, *Collagens: molecular biology, diseases, and potentials for therapy.* Annual review of biochemistry, 1995. **64**(1): p. 403-434.
197. Wottawah, F., et al., *Optical rheology of biological cells.* Physical review letters, 2005. **94**(9): p. 098103.
198. Chaudhuri, O., et al., *Substrate stress relaxation regulates cell spreading.* Nature communications, 2015. **6**.
199. Sloane, B.F., et al., *Functional imaging of tumor proteolysis.* Annu Rev Pharmacol Toxicol, 2006. **46**: p. 301-15.
200. Fraley, S.I., et al., *Three-dimensional matrix fiber alignment modulates cell migration and MT1-MMP utility by spatially and temporally directing protrusions.* Scientific reports, 2014. **5**: p. 14580-14580.
201. Kakkad, S.M., et al., *Collagen I fiber density increases in lymph node positive breast cancers: pilot study.* Journal of biomedical optics, 2012. **17**(11): p. 116017-116017.
202. Friedl, P. and K. Wolf, *Tumour-cell invasion and migration: diversity and escape mechanisms.* Nature Reviews Cancer, 2003. **3**(5): p. 362-374.
203. Frantz, C., K.M. Stewart, and V.M. Weaver, *The extracellular matrix at a glance.* Journal of Cell Science, 2010. **123**(24): p. 4195-4200.
204. Seewaldt, V., *ECM stiffness paves the way for tumor cells.* Nature medicine, 2014. **20**(4): p. 332.
205. Lewis, D.M., et al., *O 2-controllable hydrogels for studying cellular responses to hypoxic gradients in three dimensions in vitro and in vivo.* nature protocols, 2017. **12**(8): p. 1620.
206. Xia, Z., et al., *Structure and relaxation in cellulose hydrogels.* Journal of Applied Polymer Science, 2015. **132**(24).
207. McCaffery, J.M. and M.G. Farquhar, *[29] Localization of GTPases by indirect immunofluorescence and immunoelectron microscopy*, in *Methods in enzymology*. 1995, Elsevier. p. 259-279.
208. Tang, Z., et al., *GEPIA: a web server for cancer and normal gene expression profiling and interactive analyses.* Nucleic Acids Research, 2017.
209. Lessey, B.A. and R.F. Savaris, *Comparison of HSCORE assessment of endometrial β3 integrin subunit expression with digital HSCORE using computerized image analysis (ImageJ).* Analytical and quantitative cytopathology and histopathology, 2013. **35**(4): p. 210.

210. Gjaltema, R.A.F., et al., *Procollagen lysyl hydroxylase 2 expression is regulated by an alternative downstream transforming growth factor β-1 activation mechanism.* Journal of Biological Chemistry, 2015. **290**(47): p. 28465-28476.
211. Laklai, H., et al., *Genotype tunes pancreatic ductal adenocarcinoma tissue tension to induce matricellular fibrosis and tumor progression.* Nature medicine, 2016. **22**(5): p. 497-505.
212. Remst, D.F., et al., *TGF-ss induces Lysyl hydroxylase 2b in human synovial osteoarthritic fibroblasts through ALK5 signaling.* Cell and tissue research, 2014. **355**(1): p. 163-171.
213. Taylor, M.A., et al., *Lysyl oxidase contributes to mechanotransduction-mediated regulation of transforming growth factor-β signaling in breast cancer cells.* Neoplasia, 2011. **13**(5): p. 406-IN2.
214. Chen, Y., et al., *PKCα-induced drug resistance in pancreatic cancer cells is associated with transforming growth factor-β1.* Journal of Experimental & Clinical Cancer Research, 2010. **29**(1): p. 104.
215. Xu, F., et al., *Hypoxia and TGF-β1 induced PLOD2 expression improve the migration and invasion of cervical cancer cells by promoting epithelial-to-mesenchymal transition (EMT) and focal adhesion formation.* Cancer cell international, 2017. **17**(1): p. 54.
216. DuFort, C.C., M.J. Paszek, and V.M. Weaver, *Balancing forces: architectural control of mechanotransduction.* Nature reviews Molecular cell biology, 2011. **12**(5): p. 308.
217. Dupont, S., et al., *Role of YAP/TAZ in mechanotransduction.* Nature, 2011. **474**(7350): p. 179.
218. Schaub, F.X., et al., *Fluorophore-NanoLuc BRET reporters enable sensitive in vivo optical imaging and flow cytometry for monitoring tumorigenesis.* Cancer research, 2015. **75**(23): p. 5023-5033.
219. Park, K.M., D. Lewis, and S. Gerecht, *Bioinspired hydrogels to engineer cancer microenvironments.* Annual review of biomedical engineering, 2017. **19**(1).
220. Huh, D., et al., *Reconstituting organ-level lung functions on a chip.* Science, 2010. **328**(5986): p. 1662-1668.
221. Lewis, D.M. and S. Gerecht, *Microfluidics and biomaterials to study angiogenesis.* Current Opinion in Chemical Engineering, 2016. **11**: p. 114-122.
222. Dickinson, L.E., et al., *Patterning microscale extracellular matrices to study endothelial and cancer cell interactions in vitro.* Lab on a chip, 2012. **12**(21): p. 4244-4248.
223. Highley, C.B., C.B. Rodell, and J.A. Burdick, *Direct 3D printing of shear‐thinning hydrogels into self‐healing hydrogels.* Advanced Materials, 2015. **27**(34): p. 5075-5079.
224. Jonas, O., et al., *An implantable microdevice to perform high-throughput in vivo drug sensitivity testing in tumors.* Science translational medicine, 2015. **7**(284): p. 284ra57-284ra57.

CURRICULUM VITAE

Johns Hopkins University, Department of Chemical and Biomolecular Engineering
Johns Hopkins Physical Sciences-Oncology Center (JHU-PSOC)
Institute for NanoBioTechnology (INBT)

Education

2015 – May 2018	**Ph.D. Johns Hopkins University** – *Chemical and Biomolecular Engineering* **Certificate –** *NanoBiotechnology*
2014	**M.S.E. Johns Hopkins University** – *Chemical and Biomolecular Engineering*
2010-2014	**B.S. Johns Hopkins University** –*Chemical and Biomolecular Engineering*

Research Experience

Doctoral Research: Department of Chemical and Biomolecular Engineering, Johns Hopkins University, Baltimore, MD, 2015-Present (research advisor: Dr. Sharon Gerecht)

- Developed a platform to control the stress relaxation of collagen gels to examine the effects of stress relaxation of sarcoma cell migration and metastatic potential.
- Created a novel collagen gel platform to independently control oxygen concentration from collagen fiber density in order to explore the effects of fiber density on sarcoma cell migration.
- Establishing a novel model to study sarcoma cell migration, metastasis, and drug response by incorporating single cells and biopsy tissue in a hypoxic-inducible hydrogel, with the eventual goal to validate multiple cancer types as a potential predictive personalized medicine platform.
- Integrating impedance spectroscopy into existing microfluidic device in order to have real-time imaging and impedance measurements of endothelial cells as they respond to shear stress.
- Validated and helped design self-healing injectable hydrogels for the potential therapeutic and *in-vitro* culture platform.

Masters Research: Department of Chemical and Biomolecular Engineering, Johns Hopkins University, Baltimore, MD, 2014 (research advisor: Dr. Sharon Gerecht)

- Designed and developed a microfluidic model to explore wound healing and to enhance endothelial cell repair and recruitment in hypoxic and non-hypoxic environments under physiologically relevant shear stress.

Undergraduate Research: Department of Chemical and Biomolecular Engineering, Johns Hopkins University, Baltimore, MD, 2010-2014 (research advisor: Dr. Sharon Gerecht)

- Created a co-culture platform using micro-patterning to explore the interactions between breast cancer and endothelial cells by precisely controlling the extracellular matrix components and distribution.

Awards, Fellowships, and Honors

1. **Siebel Scholarship Award** 2017
2. **NCI Nanotechnology for Cancer Research Fellowship** 2015-2017
3. **Graduate Student Excellence in Research Award Dept. of Chemical and Biomolecular Engineering** 2017
4. **School of Engineering Dean's List** 2014
5. **Outstanding Senior Design Project** 2014
6. **Undergraduate Student Excellence in Research Award Dept. of Chemical and Biomolecular Engineering** 2012-2014
7. **Joseph F. McElvery Memorial Award for Excellence in Research** 2014
8. **Provost Undergraduate Research Award** 2012
9. **American Red Cross Scholarship in Memory of Dwight H. Renfrew II and John E. Schmeltzer IV Award** 2010-2014
10. **Friends of Greenwich Point Award** 2010-2014
11. **Greenwich High School PTA Council Award** 2010-2014
12. **Charlton Fund** 2010-2014
13. **Countess Frances Thorley Palen-Klar Scholarship Fund** 2010-2014

Publications and Patents (*denotes equal contribution)

1. **Lewis DM,** Mavrogiannis N, Gagnon Z, Gerecht S. Real-time Imaging and Impedance Spectroscopy in physiologically relevant flow. In preparation
2. **Lewis DM,** Pruitt HC, Jain N, Ciccaglione M, McCaffery JM, Xia Z, Weber K, Eisinger-Mathason TSK, Gerecht S. Quicker Stress Relaxation Increases Migration Speed of Sarcoma Cells in Hypoxic Gradients. In preparation
3. Jaber SM, Bordt EA, Bhatt NM, **Lewis DM**, Gerecht S, Fiskum G, Polster BM. Sex differences in the mitochondrial bioenergetics of astrocytes but not microglia at a physiologically relevant brain oxygen tension. *Neurochemistry international*. (2017).
4. **Lewis DM***, Blatchley M*, Park KM, Gerecht S. O2-controllable hydrogels to study cellular responses to hypoxic gradients in three dimensions. *Nature Protocols.* (2017). 12 (8), 1620
5. Wei Z., **Lewis DM**, Xu Y., Gerecht S. Dual crosslinked bio-functional gradient hydrogels with injectable and self-healing properties. *Advance Health Care Materials*. (2017). 6 (16)
6. Gerecht, S; **Lewis, DM**; Park KM; Eisinger-Mathason TK; Simon C. "Oxygen Gradient Hydrogels to Study and Screen Potential Cancer Therapeutics." **July 2016.** U.S. Provisional application, pending.
7. **Lewis DM,** Tang V, Jain N, Isser A, Xia Z, Gerecht S. Collagen Fiber Density and Characteristic Stress Relaxation Regulate Hypoxic Sarcoma Cell Migration. *ACS Biomaterials Science & Engineering* (2017).
8. Park KM*, **Lewis DM*,** Gerecht S*. Bioinspired Hydrogels to Engineer Cancer Microenvironments. *Annual Review of Biomedical Engineering* 19.1 (2017).
9. **Lewis DM***, Park KM*, Tang V, Xu Y, Pak K, Eisinger-Mathason TK, Simon MC, Gerecht S. Intratumoral oxygen gradients mediate sarcoma cell invasion. *Proceedings of the National Academy of Sciences.* Aug 16:113(33):9292-9297 (2016)
10. **Lewis DM**, Gerecht S. Microfluidics and biomaterials to study angiogenesis." *Current Opinion in Chemical Engineering* 11: 114-122 (2016)
11. **Lewis DM**, Abaci H, Xu Y, Gerecht S. Endothelial Progenitor Cell Recruitment in a Microfluidic Vascular Model. *Biofabrication* 7.4: 045010. (2015)
12. Dickinson LE, Lütgebaucks C, **Lewis DM**, Gerecht S. Patterning microscale extracellular matrices to study endothelial and cancer cell interactions in vitro. *Lab Chip.* 12:4244-4248. (2012)

Master's Thesis

1. **Lewis, DM.** Endothelial Progenitor Cell Recruitment in a Wound Healing Microfluidic Vascular Model. Diss. Johns Hopkins University, 2014.

Conferences, Posters and Presentations (*denotes equal contribution)

1. **Lewis DM,** Eisinger-Mathason TSK, Simon C, Gerecht S. Hydrogels to study of ECM and oxygen gradient interactions. NIH/NCI Physical Sciences in Oncology Investigator Meeting. October 2017. ***Poster Presentation. Was selected to student oral presentation.***
2. **Lewis DM,** Eisinger-Mathason TSK, Simon C, Gerecht S. Hydrogels to study of ECM and oxygen gradient interactions. Institute for NanBiotechnology at Johns Hopkins University Annual Symposium. May 2017. ***Poster Presentation***
3. **Lewis DM,** Eisinger-Mathason TSK, Simon C, Gerecht S. Hydrogels to study of ECM and oxygen gradient interactions. Annual Meeting for the American Association for Cancer Research. April 2017. ***Poster Presentation***
4. **Lewis DM,** Eisinger-Mathason TSK, Simon C, Gerecht S. Hydrogels to study of ECM and oxygen gradient interactions. Cancer Systems. National Cancer Institute Nanotechnology Characterization Lab. October 2016. ***Poster Presentation***
5. **Lewis DM,** Eisinger-Mathason TSK, Simon C, Gerecht S. Hydrogels to study of ECM and oxygen gradient interactions. Cancer Systems. NCI Division of Cancer Biology's joint meeting of the Cancer Systems Biology Consortium (CSBC) and the Physical Sciences-Oncology Network (PS-ON). Auguts 2016. ***Poster Presentation***
6. **Lewis DM*,** Park KM*, Eisinger-Mathason TSK, Simon C, Gerecht S. Intratumoral oxygen gradients mediate sarcoma cell invasion. American Association for Cancer Research: Physical Sciences in Oncology Meeting. June 2016. ***Poster Presentation***
7. **Lewis DM*,** Park KM*, Eisinger-Mathason TSK, Simon C, Gerecht S. Intratumoral oxygen gradients mediate sarcoma cell invasion. Institute for NanBiotechnology at Johns Hopkins University Annual Symposium. May 2016. ***Poster Presentation***
8. **Lewis DM*,** Baker J*, McIntyre C*. FlowOx Bandage- A Topical Oxygen Microfluidic Bandage for Wound Healing. Senior Design Presentations for the Department of Chemical and Biomolecular Engineering at Johns Hopkins University. May 2014. ***Poster Presentation***
9. **Lewis DM,** Abaci H, Xu Y, Gerecht S. Endothelial Progenitor Cell Recruitment in a Microfluidic Vascular Model. Provost Undergraduate Research Award Ceremony. April 2013. ***Poster Presentation***

Mentored Students

1. Yu Xu. B.S. in Biomedical Engineering. Johns Hopkins University, Baltimore MD. Mentored 2014-Present-Undergraduate and Master student
2. Vitor Tang. B.S. in Chemical and Biomolecular Engineering. Johns Hopkins University, Baltimore MD. Mentored 2015-2017. Undergraduate student
3. Nupur Jain. B.S. in Chemical and Biomolecular Engineering. Johns Hopkins University, Baltimore MD. Mentored 2017-Present. Undergraduate student
4. Mark Ciccaglione. B.S. in Chemical and Biomolecular Engineering. Johns Hopkins University, Baltimore MD. Mentored 2017-Present. Undergraduate student
5. Dani Zamalin. **PSOC Undergraduate Research**. B.S. in Biology. Georgetown University, Washington D.C. Mentoring summer 2017.

Outreach, Leadership and Community Engagement

1. **Recruitment Committee for the Department of Chemical and Biomolecular Engineering, JHU** 2017
2. **Sports Chair for Graduate Student Liaison Committee, JHU.** 2017
3. **Institute for NanoBioTechnology Undergraduate Research Leader, JHU** 2013-2014
4. **Leadership Committee Member for Senior Class Gift, JHU** 2013-2014
5. **Corresponding Secretary for Theta Tau (Professional Engineering Fraternity)-** Participates in philanthropy and other fraternity events. Organized events and communicated with alumni.
6. **Presidents Day of Service, JHU** 2011-2014

7. **Tower of Power, JHU** 2011-2014
8. **Pathology Lab Volunteer, Greenwich Hospital, Greenwich, CT** 2011

Industry and Engineering Project Experience

Senior Associate of Therapeutic Research New York, New York
Leading BioSciences Inc May 2014 – August 2014

- Established project management protocol for running a Phase 2 clinical trial.
- Identified the top critical care physicians to establish a Phase 2 clinical trial protocol.
- Wrote and helped complete sections for an Investigation New Drug Filing.

Associate of Therapeutic Research New York, New York
Leading BioSciences Inc December 2013 – February 2014

- Generated market strategy and analysis of critical care standard of care.
- Restructured clinical trial strategy from market analysis.
- Explored new therapeutic areas using the company's existing drug development pipeline.

Rotational Program Intern New York, New York
Mesoblast, Ltd June 2013 – August 2013

- Rotated through Mesoblast's clinical, pre-clinical, project management, quality, manufacturing, and regulatory departments to assist in the development of new stem cell therapies.
- Edited and reviewed a European Medical Agency submission for a Phase 3 clinical trial.
- Created project management standard operating procedures for the data management division of Mesoblast.
- Repurposed existing therapeutics to look for alternative disease designation.
- Collaborated and coordinated evaluation of possible contract research organizations for new clinical programs.

Clinical Practice Manager Greenwich, Connecticut
Diagnostic and Medical Specialist of Greenwich May 2011 – August 2011

- Optimized patient inflow and outflow through the development of standard operating procedures to maximize the number of patients seen by general practitioners.

Skills

Teaching:	Teaching Assistant for Introduction to Chemical & Biological Process Analysis and Bioengineering in Regenerative Medicine.
Computer:	Microsoft Excel, Word, PowerPoint, Project, MATLAB, Python, Zen, AutoCAD, COMSOL.
Clinical Research Skills:	Contract Research Organization negotiations and analysis, clinical trial management, batch reconciliation, FDA and EMA regulatory knowledge, key opinion leader recruitment, market and scientific analysis, Phase 2 clinical trial design, created investigator brochures.
Laboratory:	In-vivo dissection, hydrogel and alginate encapsulation, confocal and fluorescent microscopy, fluid flow assay analysis, fluorescent staining, hydrogels, rheology, flow cytometry, cell culture, microfabrication, microfluidics, electrode systems, impedance spectrometry, device design and fabrication, AFM, dynamic materials analysis and PCR.
Language:	English and Basic Spanish.